Dispersion and Stabilization of Gold and Silver Nanoparticles by Topology Effect of Cyclic Poly(Ethylene Glycol)

A Dissertation for the Degree of Doctor of Philosophy

Yubo Wang

Hokkaido University

March 24, 2023

Acknowledgements

This research work was performed under the direction of my supervisor, Associate Professor Takuya Yamamoto, Division of Applied Chemistry, Faculty of Engineering, Hokkaido University, during April 2020 – March 2023. The author is deeply grateful for his kind instruction, supervision, and advice. His passion for research and positive attitude towards work inspires me deeply. This thesis wouldn't have been possible without him. The author also thanks to Associate Professor Shin-ichiro Sato, Professor Toshifumi Satoh, Associate Professor Kenji Tajima, Associate Professor Takuya Isono, and Assistant Professor Feng Li for their kind comments and suggestion.

The author sincerely thanks to the members in Associate Professor Yamamoto's Laboratory and Professor Satoh's Laboratory, Jose Enrico Quijano Quinsaat, Masaaki Hosokawa, Shota Yoshino, Yuta Miyata, Minato Nakamura, Satoru Chimura, Atsuo Utagawa, Masaya Kawamura, Choike Onyinyechukwu-Justina, Moka Takashima, Xueming Su, Rika Kudo, Tomoko Ono, Suzuki Kazushige, Tomohisa Watanabe, Yuna Kinoshita, Yuto Okuma, Huimin Wang, Tsuyoshi Nakai, Akira Takatsuka, Masato Yamasaki, Katsuyuki Namai, Kenta Koumura, Ayaka Otsuka, Satoshi Katsuhara, Tianle Gao, Chaehun Lee, Minami Ebe, Ryota Suzuki, Taiki Nishimura, Satoru Takagi. It was a precious memory and the author would never forget. The author will thank to my parents, Jingbo Li and Xin Wang. Thanks to them for giving me life and raising me with a good education. Finally, the author will thank to my supervisor, Associate Professor Takuya Yamamoto again.

March 2023

Yubo Wang

Contents

Chapter1.General Introduction 6

1.1 Topological effect of polymer.....7

1.2 Potential materials of nanoparticles.....11

1.3 Metal nanoparticles…….....13

1.3.1 Gold nanoparticles.....13

1.3.2 Silver nanoparticles.....14

1.4 Influencing factors on the dispersion stability of metal nanoparticles.....15

1.4.1 Factor of salt concentration….....15

1.4.2 Factor of temperature and pH….....16

1.5 Dispersant of metal nanoparticles…….....17

1.6 Objectives and main theme of dissertations.....19

1.7 References 23

Chapter 2 Cyclic Poly(ethylene glycol) : A Dispersion Stabilizer for Gold Nanoparticles by Physisorption.....30

2.1 Introduction 31

2.2 Experimental section.....34

2.2.1 Materials.....34

2.2.2 NMR 34

2.2.3 SEC..... 35

2.2.4 Recycling Preparative SEC 35

2.2.5 MALDI–TOF MS…….....35

2.2.6 UV–Vis Spectroscopy…….....35

2.2.7 Synthesis of *c*-PEG……...35

2.2.8 Synthesis of MeO–PEG–OMe…….……..…36

2.2.9 Preparation of AuNPs/HO–PEG–OH, AuNPs/MeO–PEG–OMe, AuNPs/HS–PEG–OMe, AuNPs/HS–PEG–SH, and AuNPs/*c*-PEG……..……..37

2.2.10 Dispersion stability against freezing……..……....37

2.2.11 Dispersion stability against lyophilization……..……....37

2.2.12 Dispersion stability against heating……..……..….37

2.2.13 Dispersion stability against a PBS buffer solution……..……38
2.2.14 Stabilization of AuNPs with various diameters…….…….…38
2.2.15 PEG concentration-dependent stabilization of AuNPs……..…….…….……39
2.2.16 DLS and ζ-potential …….…….....39
2.2.17 FT-IR……..……..…...39
2.2.18 Cell lines and animals…….…....39
2.3. Results and Discussion……...…….……...….40
2.3.1 Synthesis of *c*-PEG……...….40
2.3.2 Dispersion stability against freezing…….…….....….49
2.3.3 Dispersion stability against lyophilization……..…..……..…..52
2.3.4 Dispersion stability against heating…….…….....….52
2.3.5 Dispersion stability against a physiological condition……....….61
2.3.6 Size-dependence of AuNPs dispersion stability against a physiological condition….....64
2.3.7 Molecule weight-dependence of *c*-PEG of AuNPs dispersion stability against a physiologicalcondition…….....….66
2.3.8 Concentration-dependence of *c*-PEG of AuNPs dispersion stability against a physiological condition…….....….68
2.3.9 DLS and ζ-potential for AuNPs/PEG…….....….69
2.3.10 *c*-PEG concentration-dependence of the layer thickness and ζ-potential…….71
2.3.11 FT-IR for AuNPs/PEG…….…….74
2.3.12 Animal experiments by AuNPs/PEG…….…….…77
2.4. Conclusions…….....79
2.5. References…….…….....81

Chapter 3. Size Control and Enhanced Stability of Silver Nanoparticles by Cyclic Poly(Ethylene Glycol) 84
3.1 Introduction 85
3.2 Experimental section.....87
3.2.1 Materials. ……...……..……87
3.2.2 NMR……..…….…….....87
3.2.3 SEC. ……..…...87

3.2.4 TEM……..……..……..….87
3.2.5 MALDI–TOF MS …….……...…….....88
3.2.6 UV–Vis Spectroscopy……..……..…..….88
3.2.7 Synthesis of AgNPs Through the Tollens Process…….…….…….…….....88
3.3 Results and Discussion.....89
3.3.1 Synthesis of AgNPs. 89
3.3.2 Stability of AgNPs.....98
3.4 Conclusions.....104
3.5 References.....105

Chapter 4. Conclusions.....108

Chapter 1

General Introduction

1.1 Topological effect of polymer

Many smaller chemical units are connected to each other and arranged in a regular or irregular manner to form larger molecules, which is called polymer. Based on the number or segment of molecules, the order of arrangements or connections, many researchers have synthesized and successfully isolated various structures of topological shapes such as 'linear', 'star', 'cyclic', '8-shape', 'multicyclic', 'H-shape', 'cross linked', 'branched' etc polymers (Figure 1.1).[1] Interestingly, different topologies affect the intrinsic properties of polymer like hydrodynamic volumes, viscosity, crystallization or melting points, diffusion coefficients, as well as phase separation in films, solution and bluk.[2] Among all the topological structures, 'cyclic' polymers without any end-groups exhibits unique physical/chemical properties.[3] For example, compared with the respective linear counterparts, cyclic polymers always give a higher glass transition temperature,[4] reduced hydrodynamic volume,[5] higher density,[6] slower degradation profile,[7] lower viscosity,[8] faster crystallization capability,[9] higher melting temperature,[10] smaller radius of gyration,[11] more orderly entanglement,[12] as well as higher tolerance towards temperature[13] and salinity of micelles[14] in the same molecule weight condition.

Dating back as far as ancient times, the composition of cell membrane in extremophile archaea is a diether or the tetraether lipid monolayer.[15] In order to resist the extremely high temperature, variations in chain length and cyclization lead to diversification of these lipids.[16] The presence of cyclic DNA in *Escherichia coli* was first hypothesized by Jacob and Wollman in 1958 and since then various types of cyclic DNA have been found in bacteria and viruses.[17] With intensive research and observation of bio-cyclic macromolecules, it was found that the thermal and chemical stability of cyclic macromolecules was greatly improved compared to their respective linear counterparts.[18] Thus, much interest had been focused on cyclic macromolecules.

For example, it has been reported that cyclic peptides show unusual properties in biochemical such as antibacterial activity,[19] immunosuppressive activity,[20] effective enzyme inhibitor,[21] and anti-tumor activity.[22] In addition, cyclic oligosaccharides and polysaccharides like cyclodextrins, are well known for their ability to incorporate various organic compounds into their cavities and for exhibiting catalytic activity.[23]

With advances in precision synthesis, separation, and purification, the yield and purity of cyclic polymers increased dramatically, which facilitates comparison upon topological conversion between linear and cyclic polymers of the physical and chemical properties. Firstly, significant differences between linear and cyclic polymer of self-assembly behavior in aqueous solution of micelles formed by block polymers composed of different hydrophilic and hydrophobic segments was found.[24] Booth et al. reported cyclic copolymer of ethylene glycol and 1,2-butylene oxide formed larger micelles than the corresponding the linear triblock copolymer through the measurement of dynamic and static light scattering, surface tension, as well as micellar molar mass

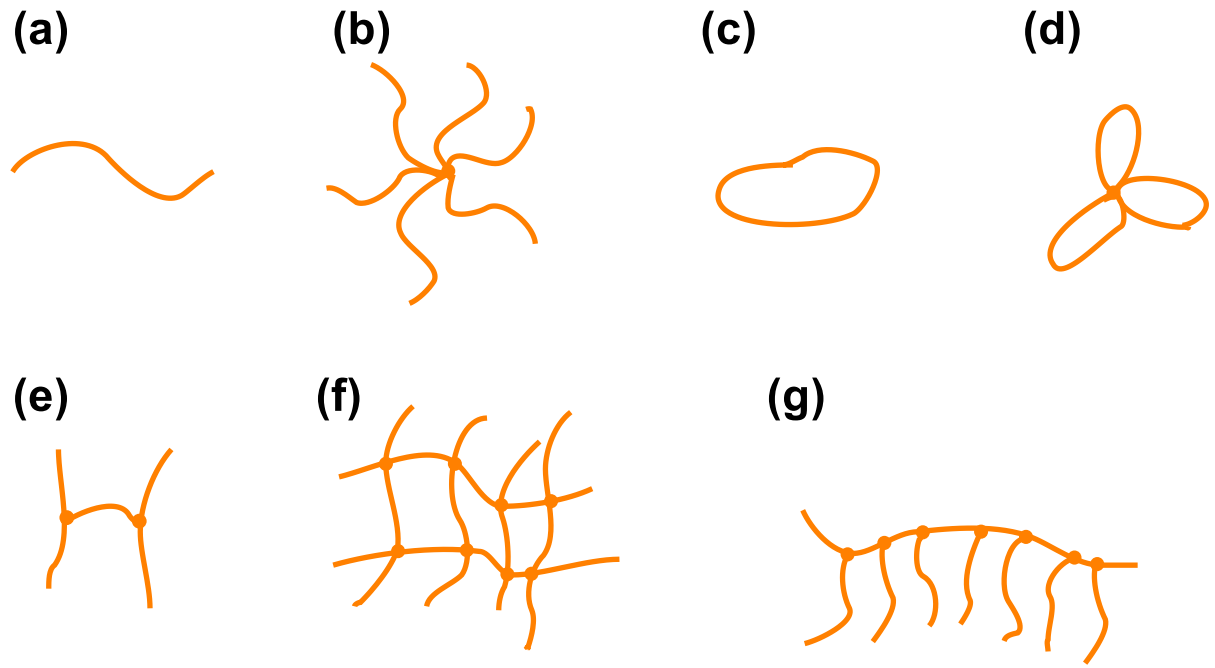

Figure 1.1 Schematic illustrations of polymer topological shapes of (a) linear, (b) star, (c) cyclic, (d) multicyclic, (e) H-shape, (f) cross linked, and (g) branched.

and size.[25] Similar result was also found in cyclic oxyethylene/oxybutylene copolymers formed micelles with a lower critical micellization concentration (CMC) in aqueous solution.[26] In addition, in the case of gelation of concentrated solutions, the cyclic triblock copolymer of propylene glycol/ethylene glycol formed micelles exhibits temperature dependence of CMC, larger association numbers and hard-sphere volumes at 50−55 °C.[27] Tezuka et al. reported that the cloud point of cyclic poly(butyl acrylate)-block-poly(ethylene oxide) (PBA-*b*-PEG) formed flower-like micelles was elevated by more than 40 °C, by compared with linear poly(butyl acrylate)-block-poly(ethylene oxide)-block-poly(butyl acrylate) (PBA-*b*-PEG-*b*-PBA), which remarkably enhanced the thermal stability of a self-assembled micelle.[28] Especially, the cyclized polymeric amphiphiles micelles of PBA-*b*-PEG feature a higher tolerance towards a wide range of temperature and salt concentration compared to their linear counterparts of PBA-*b*-PEG-*b*-PBA (Figure 1.2).[24] Furthermore, cyclic copolymer surfactant of PS-*b*-PEG exhibits a faster phase separation kinetic and a better emulsion stabilization in the emulsion system, by compared with the linear PS-*b*-PEG-*b*-PS.[29] Moreover, a faster crystallization rate was observed for cyclic poly(ε-caprolactone) in comparison with its linear counterpart in the crystallization kinetic behavior.[30] In addition, a reversible linear-cyclic topological conversion of hydrophilic and hydrophobic

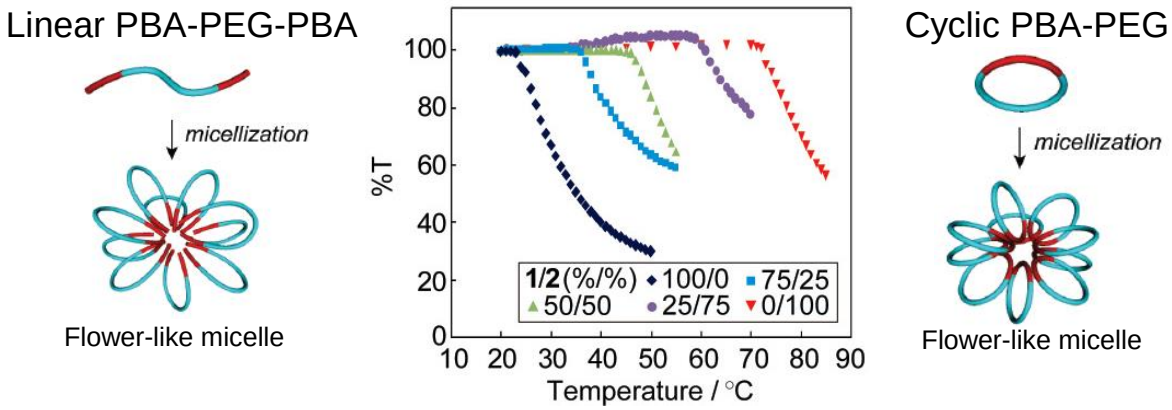

Figure 1.2 Thermal stability measurement of flower-like micelles formed by linear PBA-PEG-PBA and cyclic PBA-PEG.[24]

polymers was also found in linear and cyclic poly(ethylene glycol) telechelics with coumarinyl end groups through light or heat, providing the possibilities for comprehensive topological transformations.[31]

In recent 20 years, polyethylene glycol (PEG) and its analogue as a commercial product have been on the market due to its non-ionic water-soluble property and superior biocompatibility with a flexible backbone. It is widely used as a surface covalent modifier of biological macromolecule like proteins and liposomes,[32] nanoparticles like gold,[33] silver,[34] or copper,[35] as well as a drug carrier with the advantages of enhanced solubility of hydrophobic drugs, reduced tendency of drug particles to aggregate, prolonged circulation time, reduced blood clearance of drug carriers, decreased non-specific uptake, and allowed for specific tumor-targeting.[36] It has been reported that coating of PEG on the surface of gold or silver nanoparticles, enhanced their water-solubility and biocompatibility is the usual method for functioning the nanoparticles.[37] Jiang et al. reported that looped poly(ethylene glycol) with thiol termini groups are much thicker and denser than the linear counterparts on gold nanoparticles, which supplies a more stable in a high-salt environment, a better hydrophilicity, excellent biocompatibility, protein resistance and cell viability (Figure 1.3).[38] Benetti et al. compared the differences between the linear and cyclic poly-

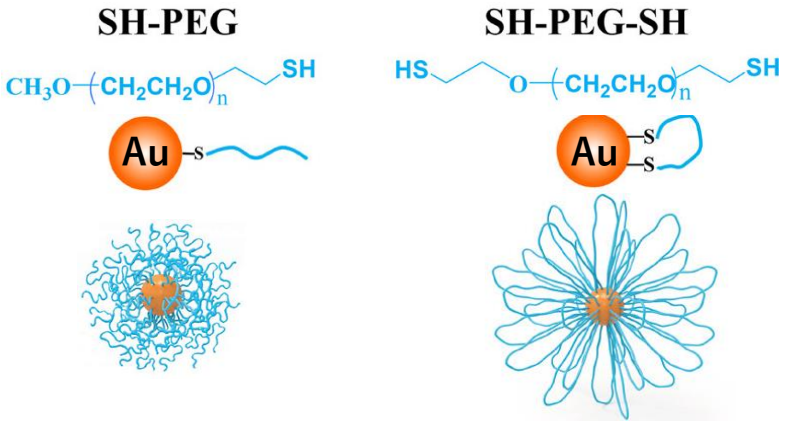

Figure 1.3 Chemical structure and scheme of AuNPs stabilized by PEG with one end group of thiol (left) and two end groups of thiol (right).[38]

2-ethyl-2-oxazoline (PEOXA) grafts assembled on titanium oxide surface, found that cyclic PEGXA favors the formation of denser brusher with respect to linear analogs, which produces surfaces to display a super-lubricating character when they are sheared against each other.[39] In addition, the ultra-dense and highly compact shells of cyclic PEGXA also prevents superparamagnetic Fe_3O_4 nanoparticles nonspecific interaction with proteins.[40]

1.2 Potential materials of nanoparticles

Nanomaterials date back as far as the Lycurgus Cup in the 4th century A.D., which exhibits various colors depending on the incident light due to the presence of nanoparticles of gold and silver.[41] The interest of red color in gold nanoparticle colloidal solution was found in 1850 by Faraday. M., who started the first systematic synthesis of gold nanoparticles using the reduction of gold chloride (Figure 1.4).[42] Five decades later, a scientific theoretical explanation of surface plasmon resonance was put forward. When a beam of light is illuminated onto the surface of nanoparticle colloidal solution, colors are formed due to the interaction of photons and electrons in the transmission band of the nanoparticles, leading to collective oscillations of the free conduction band electrons and subsequent light absorption.[43] The color of the colloidal solution formed varies depending on the material,[44] size,[45] shape,[46] and structure[47] of the nanoparticles, resulting in different physical or chemical properties (Figure 1.5). It is usually defined that the diameter of a nanoparticle is between 1 and 100 nm, which is widely applied in the life and science yield of photothermal therapy,[48]

Figure 1.4 A 4th-century Roman glass cage of Lycurgus cup, which the color changed depending on the location of the light source due to the presence of colloidal AuNPs.[42]

Figure 1.5 Various sizes (5-100 nm) of AuNPs aqueous solution.

energy,[49] electronics,[50] optics,[51] pharmaceuticals,[52] cancer treatment,[53] drug delivery,[54] as well as catalysts.[55] For example, James et al. reported that the gold nanorods were found to have two times the photothermal transduction efficiency than the gold nanoshells,[56] which is more efficiently applied in the near-infrared (NIR) absorbing plasmonic nanoparticles enhance photothermal therapy of tumors. Xin et al. announced that the nanoparticle-based drug delivery system shows improved advantages by accelerating the half-life of vulnerable drugs and proteins, improving the water-solubility of hydrophobic drugs, and allowing controlled and targeted release of drugs.[57] Xiao et al. compared the metal nanoparticles (platinum, palladium, rhodium and silver) and zeolite catalysts exhibit long reaction lifetimes than commercial catalysts, including the water-gas shift reaction, CO oxidation, oxidative reforming of methane and CO_2 hydrogenation.[58] Moreover, nanoparticle suspension is promising heat transfer fluid in the heat transfer enhancement, having a plethora of applications because of its superior thermal conductivity.[59] However, the dispersion stability of nanoparticles is considered as a priority in a variety of applications due to the aggregation,[60] dissolution,[61] loss of activity,[62] changes in shape and size[63] during synthesis and application of nanoparticles. Therefore, improving the stability and dispersion of nanoparticles as well as preventing and controlling the degree of aggregation of nanoparticles have always been pursued by scientific researchers.

1.3 Metal nanoparticles

1.3.1 Gold nanoparticles

Gold is a precious metal element used by ruling classes around the world since ancient times. The materials gold with dimensions in the nanoscale (1-100 nm) is the most representative metal-based nanoparticles. Unlike gold at the bulk or molecular scale, gold at the nanoscale can exhibit red wine colors, making them a very popular subject of study for chemists, biologists, and physicists. The strong scattering or absorption[64] make it ease of monitoring the light signal and applied in the field of optics,[65] unique sensing properties,[66] and bio-imaging.[67] Gold nanoparticles effectively convert light into heat, allowing for precise thermal therapy[68] of cancerous tissue. Especially, gold nanoparticles can shield slightly soluble imaging contrast agents and delivery to the inaccessible regions of the body due to its multivalency.[69] Importantly, the size of protein, liposomes, some biomolecules, and gold nanoparticles are almost the similar size, enabling gold nanoparticles to pass through cell membranes and influence cellular processes, with the potential to act as biomedicines.[70] Moreover, the simple surface chemistry reaction makes it possible to vary the density of bound ligands on its surface, which is beneficial for the precise treatment of diagnosis detection[71] and biomolecule identification (Figure 1.6).[72,104]

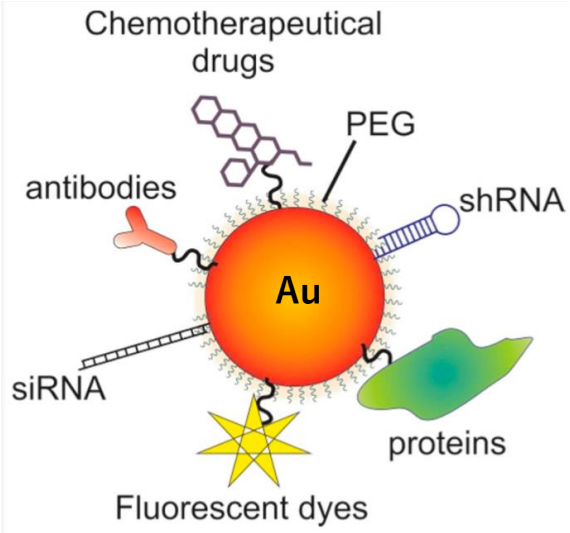

Figure 1.6 AuNPs functionalized by a variety of molecules, including drugs, antibodies, shRNA, siRNA, proteins, and fluorescent dyes for theranostics.[104]

1.3.2 Silver nanoparticles

Silver nanoparticles can be synthesized through two approaches (physical and chemical routes) in general. Physical methods[73] include evaporation/condensation and laser ablation, the former of which always requires a very spacious tube furnace and consumes a lot of energy to achieve thermal stability of the silver nanoparticles, while the latter also has the disadvantage that the size and structure of the silver nanoparticles can be affected due to further interaction with the passing laser light.[74] On the other hand, chemical reduction is the common approach for preparing colloidal dispersions of silver nanoparticles that are stable in water or organic solvents. Using a strong reducing agent such as borohydride produces small monodisperse nanoparticles, but the larger cluster is difficult to control.[75] In contrast, the utilization of weak reductant like citrates results in slower reduction rates with a wide size distribution.[76] In general, the process of synthesizing silver nanoparticles need suitable dispersion stabilizer to prevent the nanoparticles aggregation or agglomeration. The synthesized small size and regular shape[105] of silver nanoparticles attract much interest in the field of functional textiles,[77] daily cosmetics,[78] bio-probes,[79] foodstuffs packaging,[80] electronics,[81] antibacterial activity,[82] paints,[83] and drug and gene delivery (Figure 1.7).[84]

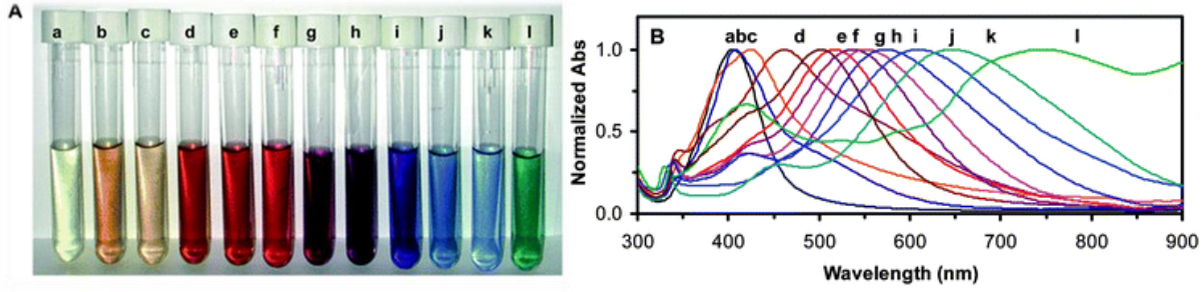

Figure 1.7 Various absorption and scattering plasmonic optical properties of colloidal AgNPs due to the different sizes and shapes.[105]

1.4 Influencing factors on the dispersion stability of metal nanoparticles

Metal nanoparticles are not a stable material and can be affected by a number of factors during and after the synthesis process. During the synthesis of nanoparticles, pH of reaction solution,[85] reaction temperature,[86] pressure,[87] reaction time[88] influence the degree of dispersion, quality, size and quantity of the nanoparticles. Even upon the synthesis, metal nanoparticles need to be kept as a solution at low temperature to prevent form agglomerate to lose surface plasmon resonance absorbance. Thus, the dispersion stability of metal nanoparticles colloidal solution is affected by various parameters such as salt concentration,[89] temperature[90] or pH,[91] all of which eventually lead to particle dissolution or agglomeration (Figure 1.8).

1.4.1 Factor of salt concentration

The increase of ionic strengths in colloidal nanoparticle will lead to the aggregation of the metallic nanoparticles due to the change of local environment around the nanoparticle. It is reported that silver nanoparticles surface modified by poly(diallyldimethylammonium chloride), poly(allylamine hydrochloride) or poly(ethylene glycol) all can lead to aggregation in the condition of 0.5 M NaCl.[89] Gold nanoparticles also form big cluster rapidly when a critical electrolyte ionic concentration is exceeded, leading to instability and precipitation.[92] Polyelectrolyte-coated gold nanoparticles also shows instability and irreversible aggregation when the salt concentration above 50 mM.[93] Christau et al. reported that the surface plasmon of citrate-coated gold nanoparticles confined within poly(N-isopropylacrylamide) broadens and redshifts

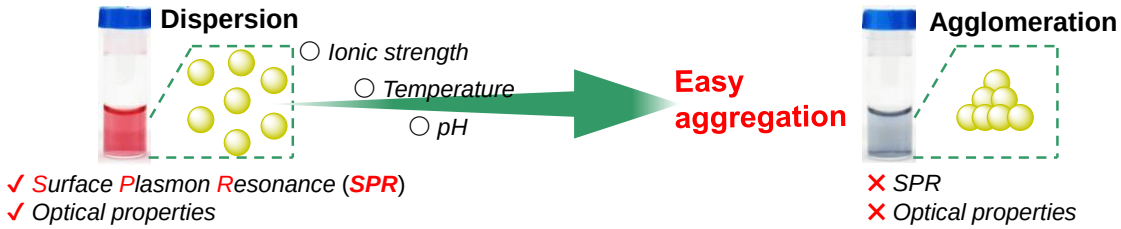

Figure 1.8 Photographs and schematic illustrations of AuNPs aqueous solution influenced by ionic strength, temperature, and pH.

upon immersion in aqueous 1 M salt solutions (NaF, NaCl, NaBr, and KCl).[94] It can be concluded that increasing the salt concentration in a colloidal solution decreases the ζ-potential on the surface of the metal nanoparticles, leading to a weakening of the repulsive forces and a shortening of the distance between the nanoparticles, thus causing them to aggregate, dissolve, or agglomerate.

1.4.2 Factor of temperature and pH

The synthesis reaction temperature and the ambient temperature of the metal nanoparticles will also affect the dispersion stability of the colloidal solution. Especially, when nanoparticles treated by heating or freezing, the irreversible aggregation will lead to loss surface plasmon resonance or optical properties of nanoparticles. Matyjaszewski reported that gold nanoparticles coated by *n*-butyl acrylate aqueous solution turned to be grayish blue after a 3.5 h heating at 80ºC or a 1 h heating at 110ºC, suggesting aggregation, but the same gold nanoparticles stabilized by a dimethacrylate-based cross-linker still maintain the red color due to the surface plasmon resonance even heated for 24 h.[90] Moreover, strongly temperature-dependence in the synthesis of silver nanoparticle that 100ºC synthesis reaction displays a sharp UV absorption and a smaller size of AgNPs, by compared with lower reaction temperature of 25 ºC or 60 ºC.[95]

On the other hand, the pH is also an important factor to the stabilization which modifies the surface charge and the oxidative dissolution of metallic nanoparticle. As a result, the particle behavior varied in acidic and alkaline conditions. For example, Hiemstra et al. reported the Ag^+ release from the surface of silver nanoparticles is much faster in the case of pH=3, by compared in the neutral solution condition.[96] Importantly, silver nanoparticles exhibit a cleaner and narrower surface plasmon resonance with a UV absorbance as the pH increasing in the process of silver nanoparticles.[97] The pH of the solution also affects the size of the gold nanoparticles. Hodak et al.

reported that during the synthesis of gold nanoparticles through the reduction of $AuCl_4^-$, the smaller size and narrower distribution with the pH increasing in the range from 4 to 6.5.[98]

It can be concluded that the dispersion stability of metal nanoparticles was easily influenced by the external environment of ionic strength, temperature, or pH in the synthesis or during the storage. It is necessary to apply the suitable dispersant or stabilizer for preventing the nanoparticles aggregating or forming the clean and regular size of nanoparticles.

1.5 Dispersant of metal nanoparticles

Surfactants or dispersants are generally applied to stabilize the gold or silver nanoparticles. In general, there are two mechanisms of ionic surfactants and nonionic surfactant for disperse and stabilize nanoparticles. The surfactants of sodium dodecyl sulfate (SDS) and Cetyltrimethyammonium bromide (CTAB) belong to the ionic surfactants which will give an electrostatic stabilization to nanoparticles. Existence of an electric charge on the surfaces of particles is a major source of kinetic stability. Electrostatic stabilization occurs by adsorption of ions to the electrophilic metal surface. On the other hand, nonionic surfactant such as Polyvinylpyrrolidone (PVP) and polyethylene glycol belong to the which will give a steric stabilization to nanoparticles. Steric stabilization of nanoparticles is achieved by graft or chemisorption attaching macromolecules such as polymers or surfactants to the surfaces of the particles. The stabilization is due to the large adsorbents which provide steric barrier to prevent particles coming close to each other. In addition, Cooper et al. reported that poly(sodium acrylate) with polymer backbone structure and charges can also stabilize silver or gold nanoparticles through above both two dispersion mechanisms (Figure 1.9).[99]

Notably, poly(ethylene glycol) (PEG) is a biocompatible polymer that is often used for stabilizing nanoparticles because its flexible and long alkoxy chain can provide steric hindrance and/or the end-groups can react with the surface of the nanoparticles. In particular, the coverage density of PEG coating on the surface of nanoparticles is a crucial factor for the biophysical and chemical properties of nanoparticles.[100] Mirkin et al. reported that the molecular weight and density of PEG ligands will also influence the shape of nanocrystals' growth.[101] Especially, PEG can protect nanoparticles aggregation and improve drug and gene delivery *in vitro* and *in vivo* as well as from detection by the immune system.[102] It is a common methodology to use the water-

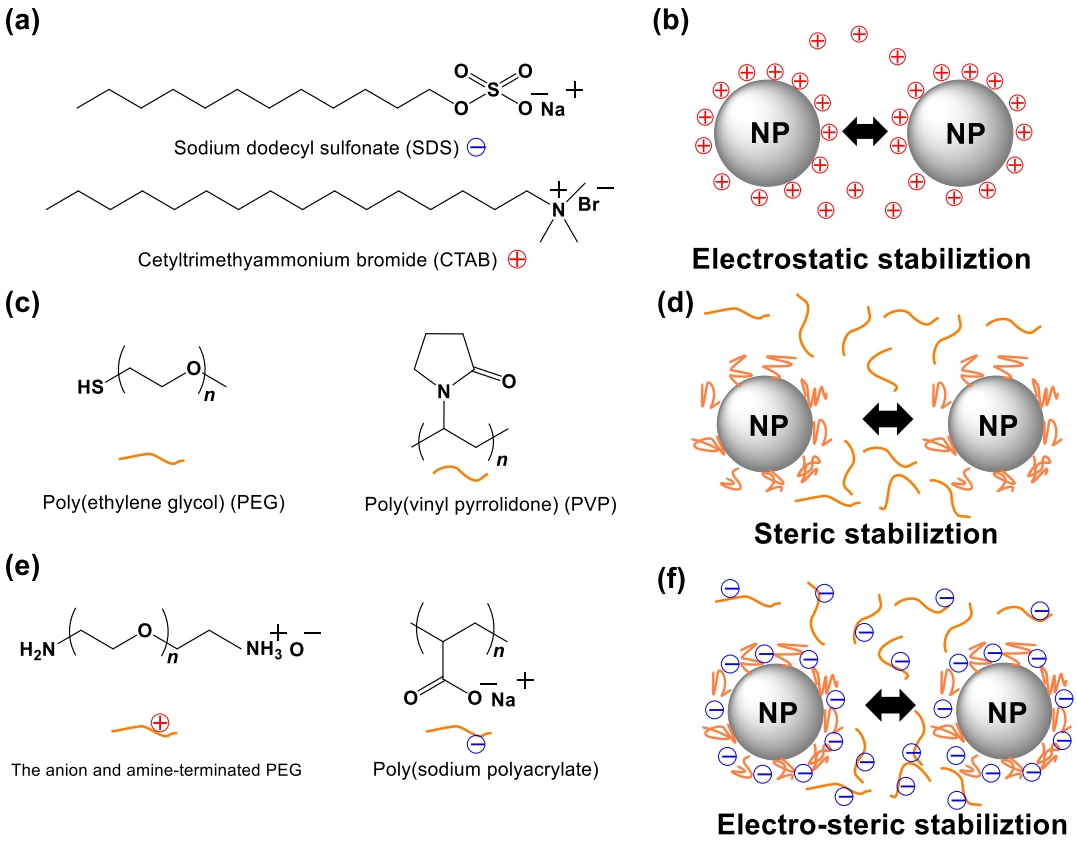

Figure 1.9 Molecule dispersants of (a) sodium dodecyl sulfonate and cetyltrimethyammonium bromide, and (b) schematic illustrations of interaction with nanoparticles. Neutral polymer dispersants of (c) poly(ethylene glycol) and poly(vinyl pyrrolidone), and (d) schematic illustrations of interaction with nanoparticles. Ionic polymer dispersants of (e) the anion and amine-terminated PEG and poly(sodium polyacrylate), and (f) schematic illustrations of interaction with nanoparticles.

soluble property of PEG to encapsulate nanoparticles and some hydrophobic drugs in order to apply them in biological experiments.[103] Until today, PEG has been approved by U.S. Food and Drug Administration (USFDA) have led to a clinically approved product due to its tunable properties and well-established safety profile.[36] PEG is applied in various application field such as medical, pharmaceutical, food, cosmetic, and drug delivery system. Thus, the importance and potential value of PEG is worthy of further study and exploration.

1.6. Objectives and main theme of dissertations

With above-mentioned understanding and insights about polymer topology effect, metal nanoparticles, as well as suitable dispersion stabilizer in mind, cyclic poly(ethylene glycol) (*c*-PEG) was applied to provide polymer topology-dependent stabilization for the surface modification of gold nanoparticles (AuNPs) and in the preparation process of silver nanoparticles (AgNPs), which was found that the *c*-PEG supplies superior dispersion stability to gold nanoparticles through physisorption as well as the effect on the size and stability against NaCl of silver nanoparticle. In this research, based on the effect of polymer topology, linear PEG with the end groups of hydroxy (HO–PEG–OH), methoxy (MeO–PEG–OMe), and thiol (HS–PEG–OMe) were compared with *c*-PEG to be a dispersion stabilizer for AuNPs. Thus, (i) the influence of external environment factors such as freezing, lyophilization, heating, a physiological condition on AuNPs stabilized by PEG; (ii) the influence of concentration, molecular weight of PEG and polymer topology on AuNPs; (iii) the influence of AuNPs size; (iv) the optimal thickness, density, chains and ζ-potential of PEG layer on the surface of AuNPs; (v) the interaction of PEG and AuNPs by FT-IR; (vi) an animal experiment of blood circulation and tumor accumulation were investigated. On the other hand, the polymer topology effect of PEG also affects the size and resistance to NaCl of the synthesized AgNPs. Thus, the factors were discussed in the AgNPs

synthesis process such as (i) the influence of polymer topology of HO–PEG–OH, MeO–PEG–OMe and *c*-PEG to the size of synthesized AgNPs by TEM and UV-Vis spectroscopy; (ii) the influence on molecular weight and molar ratio of PEG; (iii) the stability of synthesized AgNPs against various concentration of NaCl aqueous solution.

In order to obtain the pure *c*-PEG with homogeneity and low polydispersity index, HO–PEG–OH was applied to form a *c*-PEG via etherification in large dilute alkaline solution. Size exclusion chromatography (SEC), nuclear magnetic resonance (NMR), and matrix-assisted laser desorption ionization-time of flight mass spectrometry (MALDI-TOF) were used to characterize the chemical structure and the *c*-PEG were successfully synthesized and separated. The synthesized *c*-PEG was adsorbed on AuNPs by the physisorption. By comparing the HO–PEG–OH, MeO–PEG–OMe, and HS–PEG–OMe, the AuNPs stabilized by cyclic PEG, but not linear PEGs, remained the surface plasmon resonance (SPR) in the case of freezing, lyophilization, heating, and a physiological condition. Furthermore, dynamic light scattering (DLS), ζ-potential, and Fourier transform infrared spectroscopy (FT-IR) were used to confirm the presence of PEG layer and the interaction between PEG and AuNPs. Particularly, an optimal concentration of 0.25wt% *c*-PEG was found for AuNPs. Moreover, the AuNPs stabilized by *c*-PEG supplies a prolonged blood circulation and enhanced tumor accumulation in mice. On the other hand, the AgNPs size was significantly affected in the Tollens synthesis of AgNPs. The particle size is much smaller through the *c*-PEG as a dispersant than HO–PEG–OH and MeO–PEG–OMe. Furthermore, the stability of AgNPs was enhanced by cyclization in the salt tolerance tests.

An outline of this dissertations is as follows:

Chapter two discusses the phenomena and principles of physisorption between AuNPs and *c*-PEG. By compared with linear PEG of HO–PEG–OH, MeO–PEG–OMe, and HS–PEG–OMe,

c-PEG supplies strongly dispersion stability to AuNPs under the extreme conditions such as freezing, lyophilization, and heating. Especially, this method is comparable with the traditional chemisorption of HS–PEG–OMe. After heating AuNPs coated with HS–PEG–OMe at 85 ºC for 4 h, the red color caused by SPR disappeared. Surprisingly, AuNPs coated with *c*-PEG remained red, which indicates superior dispersion stability. Furthermore, AuNPs dispersed by cyclic PEG, but not linear PEG, maintain the superior dispersion stability in a phosphate buffer saline (PBS) solution. The strong physisorption between *c*-PEG and AuNPs is confirmed by DLS, ζ-potential, and FT-IR. The thicker PEG layer and reduced ζ-potential confirms the presence of cyclic PEG layer and the strong affinity between *c*-PEG and AuNPs. It is expected that the less entropic penalty upon adsorption is the major factor strong affinity of *c*-PEG to AuNPs.

Chapter three discusses the influence of size controlling and stability in the synthesis process of AgNPs by *c*-PEG. As a dispersant of PEG, the polymer topology of linear and cyclic polymer conversion has a significant effect on the size of the synthesized AgNPs. By compared with linear PEG of HO–PEG–OH and MeO–PEG–OMe in the same molecular weight and molar ratio, the utilization of *c*-PEG in Tollens' synthesis of AgNPs allows for the smaller and more narrow size. Furthermore, the synthesized AgNPs stabilized by *c*-PEG drastically improved stability against NaCl aqueous solution, by compared with the linear counterpart dispersant. It can be concluded that cyclized polymers endow AgNPs with superior stability and high salt resistance.

Chapter four summarizes the results about this dissertation. Based on the polymer topology effect, this methodology of *c*-PEG toward gold or silver nanoparticles supplies a novel approach for the colloidal stabilization, which is not suitable for other linear counterparts. It provides a new physisorption on the surface modification of nanoparticle without undergoing chemical reactions or chemisorption, retaining the original properties of the metal nanoparticles. The high

stabilization, high dispersion, salt, and heat resistance of *c*-PEG system gives it potential for bio-medicine applications.

1.7 Reference

1. Tezuka, Y., Oike, H. *Prog. Polym. Sci.* 2002, **27**, 1069-1122.
2. Tezuka, Y., Oike, H. *J. Am. Chem. Soc.* 2001, **123**, 11570-11576.
3. Yamamoto, T., Tezuka, Y. *Polym. Chem.* 2011, **2**, 1930-1941.
4. Gao, L. F., Oh, J., Tu, Y. F., Chang, T., Li, C. Y. *Polymer* 2019, **170**, 198-203.
5. Lienard, R., De Winter, J., Coulembier, O. *J. Poly. Sci.* 2020, **58**, 1481-1502.
6. Divandari, M., Trachsel, L., Yan, W., Rosenboom, J.G., Spencer, N. D., Zenobi-Wong, M., Morgese, G., Ramakrishna, S. N., Benetti, E. M. *ACS Macro Lett.* 2018, **7**, 1455-1460.
7. Hoskins, J. N., Grayson, S. M. *Macromolecules* 2009, **42**, 6406-6413.
8. Jeong, Y., Jin, Y., Chang, T., Uhlik, F., Roovers, J. *Macromolecules* 2017, **50**, 7770-7776.
9. Shin, E. J., Jeong, W., Brown, H. A., Koo, B. J., Hedrick, J. L., Waymouth, R. M. *Macromolecules* 2011, **44**, 2773-2779.
10. Lee, C. U., Li, A., Ghale, K., Zhang, D. *Macromolecules* 2013, **46**, 8213-8223.
11. Zhang, K., Lackey, M. A., Cui, J., Tew, G. N. *J. Am. Chem. Soc.* 2011, **133**, 4140-4148.
12. Klein, J. *Macromolecules* 1986, **19**, 105-118.
13. Yamamoto, T. *Polym. J.* 2013, **45**, 711-717.
14. Yamamoto, T., Tezuka, Y. *Soft Matter* 2015, **11**, 7458-7468.
15. Bernander, R. *Mol. Microbiol.* 1998, **29**, 955-961.
16. Jain, S., Caforio, A., Driessen, A. J. M. *Front. Microbiol.* 2014, **5**, 641.
17. Prozorov, A. A. *Microbiology* 2005, **74**, 375-387.
18. Xu, J., Ye, J., Liu, S. *Macromolecules* 2007, **40**, 9103-9110.
19. Dartois, V., Sanchez-Quesada, J., Cabezas, E., Chi, E., Dubbelde, C., Dunn, C., Granja, J., Gritzen, C., Weinberger, D., Ghadiri, M. R., et al. *Antimicrob. Agents Chemother.* 2005, **49**,

3302-3310.

20. Thell, K., Hellinger, R., Sahin, E., Michenthaler, P., Gold-Binder, M., Haider, T., Kuttke, M., Liutkeviciute, Z., Goransson, U., Grundemann, C., et al. *PNAS, Proc. Natl. Acad. Sci. USA* 2016, **113**, 3960-3965.
21. Schlippe, Y. V. G., Hartman, M. C. T., Josephson, K., Szostak, J. W. *J. Am. Chem. Soc.* 2012, **134**, 10469-10477.
22. Ramadhani, D., Maharani, R., Gazzali, A. M., Muchtaridi, M. *Molecules* 2022, **27**, 4428.
23. Bai, C. C., Tian, B. R., Zhao, T., Huang, Q., Wang, Z. Z. *Molecules* 2017, **22**, 1475.
24. Honda, S., Yamamoto, T., Tezuka, Y. *Nat. Commun.* 2013, **4**, 1574.
25. Yu, G. E., Yang, Z., Attwood, D., Price, C., Booth, C. *Macromolecules* 1996, **29**, 8479-8486.
26. Yu, G. E., Zhou, Z. K., Attwood, D., Price, C., Booth, C., Griffiths, P. C., Stilbs, P. *J. Chem. Soc., Faraday Trans.* 1996, **92**, 5021-5028.
27. Yu, G. E., Garrett, C. A., Mai, S. M., Altinok, H., Attwood, D., Price, C., Booth, C. *Langmuir* 1998, **14**, 2278-2285.
28. Honda, S., Yamamoto, T., Tezuka, Y. *J. Am. Chem. Soc.* 2010, **132**, 10251-10253.
29. Baba, E., Yatsunami, T., Yamamoto, T., Tezuka, Y. *Polym. J.* 2015, **47**, 408-412.
30. Córdova, M. E., Lorenzo, A. T., Müller, A. J., Hoskins, J. N., Grayson, S. M. *Macromolecules* 2011, **44**, 1742-1746.
31. Yamamoto, T., Yagyu, S., Tezuka, Y. *J. Am. Chem. Soc.* 2016, **138**, 3904-3911.
32. Mohamed, M., Abu Lila, A. S., Shimizu, T., Alaaeldin, E., Hussein, A., Sarhan, H. A., Szebeni, J., Ishida, T. *Sci. Tech. Adv. Mater.* 2019, **20**, 710-724.
33. Rahme, K., Chen, L., Hobbs, R. G., Morris, M. A., O'Driscoll, C., Holmes, J. D. *RSC Adv.* 2013, **3**, 6085-6094.

34. Pinzaru, I., Coricovac, D., Dehelean, C., Moaca, E. A., Mioc, M., Baderca, F., Sizemore, I., Brittle, S., Marti, D., Calina, C. D., et al. *Food Chem. Toxicol.* 2018, **111**, 546-556.
35. Okyere, D., Manso, R. H., Tong, X., Chen, J. Y. *Coatings* 2022, **12**, 776.
36. D'Souza, A. A., Shegokar, R. *Expert Opin Drug Deliv.* 2016, **13**, 1257-1275.
37. Chung, Y. C., Chen, I. H., Chen, C. J. *Biomaterials* 2008, **29**, 1807-1816.
38. Du, Y., Jin, J., Liang, H., Jiang, W. *Langmuir* 2019, **35**, 8316-8324.
39. Morgese, G., Trachsel, L., Romio, M., Divandari, M., Ramakrishna, S. N., Benetti, E. M. *Angew. Chem., Int. Ed.* 2016, **55**, 15583-15588.
40. Morgese, G., Shaghasemi, B. S., Causin, V., Zenobi-Wong, M., Ramakrishna, S. N., Reimhult, E., Benetti, E. M. *Angew. Chem., Int. Ed.* 2017, **56**, 4507-4511.
41. Freestone, I., Meeks, N., Sax, M., Higgitt, C. *Gold Bull.* 2007, **40**, 270-277.
42. Rahman, M. T., Rebrov, E. V. *Processes* 2014, **2**, 466-493.
43. Duong, V. T. T., Phan, A. D., Lien, N. T. H., Hue, D. T., Hoa, D. Q., Nga, D. T., Nhung, T. H., Viet, N. A. *Phys. Status Solidi A* 2018, **215**, 1700564.
44. Khan, I., Saeed, K. *Arab. J. Chem.* 2019, **12**, 908-931.
45. Sun, H. Y., Jiao, R. Y., An, G. Y., Xu, H., Wang, D. S. *J. Environ. Sci.* 2021, **103**, 33-42.
46. Talamini, L., Violatto, M. B., Cai, Q., Monopoli, M. P., Kantner, K., Krpetic, Z., Perez-Potti, A., Cookman, J., Garry, D., Silveira, C. P., et al. *ACS Nano* 2017, **11**, 5519-5529.
47. Tighe-Neira, R., Carmora, E., Recio, G., Nunes-Nesi, A., Reyes-Diaz, M., Alberdi, M., Rengel, Z., Inostroza-Blancheteau, C. *Plant Physiol. Biochem.* 2018, **130**, 408-417.
48. Ali, M. R. K., Wu, Y., El-Sayed, M. A. *J. Phys. Chem. C* 2019, **123**, 15375-15393.
49. Tabassum, H., Mahmood, A., Zhu, B. J., Liang, Z. B., Zhong, R. Q., Guo, S. J., Zou, R. Q. *Energy Environ. Sci.* 2019, **12**, 2924-2956.

50. Son, D., Bao, Z. A. *ACS Nano* 2018, **12**, 11731-11739.

51. Kelly, K. L., Coronado, E., Zhao, L. L., Schatz, G. C. *J. Phys. Chem. B* 2003, **107**, 668-677.

52. Mitchell, M. J., Billingsley, M. M., Haley, R. M., Wechsler, M. E., Peppas, N. A., Langer, R. *Nat. Rev. Drug Discov.* 2021, **20**, 101-124.

53. Shi, J. J., Kantoff, P. W., Wooster, R., Farokhzad, O. C. *Nat. Rev. Cancer* 2017, **17**, 20-37.

54. Hu, Q. Q., Li, H., Wang, L. H., Gu, H. Z., Fan, C. H. *Chem. Rev.* 2019, **119**, 6459-6506.

55. Astruc, D. *Chem. Rev.* 2020, **120**, 461-463.

56. Pattani, V. P., Tunnell, J. W. *Lasers Surg Med* 2012, **44**, 675-684.

57. Xin, Y. R., Yin, M. M., Zhao, L. Y., Meng, F. L., Luo, L. *Cancer Biol. Med.* 2017, **14**, 228-241.

58. Zhang, J., Wang, L., Zhang, B. S., Zhao, H. S., Kolb, U., Zhu, Y. H., Liu, L. M., Han, Y., Wang, G. X., Wang, C. T., et al. *Nat. Catal.* 2018, **1**, 540-546.

59. Ali, A. I., Salam, B. *Sn Applied. Sci.* 2020, **2**, 1636.

60. Shrestha, S., Wang, B., Dutta, P. *Adv. Colloid Interface Sci.* 2020, **279**, 102162.

61. Steinmetz, L., Geers, C., Balog, S., Bonmarin, M., Rodriguez-Lorenzo, L., Taladriz-Blanco, P., Rothen-Rutishauser, B., Petri-Fink, A. *Nanoscale Adv.* 2020, **2**, 5760-5768.

62. Ament, K., Wagner, D. R., Gotsch, T., Kikuchi, T., Krohnert, J., Trunschke, A., Lunkenbein, T., Sasaki, T., Breu, J. *ACS Catal.* 2021, **11**, 2754-2762.

63. Khodashenas, B., Ghorbani, H. R. *Arab. J. Chem.* 2019, **12**, 1823-1838.

64. Lee, K. S., El-Sayed, M. A. *J. Phys. Chem. B* 2006, **110**, 19220-19225.

65. Yuan, Z. Q., Hu, C. C., Chang, H. T., Lu, C. *Analyst* 2016, **141**, 1611-1626.

66. Sabela, M., Balme, S., Bechelany, M., Janot, J. M., Bisetty, K. *Adv. Eng. Mater.* 2017, **19**, 1700270.

67. Si, P., Razmi, N., Nur, O., Solanki, S., Pandey, C. M., Gupta, R. K., Malhotra, B. D., Willander, M., De la Zerda, A. *Nanoscale Adv.* 2021, **3**, 2679-2698.

68. Vines, J. B., Yoon, J. H., Ryu, N. E., Lim, D. J., Park, H. *Front. Chem.* 2019, **7**, 167.

69. Dreaden, E. C., Alkilany, A. M., Huang, X. H., Murphy, C. J., El-Sayed, M. A. *Chem. Soc. Rev.* 2012, **41**, 2740-2779.

70. Yang, X., Yang, M. X., Pang, B., Vara, M., Xia, Y. N. *Chem. Rev.* 2015, **115**, 10410-10488.

71. Zheng, T. Y., Pierre-Pierre, N., Yan, X., Huo, Q., Almodovar, A. J. O., Valerio, F., Rivera-Ramirez, I., Griffith, E., Decker, D. D., Chen, S. X., et al. *ACS Appl. Mater. Interfaces* 2015, **7**, 6819-6827.

72. Devi, R. S., Girigoswami, A., Siddharth, M., Girigoswami, K. Applications of Gold and Silver Nanoparticles in Theranostics. *Appl. Biochem. Biotechnol.* 2022, **194**, 4187-4219.

73. Jung, J. H., Oh, H. C., Noh, H. S., Ji, J. H., Kim, S. S. *J. Aerosol Sci.* 2006, **37**, 1662-1670.

74. Mahfouz, R., Aires, F., Brenier, A., Jacquier, B., Bertolini, J. C. *Appl. Surf. Sci.* 2008, **254**, 5181-5190.

75. Shirtcliffe, N., Nickel, U., Schneider, S. *J. Colloid Interface Sci.* 1999, **211**, 122-129.

76. Bastus, N. G., Merkoci, F., Piella, J., Puntes, V. *Chem. Mater.* 2014, **26**, 2836-2846.

77. Abou Elmaaty, T., El-Nagare, K., Raouf, S., Abdelfattah, K., El-Kadi, S., Abdelaziz, E. *RSC Adv.* 2018, **8**, 25546-25557.

78. Singh, P., Mijakovic, I. *Sci. Rep.* 2022, **12**, 7902.

79. Ghosh, D., Chattopadhyay, N. *J. Lumin.* 2015, **160**, 223-232.

80. Paidari, S., Ibrahim, S. A. *Gold Bull.* 2021, **54**, 31-36.

81. Alshehri, A. H., Jakubowska, M., Mlozniak, A., Horaczek, M., Rudka, D., Free, C., Carey, J. D. *ACS Appl. Mater. Interfaces* 2012, **4**, 7006-7009.

82. Ibrahim, N., Jamaluddin, N. D., Tan, L. L., Yusof, N. Y. M. *Sensors* 2021, **21**, 5114.

83. Kumar, A., Vemula, P. K., Ajayan, P. M., John, G. *Nat. Mater.* 2008, **7**, 236-241.

84. Heinemann, M. G., Rosa, C. H., Rosa, G. R., Dias, D. *Trends Environ. Anal. Chem.* 2021, **30**, e00129.

85. Yazdani, S., Daneshkhah, A., Diwate, A., Patel, H., Smith, J., Reul, O., Cheng, R. H., Izadian, A., Hajrasouliha, A. R. *ACS Omega* 2021, **6**, 16847-16853.

86. Mott, D., Galkowski, J., Wang, L. Y., Luo, J., Zhong, C. J. *Langmuir* 2007, **23**, 5740-5745.

87. Skandan, G., Chen, Y. J., Glumac, N., Kear, B. H. *Nanostructured Mater.* 1999, **11**, 149-158.

88. Li, S. K., Shen, Y. H., Xie, A. J., Yu, X. R., Qiu, L. G., Zhang, L., Zhang, Q. F. *Green Chem.* 2007, **9**, 852-858.

89. Radziuk, D., Skirtach, A., Sukhorukov, G., Shchukin, D., Möhwald, H. *Macromol. Rapid Commun.* 2007, **28**, 848-855.

90. Dong, H. C., Zhu, M. Z., Yoon, J. A., Gao, H. F., Jin, R. C., Matyjaszewski, K. *J. Am. Chem. Soc.* 2008, **130**, 12852-12853.

91. Zhang, X., Servos, M. R., Liu, J. *J. Am. Chem. Soc.* 2012, **134**, 9910-9913.

92. Pamies, R., Cifre, J. G. H., Espin, V. F., Collado-Gonzalez, M., Banos, F. G. D., de la Torre, J. G. *J. Nanopart. Res.* 2014, **16,** 2376.

93. Fuller, M., Koper, I. *Polymers* 2018, **10**, 1336.

94. Christau, S., Moeller, T., Genzer, J., Koehler, R., von Klitzing, R. *Macromolecules* 2017, **50**, 7333-7343.

95. Shukla, M. K., Singh, R. P., Reddy, C. R. K., Jha, B. *Bioresour. Technol.* 2012, **107**, 295-300.

96. Molleman, B., Hiemstra, T. *Environ. Sci.: Nano* 2017, **4**, 1314-1327.

97. Fernando, I., Zhou, Y. *Chemosphere* 2019, **216**, 297-305.

98. Patungwasa, W., Hodak, J. H. *Mater. Chem. Phys.* 2008, **108**, 45-54.

99. Hussain, I., Brust, M., Papworth, A. J., Cooper, A. I. *Langmuir* 2003, **19**, 4831-4835.

100. Xia, X. H., Yang, M. X., Wang, Y. C., Zheng, Y. Q., Li, Q. G., Chen, J. Y., Xia, Y. N. *ACS Nano* 2012, **6**, 512-522.

101. Li, Y. W., Lin, H. X., Zhou, W. J., Sun, L., Samanta, D., Mirkin, C. A. *Sci. Adv.* 2021, **7**, eabf1410.

102. Suk, J. S., Xu, Q. G., Kim, N., Hanes, J., Ensign, L. M. *Adv. Drug Deliv. Rev.* 2016, **99**, 28-51.

103. Gref, R., Domb, A., Quellec, P., Blunk, T., Muller, R. H., Verbavatz, J. M., Langer, R. *Adv. Drug Deliv. Rev.* 2012, **64**, 316-326.

104. Baptista, P. A., et al., *Int. J. Mol. Sci*. **2017**, *18*, 162.

105. Huang, T., Xu. X. *J. Mater. Chem*., **2010**, *20*, 9867-9876.

Chapter 2

Cyclic Poly(ethylene glycol) : A Dispersion Stabilizer for Gold Nanoparticles by Physisorption

2.1 Introduction

Metal nanoparticles represent a widely interesting group of materials due to their unique properties which differ from their respective bulk state. Presently, metal nanoparticles are used in a wide range of applications which include optics,[1] sensors,[2] biomedicine,[3] electronics,[4] and catalysis.[5] Metal nanoparticles such as gold, silver and copper nanoparticles exhibit surface plasmon resonances (SPR) as a result of their interaction with light which manifests itself in the different colors of the corresponding colloidal solutions depending on the particle size and shape.[6] However, metal nanoparticles are not a stable material and easily aggregate to lose SPR absorption and thus need to be kept as a solution at low temperature. Yet, freezing the solution also causes aggregation and cannot be redispersed. Moreover, the dispersion stability in solution is also affected by various parameters such as salt concentration,[7] temperature,[8] or pH,[9] all of which eventually lead to particle dissolution or aggregation. Hence, metal nanoparticles are often either kept in a citrate solution or reacted with thiolated molecules to gain dispersion stability.[10]

Over the past decades, there have been numerous reports on the dispersion stabilization of gold nanoparticles (AuNPs), the most representative metal nanoparticles, using poly(ethylene glycol) (PEG) as a stabilizer, namely PEGylation.[11] PEG is a neutral water-soluble polymer with a flexible backbone and is well-known for its ability to bind to water through hydrogen bonding.[12] Additionally, PEG is biocompatible and can protect gold surfaces from aggregation in vitro and in vivo as well as from detection by the immune system.[13] When biological applications are considered, the stability against salts in physiological conditions is an indispensable property. The increase in the ionic strength through the addition of a salt or electrolyte reportedly leads to aggregation.[13] Therefore, proper surface modification is essential to avoid aggregation. However, PEGylation, as well as other functionalizations, of AuNPs has been almost limited to

chemisorption by the gold–sulfur reactions, and thus, it is important to establish a new PEGylation methodology for the development of nanoparticle sciences.

Although the stabilization of nanoparticles by a polymer has extensively been explored over the years by tuning various parameters such as molecular weight[14] or composition,[15] very little attention has been paid on the potential contribution of the polymer topology. Over the last decade, numerous articles on the cyclization of various polymers through different routes have been reported which yielded polymers with different topologies.[16, 17] The cyclized polymers exhibited distinct properties compared to their linear counterparts of the same molecular weight such as higher density, higher glass transition temperature, smaller hydrodynamic volume, and lower viscosity.[18, 19] In particular, the dispersion stability exhibited by the cyclic polymers is an interesting feature which could be exploited for the stability of nanoparticles. Thus, micelles composed of cyclized PEG-containing amphiphilic block copolymers feature a higher tolerance towards temperature and salinity compared to their linear counterparts in an aqueous solution was reported, which was proven by turbidity tests and dynamic light scattering.[20-22] Moreover, cyclic polyoxazoline chemisorbed to a titanium oxide surface, Fe_3O_4 nanoparticles, or a degraded cartilage formed a denser layer than the linear counterpart.[23-25]

In this work, the use of PEG as a polymeric stabilizer of AuNPs, where the effects of the polymer topology (linear vs. cyclic) as well as the end groups (–OH vs. –OMe vs. –SH) against freezing, lyophilization, heating, and a physiological condition, is investigated with the above observations in mind (Figure 2.1). In consequence, *c*-PEG endows AuNPs with enhanced dispersion stability was found.

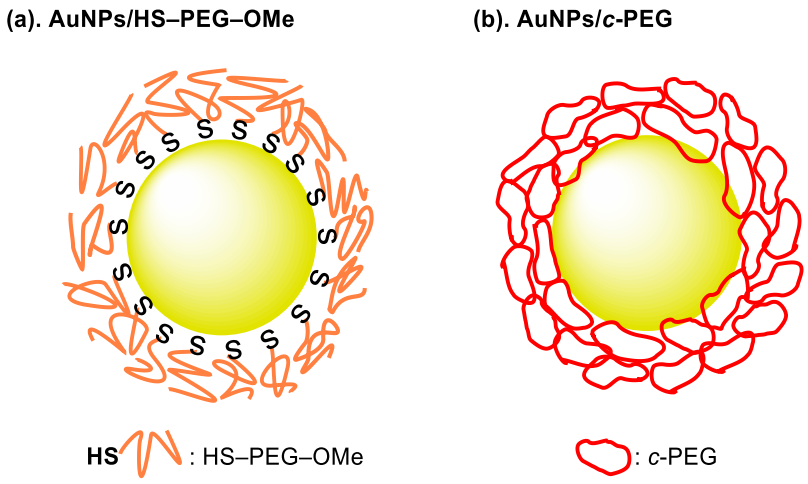

Figure 2.1 Schematic illustrations of PEGylated AuNPs of (a) AuNPs/HS–PEG–OMe and (b) AuNPs/*c*-PEG.

2.2 Experimental section

2.2.1 Materials

Gold nanoparticles (AuNPs) with a diameter of 5, 10, 15, 20, 30, 40, 50, 60, 70, 80, and 100 nm (0.05 mg/mL in aqueous 2 mM sodium citrate, nanoComposix), 4-toluenesulfonyl chloride (TsCl) (>98.0%, Junsei Chemical Co., Ltd.), sodium chloride (NaCl) (>99.0%, Kanto Chemical Co., Inc.), potassium hydroxide (KOH) (>85.5%, Kanto Chemical Co., Inc.), iodomethane (>99.5%, Kanto Chemical Co., Inc.), magnesium sulfate ($MgSO_4$) (>98.0%, Kanto Chemical Co., Inc.), *n*-heptane (>99.0%, Kanto Chemical Co., Inc.), chlorobenzene (>99.0%, Nacalai Tesque, Inc.), 18-crown 6-ether (Tokyo Chemical Industry Co., Ltd.), and dithiolated poly(ethylene glycol) (HS–PEG_{2k}–SH) (Funakoshi Co., Ltd.) were used as received. Tetrahydrofuran (THF), dehydrated stabilizer free (>99.5%, Kanto Chemical Co., Inc.), dichloromethane (CH_2Cl_2) (>99.0%, Kanto Chemical Co., Inc.), and chloroform ($CHCl_3$) (>99.0%, Kanto Chemical Co., Inc.) were purified by a solvent purification system (MBRAUN MB-SPS-Compact). Poly(ethylene glycol) 950–1050 (HO–PEG_{1k}–OH) (Sigma–Aldrich), poly(ethylene glycol) 2,000 (HO–PEG_{3k}–OH) (Sigma–Aldrich), poly(ethylene glycol) 4,000 (HO–PEG_{5k}–OH) (Kanto Chemical Co., Inc.), poly(ethylene glycol) 6,000 (HO–PEG_{10k}–OH) (Kanto Chemical Co., Inc.) were purified by passing through a silica gel column using $CHCl_3$/MeOH (90/10, v/v) as an eluent. Thiolated poly(ethylene glycol) (HS–PEG_{3k}–OMe) (Funakoshi Co., Ltd.) was purified by recycling preparative SEC. The molecular weights of PEG in the catalogues deviated from measurement result, and the measurement values are used in this paper.

2.2.2 NMR

^1H (400 MHz) and ^{13}C NMR (100 MHz) were measured in $CDCl_3$ or D_2O using a JEOL JNM-ESC400 instrument at ambient temperature.

2.2.3 SEC

Size exclusion chromatography (SEC) was performed at 40 °C with THF (flow rate, 1.0 mL/min) using a Shodex GPC-101 gel permeation chromatography system (Shodex DU-2130 dual pump, Shodex RI-71 reflective index detector, and Shodex ERC-3125SN degasser) equipped with a Shodex KF-G guard column (4.6 mm × 10 mm; pore size, 8 μm) and two Shodex KF-804L columns (8 mm × 300 mm) in series. Polystyrene standard samples were used for calibration.

2.2.4 Recycling Preparative SEC

A Japan Analytical Industry LC-908 recycling preparative HPLC system (Hitachi L-7110 pump and JAI RI detector RI-5) was used. JAIGEL-2H and 3H columns and a pre-column were connected in series. $CHCl_3$ was used as the solvent, and the flow rate was set at 3.5 mL/min.

2.2.5 MALDI–TOF MS

Matrix-assisted laser desorption/ionization time-of-flight mass spectrometry (MALDI–TOF MS) was carried out using an ABSCIEX TOF/TOF 5800 mass spectrometer at the Open Facility, Hokkaido University. A PEG sample (1.5 mg/mL, 10 μL) was mixed with a matrix (anthralin, 40 mg/mL, 25 μL) and ionization regent (silver trifluroroacetate, 40 mg/mL, 10 μL), and 0.4 μL of the mixture was drop cast on an Opti-TOF 384-Well Insert (123 × 81 mm) plate.

2.2.6 UV–Vis Spectroscopy

Absorption spectra were measured on a JASCO Ubset V-670 spectrophotometer at 25 °C in deionized water using a micro quartz cell (M25-UV-2, GL Science Inc. Japan).

2.2.7 Synthesis of *c*-PEG

HO–PEG_{1k}–OH, HO–PEG_{3k}–OH, HO–PEG_{5k}–OH, and HO–PEG_{10k}–OH were cyclized according to a previous report by Cooke et al.[26] Typically, HO–PEG_{3k}–OH (5.0 g, 2.5 mmol) and TsCl (0.63 g, 3.3 mmol) were dissolved in a dry THF (100 mL) by using a 300 mL three-neck flask

and added dropwise to a stirring suspension of KOH (3.3 g) in THF/*n*-heptane (75/25, 100 mL) through a syringe pump at 40 °C under Ar. The addition was conducted over 144 h at a rate of 0.7 mL/h. The reaction mixture was stirred for another 24 h at 40 °C. The resulting suspension was filtered and concentrated under reduced pressure. The residue was redissolved in CH_2Cl_2 and washed with a saturated NaCl solution three times. The combined organic phase was dried over $MgSO_4$ and concentrated under reduced pressure, and the residue was passed through a silica gel column using $CHCl_3$/MeOH (90/10 v/v) as an eluent. The obtained solid was dissolved in CH_2Cl_2, and *n*-heptane was added to the solution until becoming cloudy. The mixture was heated to 40 °C and cooled to 25 °C gave two separated phases. The *n*-heptane phase was collected and concentrated under reduced pressure. This step was conducted three more times to isolate *c*-PEG_{3k} (420 mg, 8.4%) as colorless solid.

The expected diameter of *c*-PEG, when the polymer forms an ideal right circular conformation, as well as that of 18-crown-6 ether, was determined by the simple geometric calculation (circumference = π × diameter) based on the length of HO–PEG–OH.

2.2.8 Synthesis of MeO–PEG–OMe

Dimethylation of HO–PEG–OH was performed using a previously reported procedure.[26] For example, a suspension of KOH (6.9 g) in chlorobenzene (60 mL) in a 300 mL three-neck flask was added dropwise to a solution of HO–PEG_{3k}–OH (5.00 g) in chlorobenzene (50 mL), followed by the slow addition of iodomethane (1.05 g) over 50 min under N_2. After the addition was completed, the mixture was stirred at 25 °C for 24 h. The resulting suspension was diluted with CH_2Cl_2 and filtered, and the filtrate was concentrated under reduced pressure. The residue was dissolved in CH_2Cl_2 and washed with a saturated NaCl solution three times, dried over $MgSO_4$, and concentrated under reduced pressure. The residue was dissolved in $CHCl_3$, passed through a

silica gel column using $CHCl_3$/MeOH (90/10 v/v) as an eluent, and concentrated under reduced pressure to give MeO–PEG_{3k}–OMe (3.26 g, 65%) as white solid.

2.2.9 Preparation of AuNPs/HO–PEG–OH, AuNPs/MeO–PEG–OMe, AuNPs/HS–PEG–OMe, AuNPs/HS–PEG–SH, and AuNPs/*c*-PEG

Typically, HO–PEG_{3k}–OH (25 mg) was added to an $AuNPs_{15}$ dispersion (1.0 mL) in a 2.0 mL vial, and PEG was dissolved by vortex mixing for 1 min to form $AuNPs_{15}$/HO–PEG_{3k}–OH with a PEG concentration of 2.5 wt%. The concentration of PEG was controlled by changing the amount of PEG.

2.2.10 Dispersion stability against freezing

$AuNPs_{15}$/No PEG, $AuNPs_{15}$/HO–PEG_{3k}–OH, $AuNPs_{15}$/MeO–PEG_{3k}–OMe, $AuNPs_{15}$/HS–PEG_{3k}–OMe, and $AuNPs_{15}$/*c*-PEG_{3k} (1.0 mL) with a PEG concentration of 2.5 wt% were frozen in a household refrigerator overnight. The frozen samples were melted at ambient temperature.

2.2.11 Dispersion stability against lyophilization

$AuNPs_{15}$/No PEG, $AuNPs_{15}$/HO–PEG_{3k}–OH, $AuNPs_{15}$/MeO–PEG_{3k}–OMe, $AuNPs_{15}$/HS–PEG_{3k}–OMe, and $AuNPs_{15}$/*c*-PEG_{3k} (1.0 mL) with a PEG concentration of 2.5 wt% were frozen in liquid nitrogen for 1 min and lyophilized overnight under reduced pressure. Deionized water (1.0 mL) was added to the residues for redispersion.

2.2.12 Dispersion stability against heating

$AuNPs_{15}$/No PEG, $AuNPs_{15}$/HO–PEG_{3k}–OH, $AuNPs_{15}$/MeO–PEG_{3k}–OMe, $AuNPs_{15}$/HS–PEG_{3k}–OMe, and $AuNPs_{15}$/*c*-PEG_{3k} (1.0 mL) with a PEG concentration of 0.25 wt% were placed in a 15 mL vial with a lid to enclose air and prevent evaporation of water and heated for 4 h in a water bath set at 85 °C. Likewise, $AuNPs_{15}$/HS–PEG_{3k}–OMe, $AuNPs_{15}$/HS–PEG_{2k}–SH, and $AuNPs_{15}$/*c*-PEG_{3k} (1.0 mL) with a PEG concentration of 0.25 wt% were placed in a 15 mL vial

with a lid and heated for 48 h in a water bath set at 85 °C. Similarly, the heating test of $AuNPs_{30}$/MeO–PEG_{3k}–OMe/*c*-PEG_{3k} and $AuNPs_{30}$/HS–PEG_{3k}–OMe/*c*-PEG_{3k} was performed. Typically, MeO–PEG_{3k}–OMe (2.25 mg, 0.225 wt%) and *c*-PEG_{3k} (0.25 mg, 0.025 wt%) were dissolved in $AuNPs_{30}$ dispersion (1.0 mL). The total PEG concentration was 0.25 wt%. The resulting dispersion was placed in a 15 mL vial with a lid and heated for 4 h in a water bath set at 85 °C. Photographs and UV–Vis spectra were recorded at the designated times.

2.2.13 Dispersion stability against a PBS buffer solution

A tenfold-concentrated phosphate-buffered saline (PBS) solution (pH 7.4, NaCl 1500 mM, Na_2HPO_4 81 mM, NaH_2PO_4 14.7 mM) was prepared in advance. Typically, $AuNPs_{15}$/No PEG, $AuNPs_{15}$/HO–PEG_{3k}–OH, $AuNPs_{15}$/MeO–PEG_{3k}–OMe, $AuNPs_{15}$/HS–PEG_{3k}–OMe, or $AuNPs_{15}$/*c*-PEG_{3k} (0.54 mL) was placed in a micro quartz cuvette to measure an absorption spectrum. Subsequently, the tenfold-concentrated PBS solution (0.06 mL) was added to the cuvette, and the resulting mixture was 0.6 mL with pH 7.4 and 150 mM of NaCl with a PEG concentration of 0.25 wt%. A time-course UV–Vis measurement was performed for 1000 min. For the long-term stability test, $AuNPs_{15}$/*c*-PEG_{3k} was kept at 37 °C for 14 d after the addition of the tenfold-concentrated PBS solution.

2.2.14 Stabilization of AuNPs with various diameters

c-PEG_{3k} (1.5 mg) was added to an AuNPs dispersion (0.54 mL) with a diameter of 5, 10, 15, 20, 30, 40, 50, 60, 70, 80, or 100 nm in a 2 mL vial and dissolved by vortex mixing for 1 min. Subsequently, the tenfold-concentrated PBS solution (0.06 mL) was added to AuNPs/*c*-PEG, and the resulting mixture was 0.6 mL with pH 7.4 and 150 mM of NaCl with a PEG concentration of 0.25 wt%. A time-course UV–Vis measurement was performed for 850 min.

2.2.15 PEG concentration-dependent stabilization of AuNPs

The tenfold-concentrated PBS solution (0.06 mL) was added to $AuNPs_5$/HO–PEG_{5k}–OH (0.54 mL) or $AuNPs_5$/*c*-PEG_{5k} (0.54 mL), and the resulting mixture was 0.6 mL with pH 7.4 and 150 mM of NaCl with a PEG concentration of 0.25, 2.5, or 10 wt% for $AuNPs_5$/HO–PEG_{5k}–OH or 0.025, 0.25, or 2.5 wt% for $AuNPs_5$/*c*-PEG_{5k}. A time-course UV–Vis measurement was performed for 1000 min.

2.2.16 DLS and ζ-potential

Zetasizer Nano ZS (Malvern Panalytical Ltd.) with a high precision micro quartz cuvette (ZEN2112, Hellma Analytics) and Zetasizer nano cells (DTS1060, Malvern Instruments Ltd.) were used to measure the diameter and ζ-potential, respectively. All measurements were performed at 25 °C with 20 scans at most with a 120 s equilibration time.

2.2.17 FT-IR

2.0 mL of $AuNPs_{15}$/No PEG (0.25 wt%), $AuNPs_{15}$/MeO–PEG_{3k}–OMe (0.25 wt%), or $AuNPs_{15}$/*c*-PEG_{3k} (0.25 wt%) was ultrafiltrated at 4,700 g for 20 min using an Amicon Ultra – 2mL centrifugal filter Ultracel – 30K twice. Deionized water was added to a total volume of 2.0 mL, and the dispersion was frozen in liquid nitrogen for 1 min and lyophilized overnight under reduced pressure. The FT-IR spectrum of the lyophilized sample was measured using a PerkinElmer Frontier MIR spectrometer equipped with a single reflection diamond universal attenuated total reflection (ATR) accessory.

2.2.18 Cell lines and animals

C26 cells (supplied by the National Cancer Center, Tokyo, Japan) were cultured with Dulbecco's Modified Eagle's Medium (high glucose, Sigma-Aldrich, D6429) plus 10% fetal bovine serum (FBS, Dainippon Sumitomo Pharma Co., Ltd.). BALB/c female mice, 6-weeks (18–

21 g) were obtained from Oriental Yeast Co., Ltd. (Tokyo, Japan) and were allowed to acclimatize for 5 days before inoculation of tumors. Animals were kept in a temperature-controlled room on 12 h / 12 h light / dark schedule at 22 ºC with food and water ad libitum. A suspension of C26 cells (1.0×10^6 cells/100 μL in PBS) was subcutaneously implanted into BALB/c female mice. Tumor growth was measured by calipebio Ar measurement and tumor volumes were calculated by the following equation: $V = (a \times b^2)/2$, where a refers to the tumor width (mm) and b refers to the tumor length (mm). Fourteen-days post-inoculation, the size tumors were reached to 50 mm^3, animals were separated into n = 3 per group and for treatment with: $AuNPs_5$/No PEG, $AuNPs_5$/MeO–PEG_{3k}–OMe, and $AuNPs_5$/*c*-PEG_{3k} (dose = 5 mg/kg on a gold basis). The mice were sacrificed 10 and 60 min after i.v, injection. The tumors were excised, washed with PBS and weighed after removing excess fluid. Blood was collected from the inferior vena cava, heparinized, and centrifuged to obtain the plasma. Acid digestion of all samples was carried out using ca. 5.0 mL of 30% HNO_3/35% HCl mixture. Obtained samples were dissolved in 3 vol% HNO_3 aq. (10 mL) and were filtered by PTFE membrane. Gold concentration was measured by inductivity coupled plasma optical emission spectrometer with yttrium as internal standard. All animal experiments were performed in accordance with the Guidelines for the Care and Use of Laboratory Animals as stated by The University of Tokyo, Tokyo Institute of Technology, and Hokkaido University.

2.3 Results and Discussion

2.3.1 Synthesis of *c*-PEG

PEG was cyclized via etherification, thus forming cyclic PEG (*c*-PEG) without inhomogeneity in the chemical structure, by using the modified tosylation method according to previous reports.[26, 27] The molecular weight was 1, 3, 5, and 10 kDa (namely, *c*-PEG_{1k}, *c*-PEG_{3k},

c-PEG_{5k}, and *c*-PEG_{10k}, respectively, shown in Table 2.1). The expected diameter of *c*-PEG_{1k}, *c*-PEG_{3k}, *c*-PEG_{5k}, and *c*-PEG_{10k} was 2.2, 7.4, 14, and 28 nm, respectively, when they form an ideal right circular conformation. The shift in the size exclusion chromatography (SEC) traces confirms the change in the polymer topology as a result of the decrease in the hydrodynamic volume upon cyclization (Figure 2.2). For example, peak top molecular weight ($M_{p,SEC}$) of PEG_{3k} decreased from 3,100 to 2,090 upon cyclization. The small values of polydispersity index (M_w/M_n), except for PEG_{1k}, allowed for clear discussion on the molecular-weight dependence.

Table 2.1 Properties of PEG by SEC

Polymer	$M_{n,SEC}$[a] (g mol^{-1})	$M_{p,SEC}$[a] (g mol^{-1})	M_w/M_n	Ideal diameter of *c*-PEG (nm)
HO–PEG$_{1k}$–OH	860	1220	1.35	-
c-PEG$_{1k}$	430	520	1.38	2.2
HO–PEG$_{3k}$–OH	2890	3100	1.06	-
MeO–PEG$_{3k}$–OMe	2990	3110	1.06	-
HS–PEG$_{3k}$–OMe	2500	2540	1.07	-
HS–PEG$_{2k}$–SH	2220	2500	1.08	
c-PEG$_{3k}$	1910	2090	1.07	7.4
HO–PEG$_{5k}$–OH	5450	5480	1.03	-
MeO–PEG$_{5k}$–OMe	5460	5480	1.03	-
c-PEG$_{5k}$	3750	3860	1.05	14
HO–PEG$_{10k}$–OH	10800	11060	1.01	-
MeO–PEG$_{10k}$–OMe	11760	12140	1.01	-
c-PEG$_{10k}$	8500	8810	1.02	28

[a]Determined by SEC in THF using polystyrene standards.

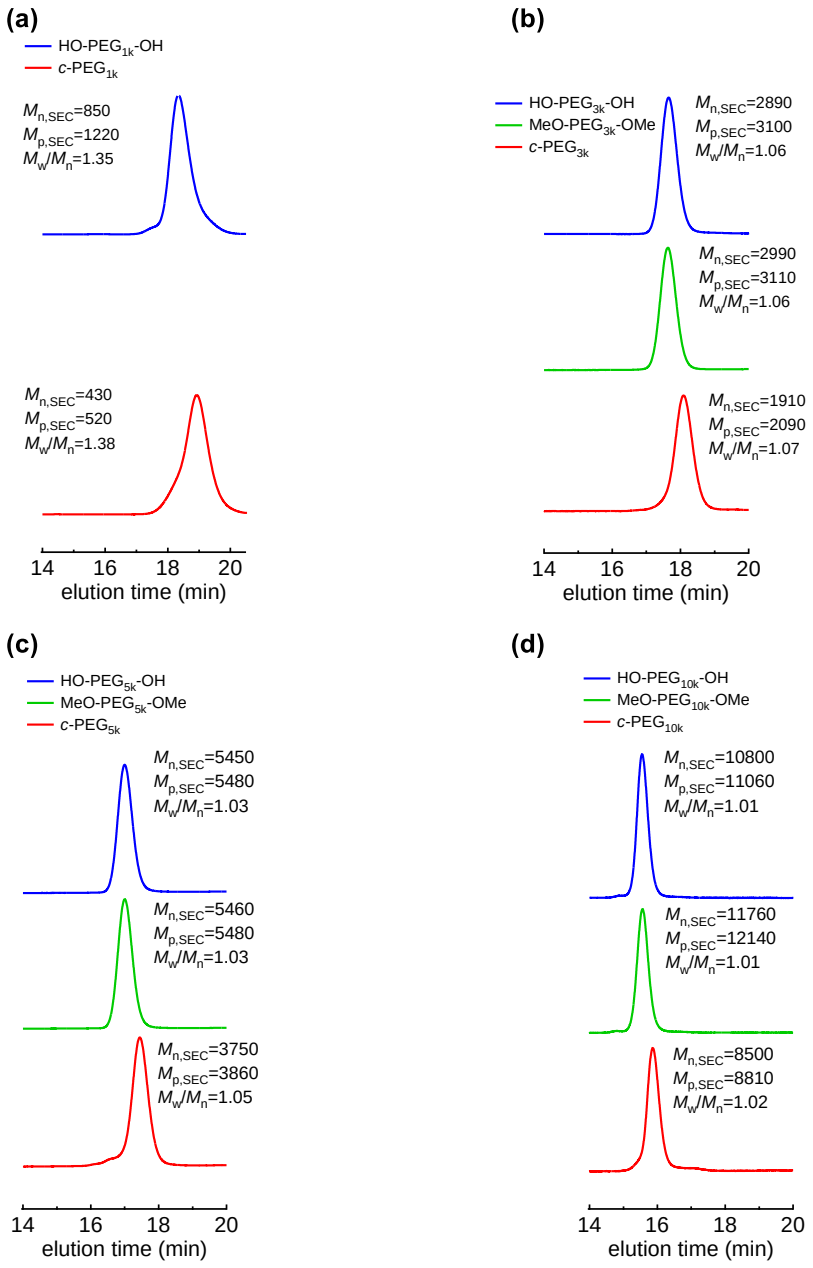

Figure 2.2 SEC traces of HO–PEG–OH (blue), MeO–PEG–OMe (green) and *c*-PEG (red) with a molecular weight of (a) 1, (b) 3, (c) 5 and (c) 10 kDa.

In the ^{13}C NMR spectra, the peak at 61.8 ppm and 72.5 ppm observed for the carbon atoms adjacent to the terminal hydroxy groups in HO–PEG–OH vanished upon cyclization thus confirming the effective elimination of the end groups (Figure 2.3).

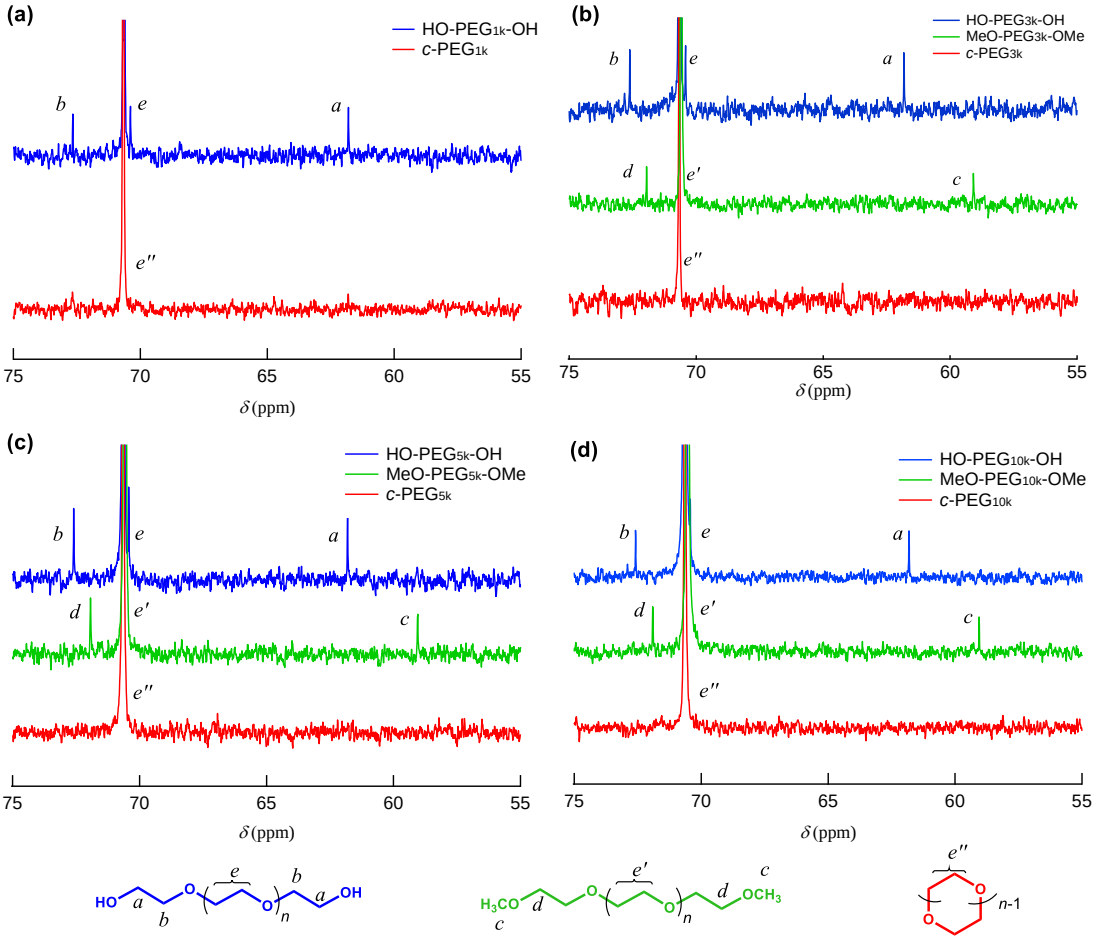

Figure 2.3 ^{13}C NMR spectra of HO–PEG–OH (blue), MeO–PEG–OMe (green), and *c*-PEG (red) with a molecular weight of (a) 1, (b) 3, (c) 5, and (c) 10 kDa.

^{1}H NMR also showed the high symmetry of *c*-PEG by the single peak of the methylene protons (Figure 2.4). MeO–PEG–OMe was synthesized from HO–PEG–OH with iodomethane under an alkaline condition.

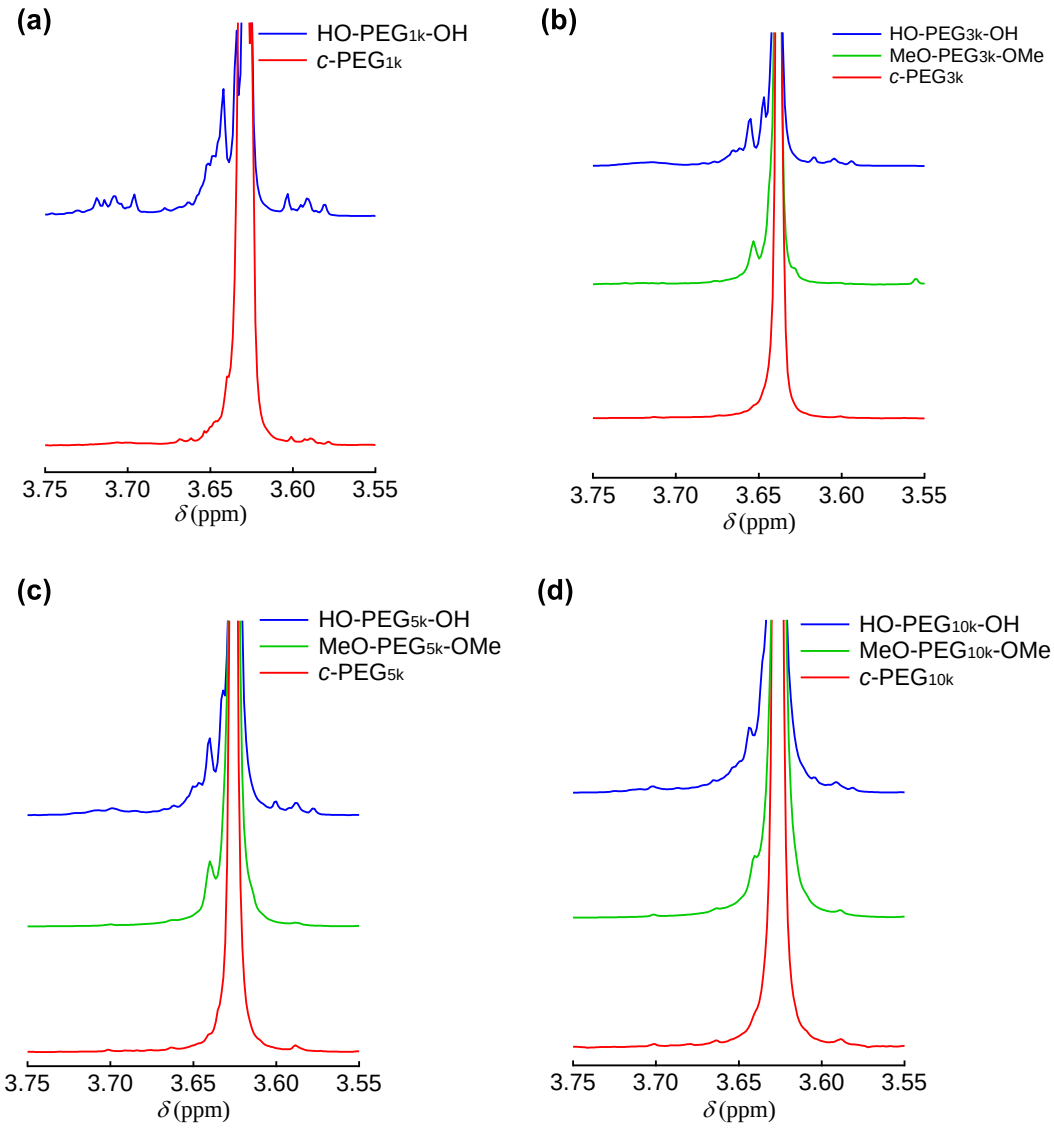

Figure 2.4 ^{1}H NMR spectra of HO–PEG–OH (blue), MeO–PEG–OMe (green), and *c*-PEG (red) with a molecular weight of (a) 1, (b) 3, (c) 5, and (c) 10 kDa.

Furthermore, matrix-assisted laser desorption ionization time-of-flight (MALDI-TOF) mass spectrometry also featured the difference between the linear and cyclic polymer species. For instance, the MALDI-TOF mass spectrum of HO–PEG_{3k}–OH showed a peak at m/z = 2062.10 (DP_n = 44, Ag^+ adduct), whereas the corresponding peak from *c*-PEG was at m/z = 2044.02; the value in the isotope distribution shifted by a mass unit of 18 due to the net elimination of a water molecule upon cyclization (Figure 2.5). The experimental m/z values for the monoisotopic mass of *c*-PEG_{3k} well matched to the calculated values for its molecular weight distribution range.

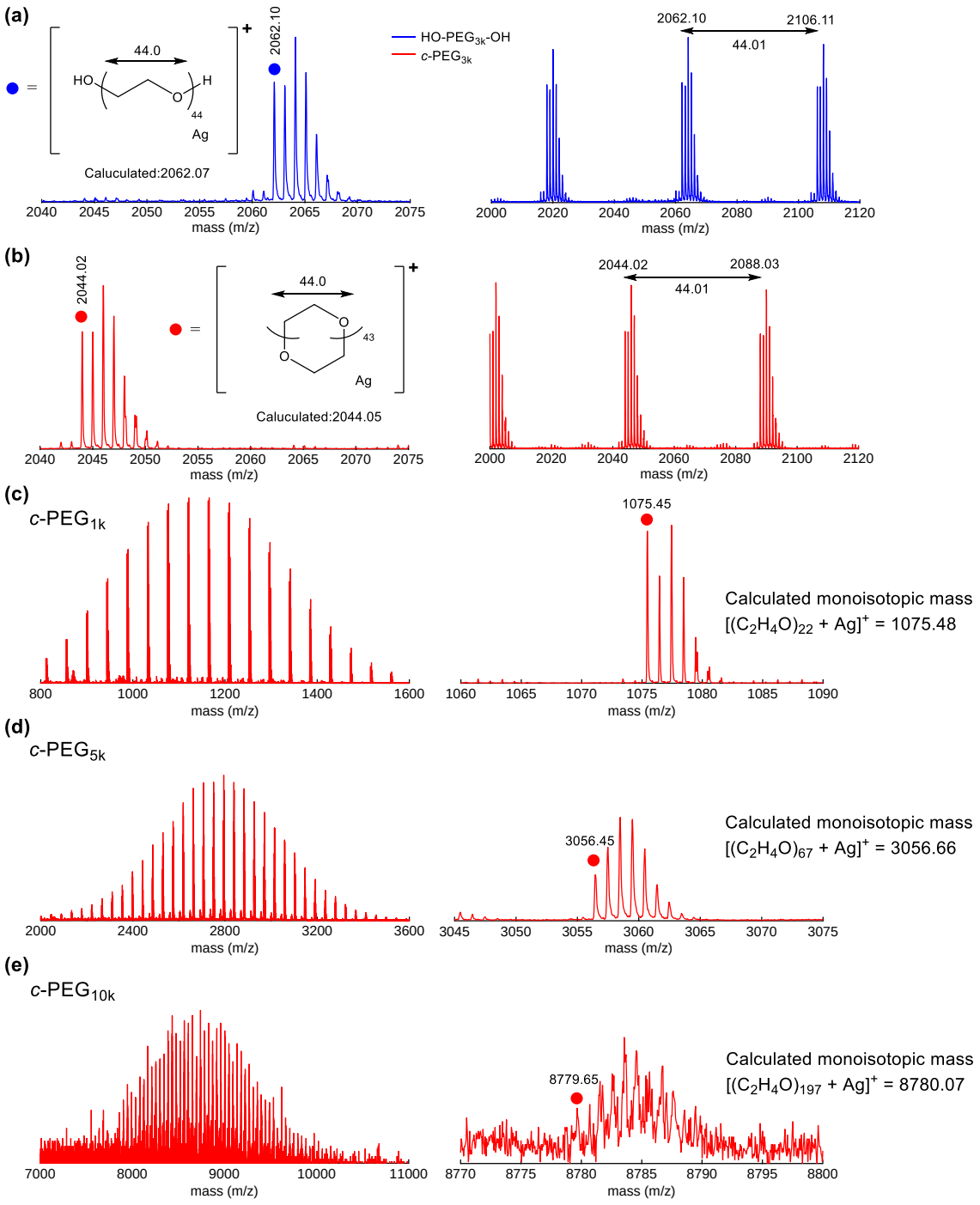

Figure 2.5 MALDI-TOF mass spectra of (a) HO–PEG–OH (blue), and (b) *c*-PEG (red) with a molecular weight of 3 kDa as well as (c) *c*-PEG_{1k}, (d) *c*-PEG_{5k}, and (e) *c*-PEG_{10k}. Calculated monoisotopic mass and experimental *m*/*z* values of typical peaks are shown.

Essentially, no absorption from purified PEG was confirmed by UV–Vis spectroscopy, allowing for the clear observation of the SPR absorption of AuNPs. The comparison of highly pure *c*-PEG with HO–PEG–OH and MeO–PEG–OMe, along with HS–PEG–OMe and HS–PEG–SH, allowed for the stringent evaluation of the effects from the topology and the end groups.

2.3.2 Dispersion stability against freezing

Based on the enhanced stability of the micelles form the cyclic block copolymers,[20-22] *c*-PEG for the dispersion stabilization of AuNPs in comparison with the linear counterparts was tested, finding significantly enhanced stability against temperature and change in the phase. Thus, HO–PEG_{3k}–OH, MeO–PEG_{3k}–OMe, HS–PEG_{3k}–OMe, or *c*-PEG_{3k} was added to a commercially available aqueous dispersion of AuNPs with 15 nm in diameter ($AuNPs_{15}$). By mixing AuNPs with these polymers, no change in the red colour by the SPR absorption was observed. UV–Vis spectroscopy showed similar spectra to those before mixing with PEG, and λ_{max} remained at around 520 nm (Figure 2.6).

Upon freezing in a household refrigerator, $AuNPs_{15}$ without PEG ($AuNPs_{15}$/No PEG) become nearly colorless due to aggregation[13] and etching by dissolved oxygen (Figure 2.7a).[28]

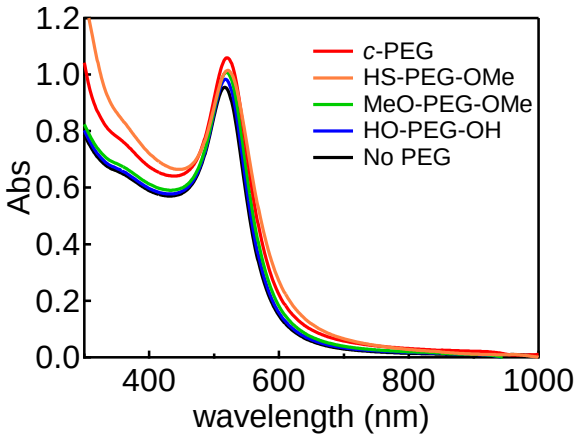

Figure 2.6 UV–Vis spectra before freezing and lyophilization. $AuNPs_{15}$/No PEG (black), $AuNPs_{15}$/HO–PEG_{3k}–OH (blue), $AuNPs_{15}$/MeO–PEG_{3k}–OMe (green), $AuNPs_{15}$/HS–PEG_{3k}–OMe (orange), and $AuNPs_{15}$/*c*-PEG_{3k} (red).

When $AuNPs_{15}$ with HO–PEG_{3k}–OH ($AuNPs_{15}$/HO–PEG_{3k}–OH) and with MeO–PEG_{3k}–OMe ($AuNPs_{15}$/MeO–PEG_{3k}–OMe) were frozen, the red colour of AuNPs disappeared and became grayish blue. After melting, UV–Vis spectra were recorded showing a strong bathochromic shift

in λ_{max} (AuNPs$_{15}$/HO–PEG$_{3k}$–OH, 667 nm; AuNPs$_{15}$/MeO–PEG$_{3k}$–OMe, 687 nm), suggesting aggregation of AuNPs. The relative absorption intensity (Rel. Abs) compared to that before freezing was 26% or less for these three specimens listed in Table 2.2. In contrast, the red colour of AuNPs$_{15}$/HS–PEG$_{3k}$–OMe (Rel. Abs = 92%) and AuNPs$_{15}$/*c*-PEG$_{3k}$ (Rel. Abs = 97%) persisted after melting with an unnoticeable change, and UV–Vis showed nearly identical spectra to those before freezing, demonstrating that the PEGylation by the two methods provide dispersibility through the frozen state.

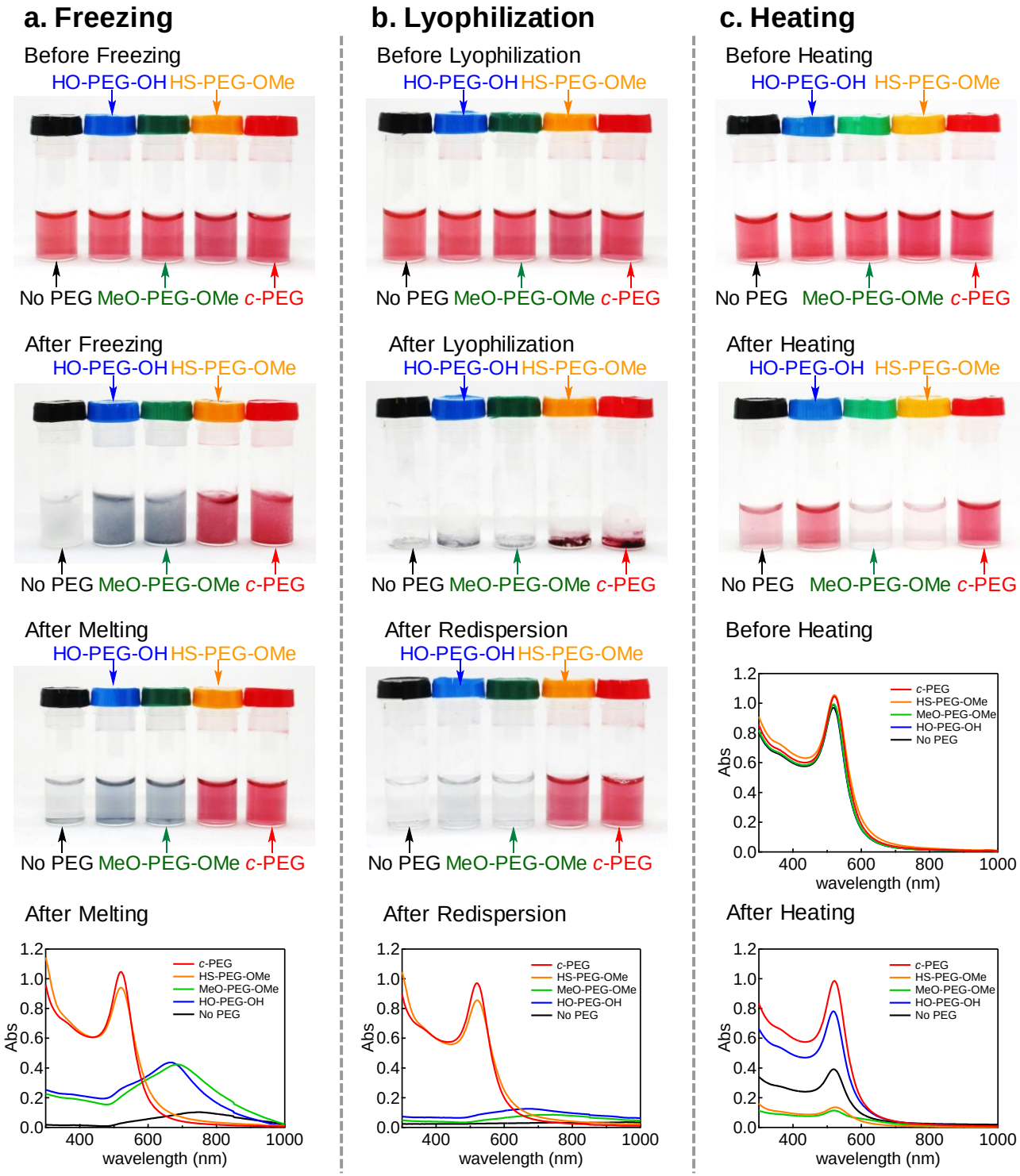

Figure 2.7 Freezing, lyophilization, and heating tests. Photographs and UV–Vis spectra of $AuNPs_{15}$/No PEG (black), $AuNPs_{15}$/HO–PEG_{3k}–OH (blue), $AuNPs_{15}$/MeO–PEG_{3k}–OMe (green), $AuNPs_{15}$/HS–PEG_{3k}–OMe (orange), and $AuNPs_{15}$/*c*-PEG_{3k} (red). (a) Freezing test using a household refrigerator. From top to bottom, photographs before freezing, after freezing, after melting, and a UV–Vis spectrum after melting. (b) Lyophilization test using liquid N_2. From top to bottom, photographs before freezing, after lyophilization, after redispersion, and a UV–Vis spectrum after redispersion. (c) Heating test at 85 °C for 4 h. From top to bottom, photographs before and after heating and UV–Vis spectra before and after heating.

Table 2.2 Relative absorption intensity (Rel. Abs) of $AuNPs_{15}/PEG_{3k}$ in freezing, lyophilization, heating, and physiological condition tests.

Test	No PEG	HO–PEG–OH	MeO–PEG–OMe	HS–PEG–OMe	*c*-PEG
Freezing	3%	26%	21%	92%	97%
Lyophilization	3%	9%	5%	84%	91%
Heating	39%	78%	12%	13%	95%
Physiological condition	1%	1%	2%	83%	88%

Rel. Abs was calculated by dividing the absorption value at λ_{max} after the tests by that before the tests.

2.3.3 Dispersion stability against lyophilization

Based on the above results, the effects of lyophilization of the dispersions were evaluated (Figure 2.7b). In this experiment, the dispersions were frozen in liquid nitrogen, and the solvent was sublimed under reduced pressure. Dried $AuNPs_{15}$/HS–PEG_{3k}–OMe and $AuNPs_{15}$/*c*-PEG_{3k} kept the red colour, suggesting that AuNPs did not aggregate even in the solid state likely by the respective PEG molecules penetrate among AuNPs. Upon addition of water, $AuNPs_{15}$/HS–PEG_{3k}–OMe (Rel. Abs = 84%) and $AuNPs_{15}$/*c*-PEG_{3k} (Rel. Abs = 91%) gave a redispersion with good restoration of the original spectra. On the other hand, $AuNPs_{15}$/No PEG, $AuNPs_{15}$/HO–PEG_{3k}–OH, and $AuNPs_{15}$/MeO–PEG_{3k}–OMe formed grayish blue solid, and redispersion was not possible (Rel. Abs ≤ 9%). These experiments indicate that the physisorption of *c*-PEG can endow AuNPs with dispersion stability against freezing and lyophilization as good as the chemisorption of HS–PEG–OMe.

2.3.4 Dispersion stability against heating

Furthermore, $AuNPs_{15}$/No PEG, $AuNPs_{15}$/HO–PEG_{3k}–OH, $AuNPs_{15}$/MeO–PEG_{3k}–OMe, $AuNPs_{15}$/HS–PEG_{3k}–OMe, and $AuNPs_{15}$/*c*-PEG_{3k} were heated at 85 °C for 4 h to determine the

thermal stability. Most of the nanoparticles in $AuNPs_{15}$/MeO–PEG_{3k}–OMe (Rel. Abs = 12%) and $AuNPs_{15}$/HS–PEG_{3k}–OMe (Rel. Abs = 13%) aggregated to deposit or etched by dissolved oxygen to give almost colourless liquid (Figure 2.7c).[28] $AuNPs_{15}$/No PEG (Rel. Abs = 39%) and $AuNPs_{15}$/HO–PEG_{3k}–OH (Rel. Abs = 78%) showed some degree of retention of the red colour but less intense than those before heating. Interestingly, the colour and UV–Vis spectrum of $AuNPs_{15}$/*c*-PEG_{3k} were nearly intact (Rel. Abs = 95%), suggesting excellent dispersion stability against heating.

In order to determine the cause of the relatively poor protection by HS–PEG_{3k}–OMe against heating, ^{1}H NMR was used to find that the thiol group turned into disulfide (–C*H*$_2$–S–S–C*H*$_2$–, 2.91 ppm) (Figure 2.8). ^{13}C NMR before and after heating also suggests the formation of disulfide (Figure 2.9). It is known that the bonding of Au and HS–PEG is dynamic,[29] and at high temperature, HS–PEG_{3k}–OMe is liberated from the surface of AuNPs and oxidized to form disulfide (MeO–PEG_{3k}–S–S–PEG_{3k}–OMe) was expected. Once disulfide is formed, the affinity to Au becomes much smaller than that of thiol,[30] leading to the less shielding on AuNPs. In the meantime, HO–PEG_{3k}–OH showed moderate dispersion stability most likely by the effects of the hydroxy chain end groups.

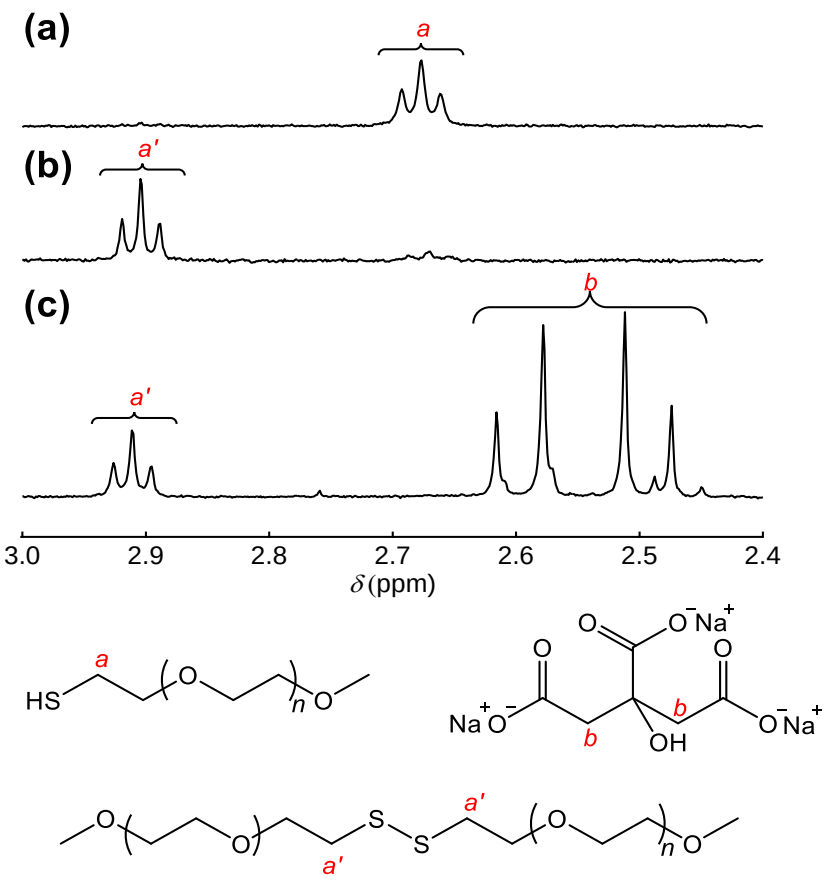

Figure 2.8 Formation of disulfide by heating. ^{1}H NMR spectra of (a) HS–PEG$_{3k}$–OMe, (b) MeO–PEG$_{3k}$–S–S–PEG$_{3k}$–OMe, and (c) AuNPs$_{15}$/HS–PEG$_{3k}$–OMe after heating at 85 °C for 4 h followed by exchange of the solvent to D_2O.

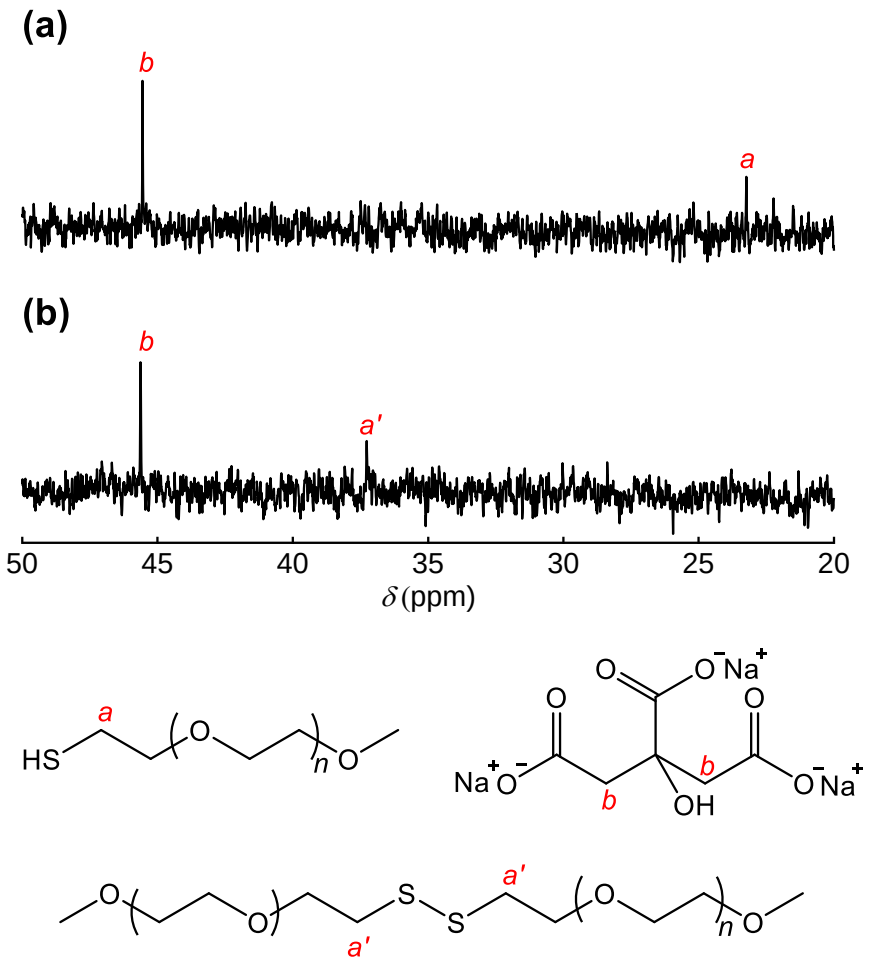

Figure 2.9 Formation of disulfide by heating. ^{13}C NMR spectra of $AuNPs_{15}$/HS–PEG_{3k}–OMe (a) before and (b) after heating at 85 °C for 4 h.

Furthermore, AuNPs$_{15}$/HS–PEG$_{2k}$–SH was also tested against heating at 85 °C, where the polymers are anchored to the surface at both chain ends (Figure 2.10).[31, 32] After 48 h, Rel. Abs was only 2% for AuNPs$_{15}$/HS–PEG$_{3k}$–OMe, 64% for AuNPs$_{15}$/HS–PEG$_{2k}$–SH, and 75% for AuNPs$_{15}$/*c*-PEG$_{3k}$. Both AuNPs$_{15}$/HS–PEG$_{2k}$–SH and AuNPs$_{15}$/*c*-PEG$_{3k}$ showed good long-term stability at high temperature. The high stability of AuNPs$_{15}$/HS–PEG$_{2k}$–SH was likely caused by that even when one chain end of HS–PEG–SH is liberated from the surface of AuNPs by heating, the polymer is held by other chain end, preventing the complete removal from AuNPs. In any case, *c*-PEG$_{3k}$ gave the best result. All of the above experiments suggest that *c*-PEG endows AuNPs with significant dispersion stability against freezing, lyophilization, and heating.

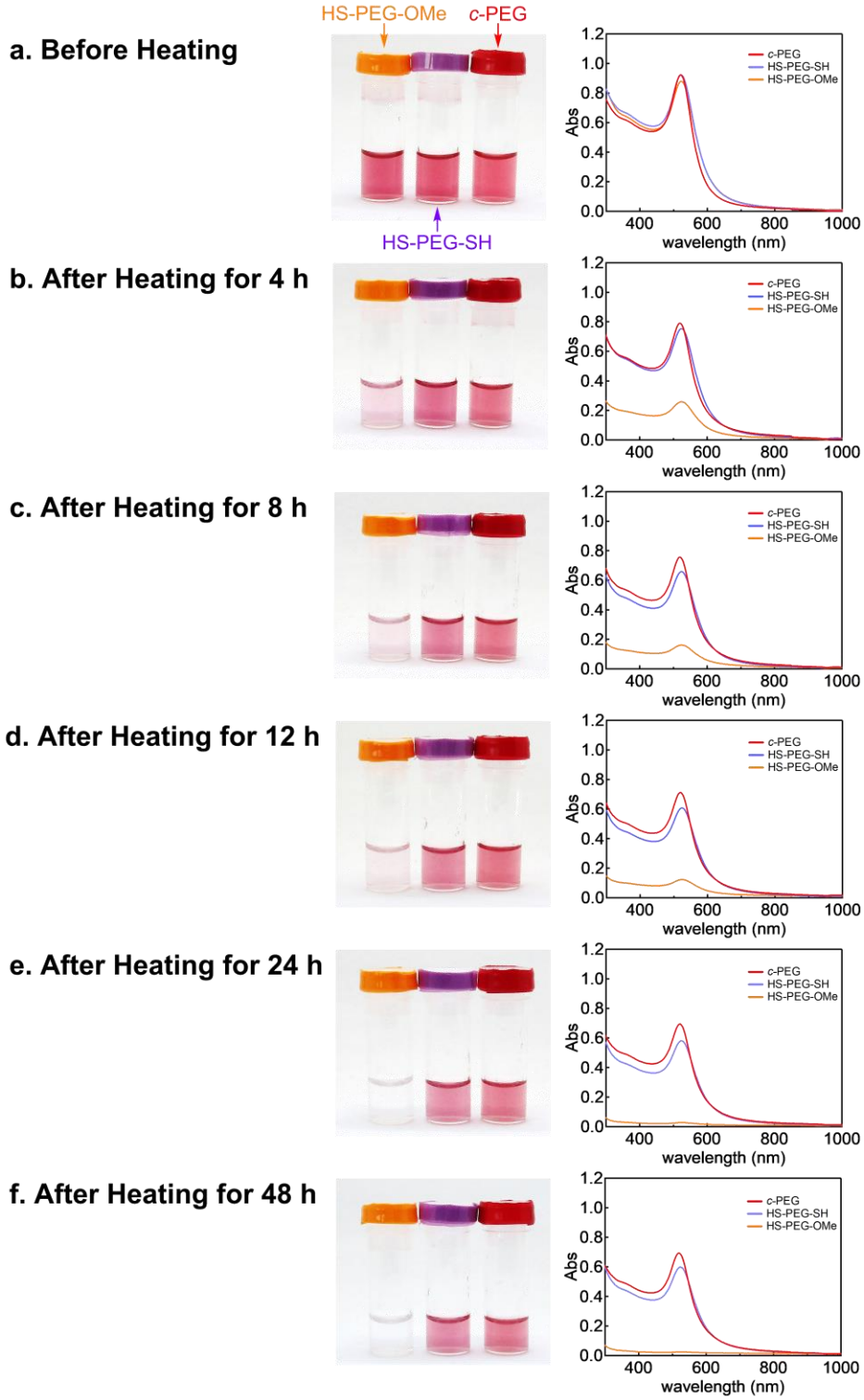

Figure 2.10 Time course heating test. Photographs and UV–Vis spectra of $AuNPs_{15}$/HS–PEG_{3k}–OMe (orange), $AuNPs_{15}$/HS–PEG_{2k}–SH (purple), and $AuNPs_{15}$/*c*-PEG_{3k} (red). (a) Before heating and after heating for (b) 4, (c) 8, (d) 12, (e) 24 , and (f) 48 h at 85 °C. Rel. Abs was 2% for $AuNPs_{15}$/HS–PEG_{3k}–OMe, 64% for $AuNPs_{15}$/HS–PEG_{2k}–SH, and 75% for $AuNPs_{15}$/*c*-PEG_{3k} after 48h.

In addition, mixtures of *c*-PEG with MeO–PEG–OMe or HS–PEG–OMe were tested against heating. Thus, MeO–PEG_{3k}–OMe (0.225, 0.125, or 0.025 wt%) and *c*-PEG_{3k} (0.025, 0.125, or 0.225 wt%, respectively) were added to $AuNPs_{30}$ to form $AuNPs_{30}$/MeO–PEG_{3k}–OMe/*c*-PEG_{3k} with a total PEG concertation of 0.25 wt%. The mixtures were heated at 85 °C for 4 h, resulting in an increase of Rel. Abs with the proportion of *c*-PEG (Rel. Abs = 67, 76, or 81%, respectively) shown in Figure 2.11. When HS–PEG_{3k}–OMe (0.225, 0.125, or 0.025 wt%) and *c*-PEG_{3k} (0.025, 0.125, or 0.225 wt%, respectively) were used, Rel. Abs significantly decreased even for the lowest concentration of HS–PEG_{3k}–OMe (Rel. Abs = 17, 17, or 46%, respectively) shown in Figure 2.12. This indicates that the presence of thiol and/or disulfide at high temperature stimulates the dissolution of AuNPs, and thus HS–PEG–OMe is not a proper capping agent against heating.

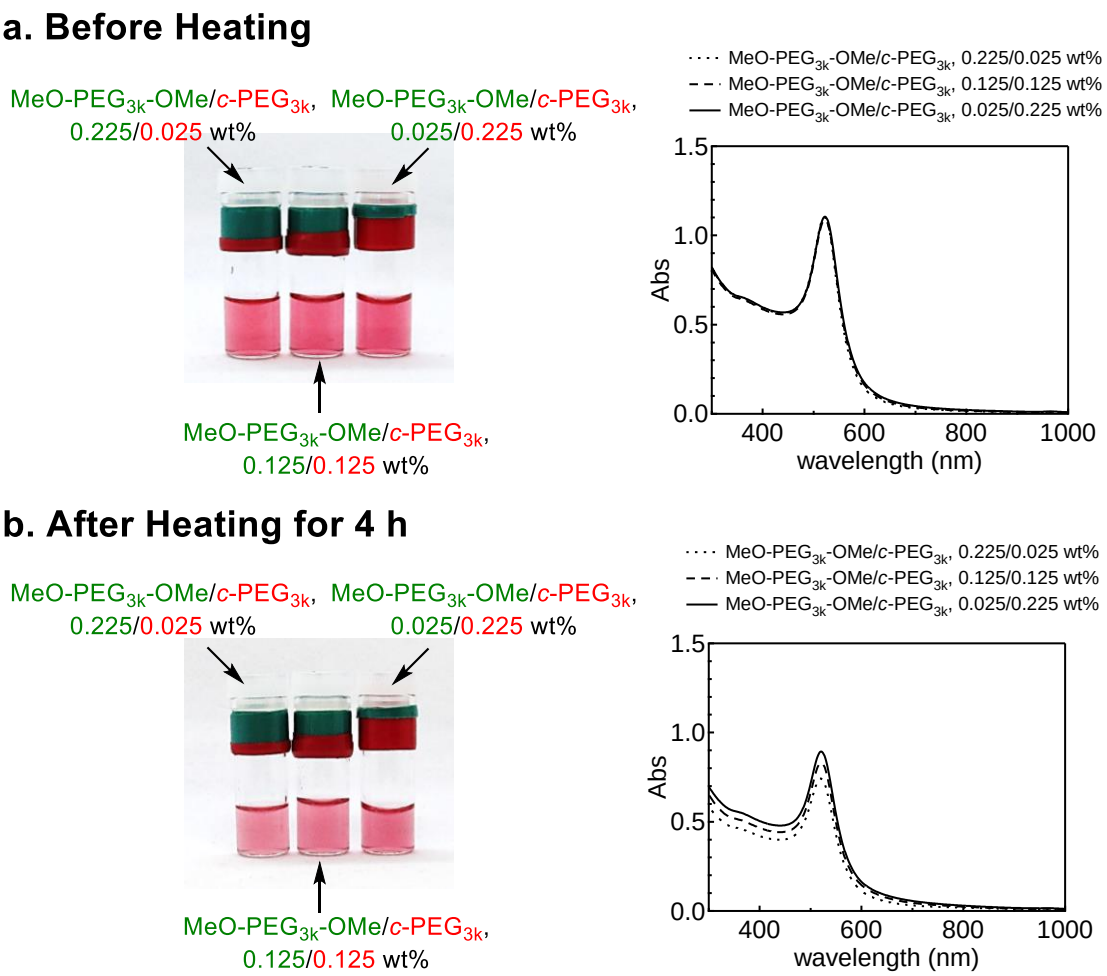

Figure 2.11 Heating test. Photographs and UV–Vis spectra of $AuNPs_{30}$/MeO–PEG_{3k}–OMe/*c*-PEG_{3k}. a Before heating and b after heating for 4 h at 85 °C. From left to right in each photograph, the concentrations of MeO–PEG_{3k}–OMe/*c*-PEG_{3k} were 0.225/0.025, 0.125/0.125, and 0.025/0.225 wt%. Rel. Abs was 67, 76, or 81%, respectively.

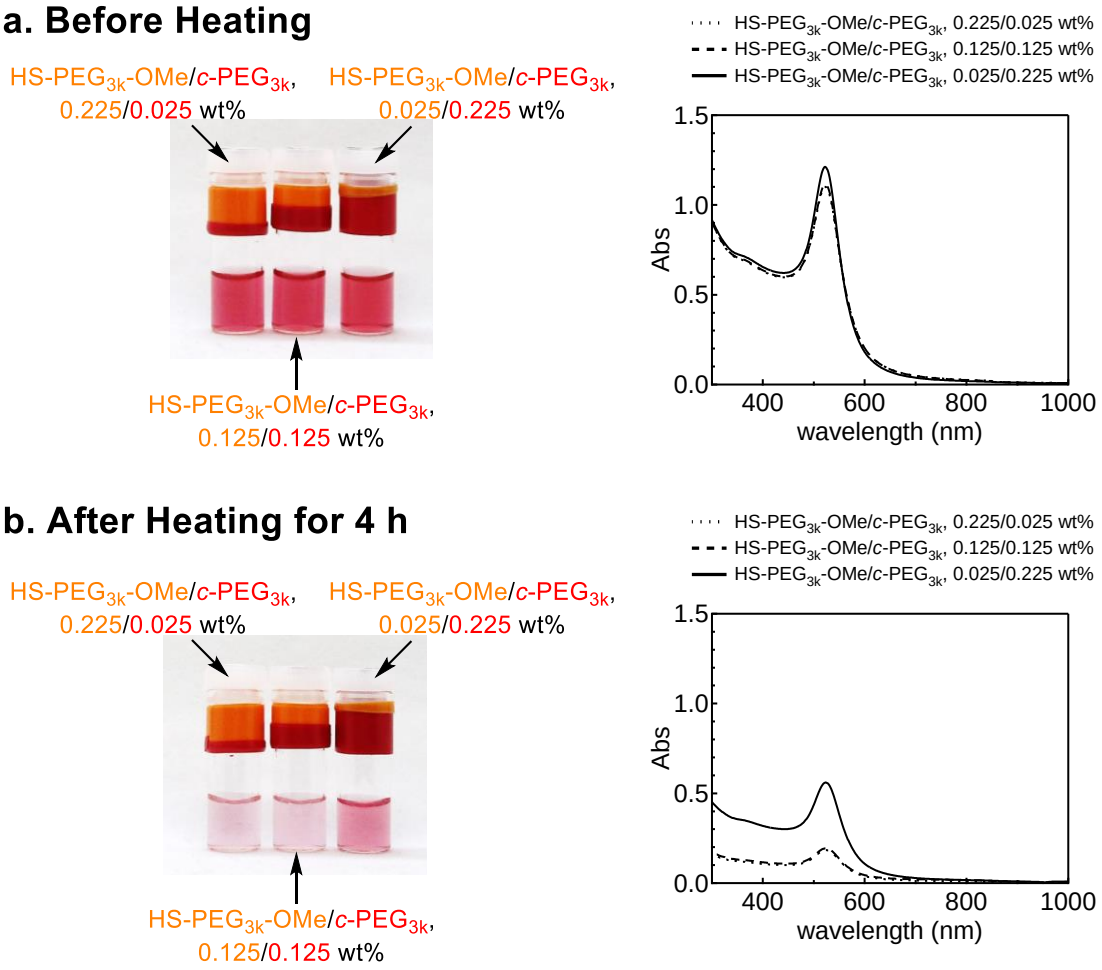

Figure 2.12 Heating test. Photographs and UV–Vis spectra of $AuNPs_{30}$/HS–PEG_{3k}–OMe/*c*-PEG_{3k}. a Before heating and b after heating for 4 h at 85 °C. From left to right in each photograph, the concentrations of HS–PEG_{3k}–OMe/*c*-PEG_{3k} were 0.225/0.025, 0.125/0.125, and 0.025/0.225 wt%. Rel. Abs was 17, 17, or 46%, respectively.

2.3.5 Dispersion stability against a physiological condition

Physiological conditions, which contain NaCl and other electrolytes, are also known to cause aggregation due to the increased ionic strength to form a salt with the citrate on the AuNPs surface to partially neutralize the charges.[13, 33] Based on the discovered enhanced dispersion stability of AuNPs provided by *c*-PEG, that in a physiological condition was examined for potential biological applications. Thus, the dispersion stability of $AuNPs_{15}$/No PEG, $AuNPs_{15}$/HO–PEG_{3k}–OH, $AuNPs_{15}$/MeO–PEG_{3k}–OMe, $AuNPs_{15}$/HS–PEG_{3k}–OMe, and $AuNPs_{15}$/*c*-PEG_{3k} was tested at a typical physiological condition of pH = 7.4 and 150 mM of NaCl. A tenfold-concentrated phosphate buffer saline (PBS) solution (0.06 mL) was added to the $AuNPs_{15}$/PEG dispersions (0.54 mL) form the intended physiological condition. The color of $AuNPs_{15}$/No PEG, $AuNPs_{15}$/HO–PEG_{3k}–OH, and $AuNPs_{15}$/MeO–PEG_{3k}–OMe changed to grayish blue immediately after the addition of the concentrated PBS solution and eventually precipitated (Figure 2.13). On the contrary, no color change was observed for $AuNPs_{15}$/HS–PEG_{3k}–OMe and $AuNPs_{15}$/*c*-PEG_{3k} even after 1000 min. UV–Vis spectra showed that there is no absorption from the SPR of $AuNPs_{15}$/No PEG, $AuNPs_{15}$/HO–PEG_{3k}–OH, and $AuNPs_{15}$/MeO–PEG_{3k}–OMe due to the precipitation (Rel. Abs ≤ 2% in Table 2.2), while $AuNPs_{15}$/HS–PEG_{3k}–OMe (Rel. Abs = 83%) and $AuNPs_{15}$/*c*-PEG_{3k} (Rel. Abs = 88%) did not exhibited a significant change from those before the addition of the concentrated PBS solution. The slight decrease in Rel. Abs was caused by the dilution of the AuNPs dispersion (0.54 mL) with the concentrated PBS solution (0.06 mL). It is assumed that the surface of AuNPs was protected by the physisorption of *c*-PEG not to contact with other nanoparticles even when AuNPs lose the repulsive surface charges by the increased ionic strength in the physiological condition, leading to the suppression of aggregation.

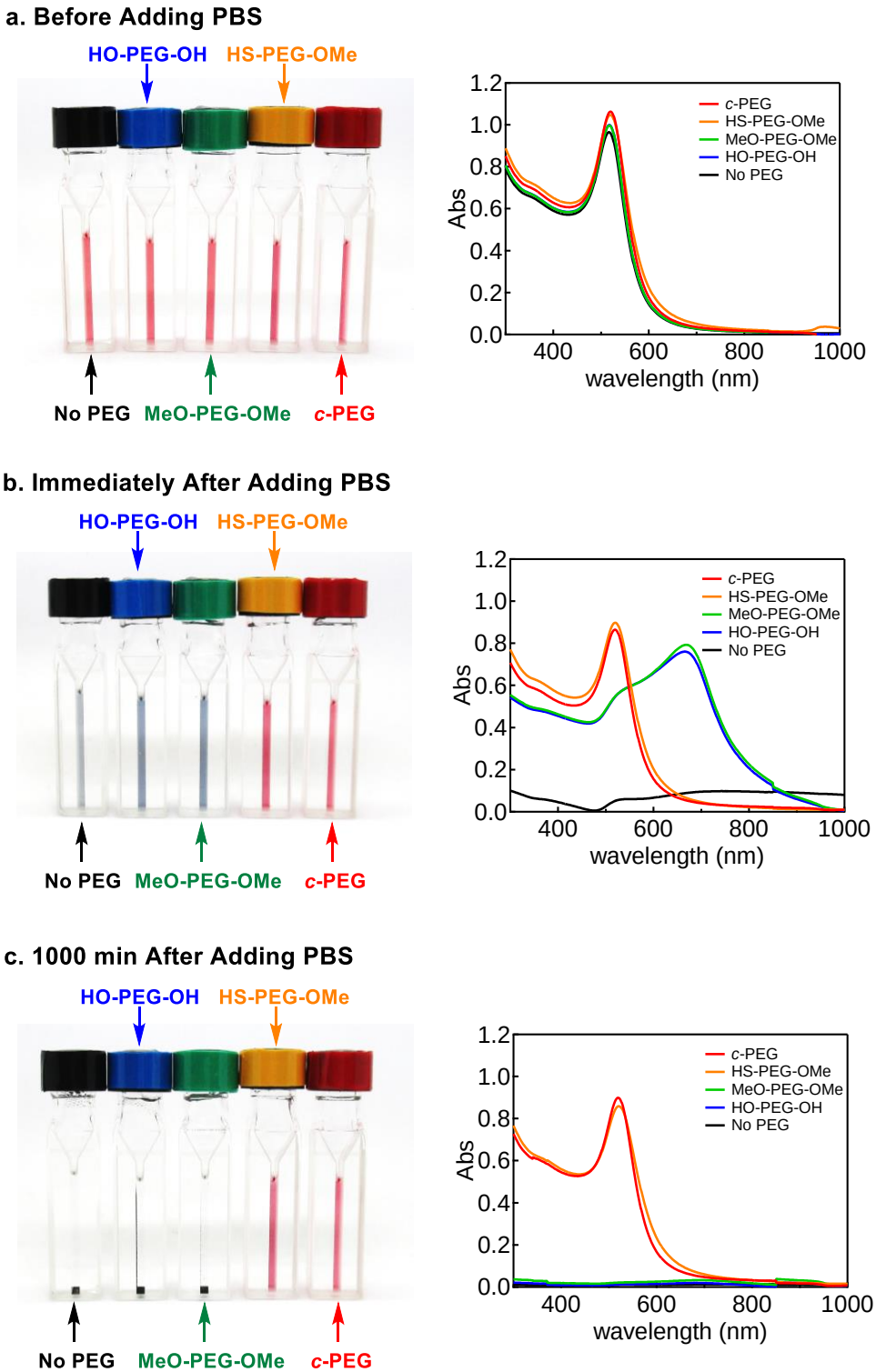

Figure 2.13 Physiological condition test. Photographs and UV–Vis spectra of $AuNPs_{15}$/No PEG (black), $AuNPs_{15}$/HO–PEG_{3k}–OH (blue), $AuNPs_{15}$/MeO–PEG_{3k}–OMe (green), $AuNPs_{15}$/HS–PEG_{3k}–OMe (orange), and $AuNPs_{15}$/*c*-PEG_{3k} (red). (a) Before, (b) immediately after, and (c) 1000 min after the addition of a tenfold-concentrated PBS solution. The resulting dispersions were pH 7.4 and 150 mM of NaCl.

Furthermore, AuNPs$_{15}$/*c*-PEG$_{3k}$ was kept under the physiological condition at 37 °C for an extended period. Rel. Abs was 81% after 7 d and 60% after 14 d, exhibiting a reasonable long-term stability (Figure 2.14).

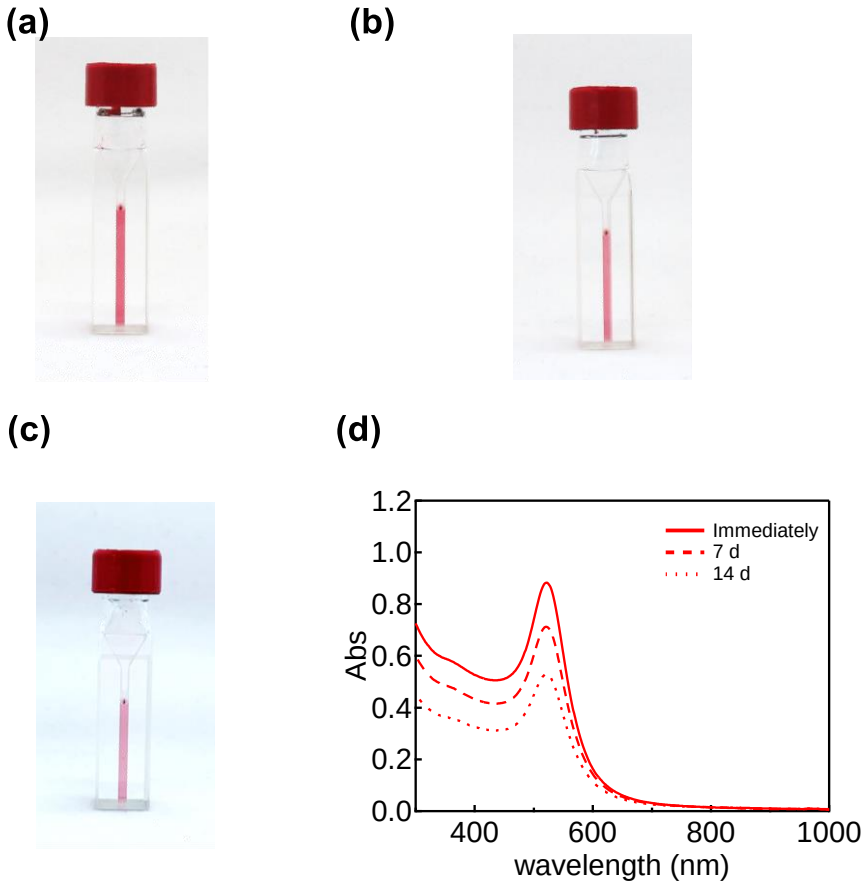

Figure 2.14 Photographs of AuNPs$_{15}$/*c*-PEG$_{3k}$ in a long-term stability test. (a) Immediately after, (b) 7 d after, and (c) 14 d after the addition of a tenfold-concentrated PBS solution kept at 37 °C as well as their (d) UV-Vis spectra.

2.3.6 Size-dependence of AuNPs dispersion stability against a physiological condition

The size-dependence of AuNPs was then examined by varying from 5 to 100 nm using *c*-PEG_{3k} for the physiological condition test. In the result, $AuNPs_{20}$ and smaller sizes persisted dispersion in the presence of *c*-PEG_{3k} (Figure 2.15). On the other hand, $AuNPs_{30}$ and larger sizes were not sufficiently stabilized, and the colour fainted after 850 min. It is known that AuNPs with a smaller size form a more stable dispersion, and the dispersion stability gradually decreases by increasing the size.[14] Thus, *c*-PEG_{3k}, which has a diameter of 7.4 nm when the molecule forms an ideal right circular conformation, showed size-dependent stabilization with a threshold between $AuNPs_{20}$ and $AuNPs_{30}$.

a. Before Adding PBS

b. Immediately After Adding PBS

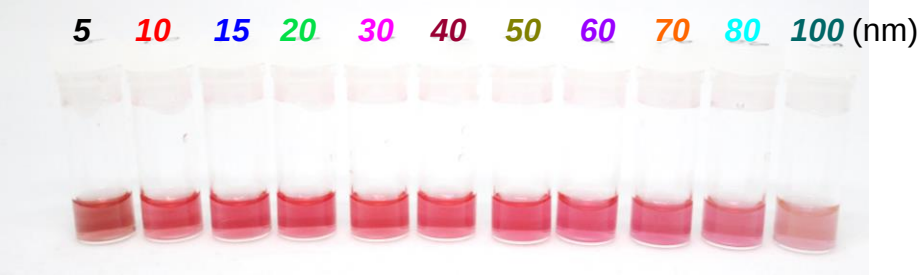

c. 850 min After Adding PBS

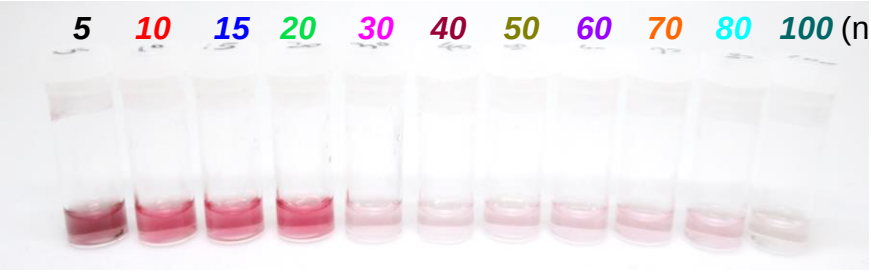

Figure 2.15 Physiological condition test with various diameters of AuNPs (5–100 nm). Photographs of AuNPs/*c*-PEG_{3k} (a) before, (b) immediately after, and (c) 850 min after the addition of a tenfold-concentrated PBS solution. The resulting dispersions were pH 7.4 and 150 mM of NaCl. From left to right in each photograph, $AuNPs_5$/*c*-PEG_{3k}, $AuNPs_{10}$/*c*-PEG_{3k}, $AuNPs_{15}$/*c*-PEG_{3k}, $AuNPs_{20}$/*c*-PEG_{3k}, $AuNPs_{30}$/*c*-PEG_{3k}, $AuNPs_{40}$/*c*-PEG_{3k}, $AuNPs_{50}$/*c*-PEG_{3k}, $AuNPs_{60}$/*c*-PEG_{3k}, $AuNPs_{70}$/*c*-PEG_{3k}, $AuNPs_{80}$/*c*-PEG_{3k}, and $AuNPs_{100}$/*c*-PEG_{3k}.

2.3.7 Molecule weight-dependence of *c*-PEG of AuNPs dispersion stability against a physiological condition

Additionally, the dependence on the *c*-PEG size was also tested by using *c*-PEG_{1k}, *c*-PEG_{5k}, and *c*-PEG_{10k} with a diameter of 2.2, 14, and 28 nm, respectively (Table 2.1). However, no significant difference was observed Figure 2.16); all of *c*-PEG_{1k}, *c*-PEG_{5k} and *c*-PEG_{10k} gave enhanced dispersion stability to $AuNPs_{15}$. On the contrary, 18-crown-6 ether with molecular weight of 264 Da with 0.7 nm in the estimated diameter did not give dispersion stability, and $AuNPs_{15}$ completely precipitated. Thus, the dispersion stabilization depended on both sizes of AuNPs and *c*-PEG.

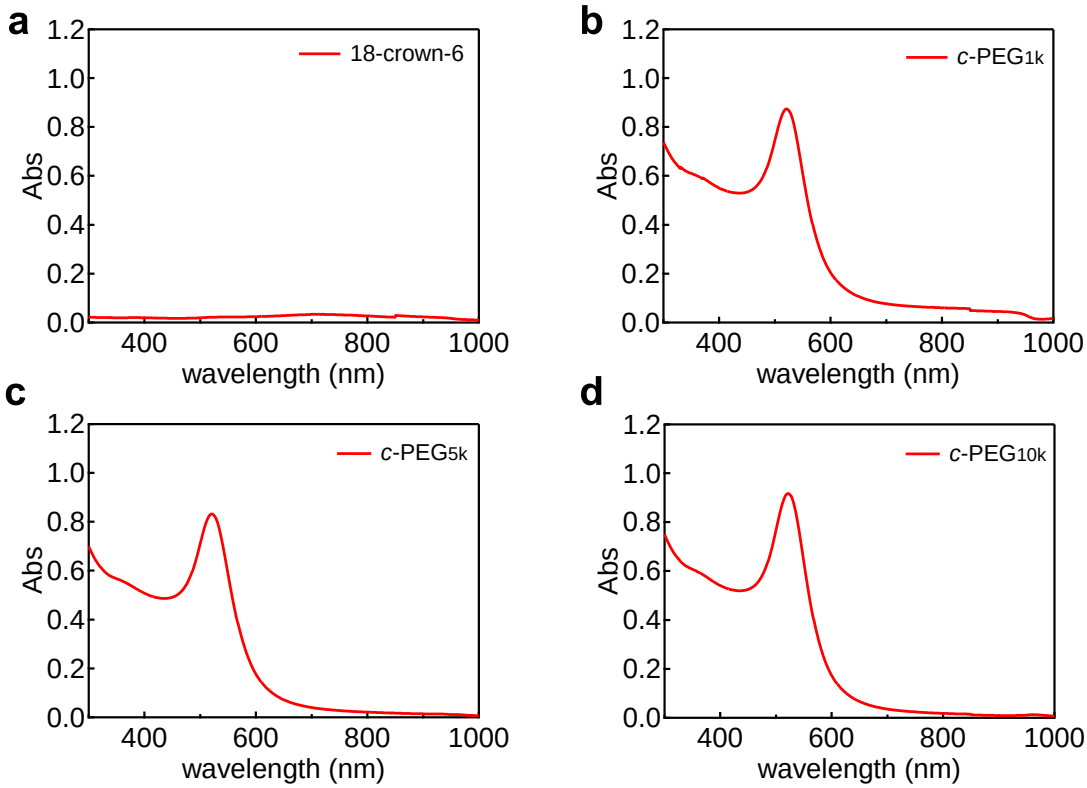

Figure 2.16 Physiological condition test of AuNPs/18-crown-6 and AuNPs/*c*-PEG with various sizes. UV–Vis spectra of (a) $AuNPs_{15}$/18-crown-6, (b) $AuNPs_{15}$/*c*-PEG_{1k}, (c) $AuNPs_{15}$/*c*-PEG_{5k}, and (d) $AuNPs_{15}$/*c*-PEG_{10k} 1000 min after the addition of a tenfold-concentrated PBS solution. The resulting dispersions were pH 7.4 and 150 mM of NaCl.

2.3.8 Concentration-dependence of *c*-PEG of AuNPs dispersion stability against a physiological condition

Moreover, the PEG concentration dependence of the dispersion stability was investigated. The *c*-PEG_{5k} concentration was changed from 0.025 to 2.5 wt% for $AuNPs_5$ (0.05 mg/mL) in the physiological condition. As shown in Figure 2.17, Rel. Abs decreased to 22% after 1000 min for *c*-PEG_{5k} solutions with 0.025 wt%. However, when the *c*-PEG concertation was 0.25 wt%, the decrease in Rel. Abs was suppressed to 78%. In the case of 2.5 wt% of *c*-PEG_{5k}, the absorption essentially quantitatively remained. In this regard, the weight ratio of $AuNPs_5$/PEG was 1/500 for 2.5 wt% of the PEG concentration. The concentration-dependence of HO–PEG_{5k}–OH was also tested for comparison. In the result, the absorption spectra of $AuNPs_5$/HO–PEG_{5k}–OH showed a strong declination even with the PEG concentration of 10 wt% (Rel. Abs = 42%).

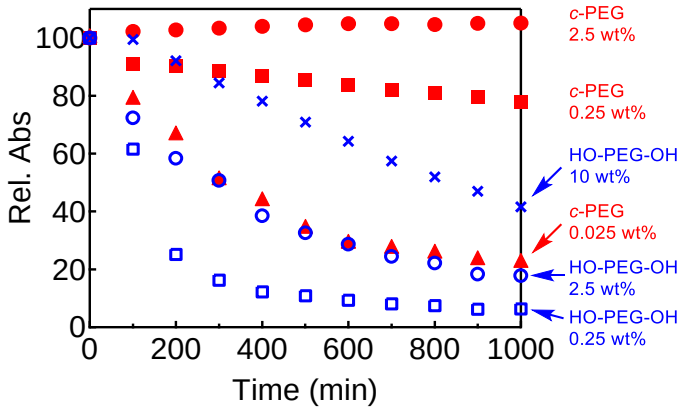

Figure 2.17 Time course of Rel. Abs of $AuNPs_5$ in the physiological condition in the presence of HO–PEG_{5k}–OH or *c*-PEG_{5k} with various concentrations. HO–PEG_{5k}–OH, 0.25 wt% (blue square); 2.5 wt% (blue circle); 10 wt% (blue cross). *c*-PEG_{5k}, 0.025 wt% (red triangle); 0.25 wt% (red square); 2.5 wt% (red circle).

2.3.9 DLS and ζ-potential for AuNPs/PEG

In order to investigate the cause of the dispersion stabilization by *c*-PEG, DLS and ζ-potentials were measured using $AuNPs_{15}$, $AuNPs_{30}$, and $AuNPs_{50}$ with no PEG, HO–PEG_{3k}–OH, MeO–PEG_{3k}–OMe, HS–PEG_{3k}–OMe, and *c*-PEG_{3k} at a polymer concentration of 0.25 wt%. The DLS size was nearly identical or slightly increased by 2 nm or less upon the addition of HO–PEG_{3k}–OH and MeO–PEG_{3k}–OMe compared to corresponding AuNPs/No PEG (Figure 2.18). In the case of $AuNPs_{15}$, the diameter was 19 nm for $AuNPs_{15}$/No PEG and 20 nm for $AuNPs_{15}$/HO–PEG_{3k}–OH and $AuNPs_{15}$/MeO–PEG_{3k}–OMe. In contrast, by the addition of HS–PEG_{3k}–OMe or *c*-PEG_{3k}, the size was significantly increased by 7 nm or more. For example, the diameter of $AuNPs_{15}$ increased to 28 and 26 nm for $AuNPs_{15}$/HS–PEG_{3k}–OMe and $AuNPs_{15}$/*c*-PEG_{3k}, respectively. The similar trends in the change in the diameter were observed for $AuNPs_{30}$ and $AuNPs_{50}$, suggesting that HS–PEG_{3k}–OMe and *c*-PEG_{3k} have a stronger affinity to the surface of AuNPs and form a thicker layer. Because the surface of AuNPs is coated with citrate, the ζ-potential of AuNPs/No PEG showed negative values such as –20 mV for $AuNPs_{15}$. It was reported that the electrically neutral PEG layer on the surface shields the negative charges of citrate to decrease in the magnitude of the ζ-potential.[34] While the ζ-potential of AuNPs/HO–PEG_{3k}–OH and AuNPs/MeO–PEG_{3k}–OMe did not significantly change from corresponding AuNPs/No PEG, that of AuNPs/*c*-PEG_{3k} strongly attenuated, which was even better shielding than AuNPs/HS–PEG_{3k}–OMe in some cases such as $AuNPs_{15}$/HS–PEG_{3k}–OMe (–13 mV) and $AuNPs_{15}$/*c*-PEG_{3k} (–7 mV). Thus, the results of the increased diameter and reduced ζ-potential for AuNPs/*c*-PEG suggest the strong interaction of *c*-PEG to AuNPs and the formation of a PEG layer with a decent density on the basis of the cyclic topology.[24]

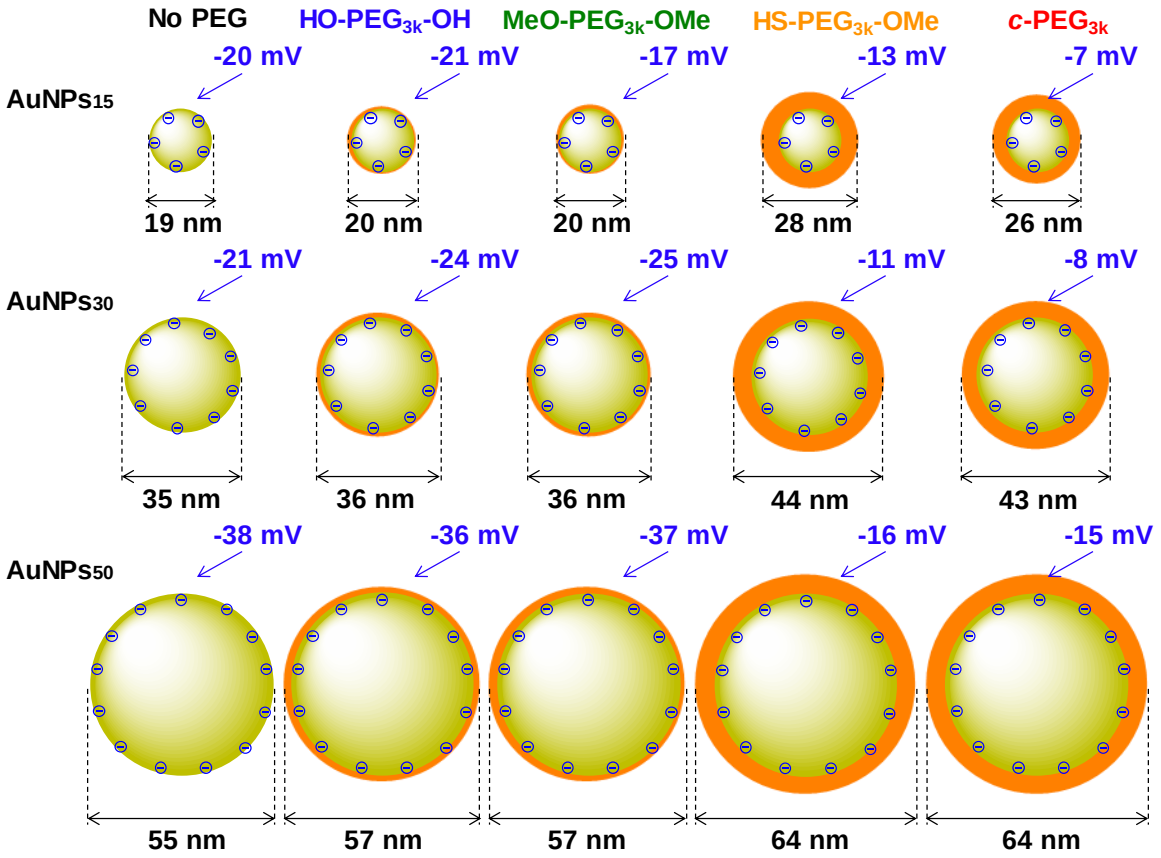

Figure 2.18 Schematic illustrations of the DLS size and ζ-potential of AuNPs/No PEG, AuNPs/HO–PEG_{3k}–OH, AuNPs/MeO–PEG_{3k}–OMe, AuNPs/HS–PEG_{3k}–OMe, and AuNPs/*c*-PEG_{3k}. The size of AuNPs was 15, 30, and 50 nm, and the concentration of PEG was 0.25 wt%. The size ratio of AuNPs and the PEG layer in the figure represents the actual ratio.

2.3.10 *c*-PEG concentration-dependence of the layer thickness and ζ-potential

Furthermore, the *c*-PEG concentration-dependence of the layer thickness and ζ-potential were determined for $AuNPs_{15}$/*c*-PEG_{3k} (Figure 2.19). Both of the thickness and ζ-potential gradually increased and essentially saturated at around 4.5 nm and –12 mV, respectively, at a PEG concentration of 0.25 wt%, suggesting this concentration is optimal. The grafting density (σ) was calculated based on the PEG layer thickness using the following formulae as reported in previous studies (Table 2.3).[35-37] Thus, the surface concentration (Γ), average distance between grafted PEG chains (D), and grafting density (σ) were calculated by:

$$\Gamma = \rho t \quad (1)$$

$$D = (M/\Gamma N_A)^{1/2} \quad (2)$$

$$\sigma = (a/D)^2 \quad (3)$$

where a is the size of a PEG monomer unit (3.5 Å), ρ is the density of PEG (1.1 g/mL), t is the thickness of the PEG layer by DLS, N_A is Avogadro's number, and M is the molecular weight of PEG. Despite that the calculation is designated for chemisorption, this helps deducing the state and environment of *c*-PEG at the AuNPs surface was considered. In the result, σ was found to be 0.13 chains/nm^2 at the *c*-PEG concentration of 0.25 wt%. This value may be comparable to 0.20–3.14 chains/nm^2 reported for HS–PEG–OMe that was determined by a different method, in which the adsorbed PEG molecules was quantitatively removed from AuNPs and analyzed by HPLC.[32] This quantitative removal as well as measuring the unadsorbed *c*-PEG in the supernatant was also attempted.[38] However, these methods need to isolate PEGylated AuNPs from the excess PEG molecules, but this was not possible for *c*-PEG-physiosorbed AuNPs. Thus, repeated centrifugation or ultrafiltration removed *c*-PEG from AuNPs, suggesting that the present

physisorption system is dynamic in contrast to the gold–sulfur chemisorption, despite providing the good dispersion stability.

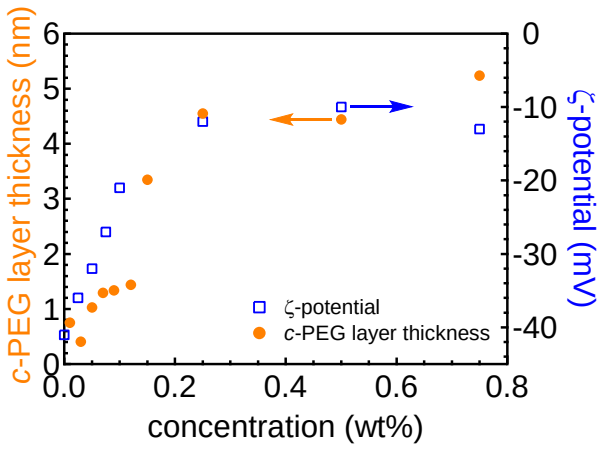

Figure 2.19 *c*-PEG layer thickness and ζ-potential for $AuNPs_{15}$/*c*-PEG_{3k} with a series of *c*-PEG_{3k} concentrations.

Table 2.3 DLS size, *c*-PEG layer thickness, and grafting density (σ) of $AuNPs_{15}$/*c*-PEG_{3k} at various concentrations of *c*-PEG_{3k}.

c-PEG conc. (wt%)	0.05	0.15	0.25	0.50	0.75
DLS size (nm)	20.3	25.0	27.4	27.1	28.7
c-PEG layer thickness (nm)	1.0	3.3	4.6	4.4	5.2
σ (chains/nm^2)	0.029	0.094	0.13	0.12	0.15

In addition, the estimated numbers of PEG molecules and Au atoms present per one AuNP are listed in Table 2.4. For example, in the case of $AuNPs_{15}$ and PEG with M_n of 3,000 Da at a concentration of 0.25 wt%, it is estimated that an average of 10.5×10^4 Au atoms form a nanoparticle,[39] and 38.2×10^4 PEG molecules exist per one nanoparticle.

Table 2.4 Estimated numbers of Au atoms and PEG molecules per one AuNP in the case of a PEG concertation of 0.25 wt%.

AuNPs size (nm)	Number of Au atoms per one AuNP (10^4)	Number of PEG (M_n = 3,000 Da) per one AuNPs (10^4)
5	0.39	1.41
10	3.10	11.3
15	10.5	38.2
20	24.8	90.4
30	83.3	303
40	198	723
50	386	1410
60	665	2430
70	1070	3880
80	1580	5780
100	3090	11300

2.3.11 FT-IR for AuNPs/PEG

In order to determine the interaction between the surface of AuNPs and PEG, FT-IR spectroscopy was performed on $AuNPs_{15}$/No PEG, $AuNPs_{15}$/MeO–PEG_{3k}–OMe, and $AuNPs_{15}$/*c*-PEG_{3k}. The samples were prepared by moderately removing excess PEG and sodium citrate by ultrafiltration followed by lyophilization. Lyophilization was necessary because water has strong absorptions in the intended wavenumber range. Although FT-IR spectroscopy of the lyophilized samples may not fully reflect the aqueous dispersion state of AuNPs/PEG, the interactions existing between AuNPs and PEG were expected to be investigated. The spectra showed noticeable difference in absorption wavenumbers between $AuNPs_{15}$/MeO–PEG_{3k}–OMe and $AuNPs_{15}$/*c*-PEG_{3k} (Figure 2.20 and Table 2.5). For example, the CH_2 rocking and twisting of PEG were higher in wavenumber for $AuNPs_{15}$/*c*-PEG_{3k} (961 cm^{-1}) than $AuNPs_{15}$/MeO–PEG_{3k}–OMe (957 cm^{-1}).[40] Moreover, the C–O and C–C stretching of PEG was also higher for $AuNPs_{15}$/*c*-PEG_{3k} (1100 cm^{-1}) than $AuNPs_{15}$/MeO–PEG_{3k}–OMe (1094 cm^{-1}), where the C–O bonds likely interacted to Na^+ of sodium citrate. $AuNPs_{15}$/MeO–PEG_{3k}–OMe exhibited an extra peak at 1455 cm^{-1} that can also be found in MeO–PEG_{3k}–OMe without AuNPs. Thus, this peak likely arose from the effect of the chain end. The asymmetric stretching of COO^- of sodium citrate appeared at 1575 cm^{-1} for $AuNPs_{15}$/No PEG, 1578 cm^{-1} for $AuNPs_{15}$/MeO–PEG_{3k}–OMe, and 1581 cm^{-1} for $AuNPs_{15}$/*c*-PEG_{3k}. This suggests that MeO–PEG_{3k}–OMe interacts with Na^+ to cause the change in the COO^- stretching wavenumber, and moreover, *c*-PEG_{3k} results in a stronger interaction. In addition, the peak at 1648–1649 cm^{-1}, not much different in all the samples, was from the asymmetric stretching of COO^- of Au-coordinated citrate.[41]

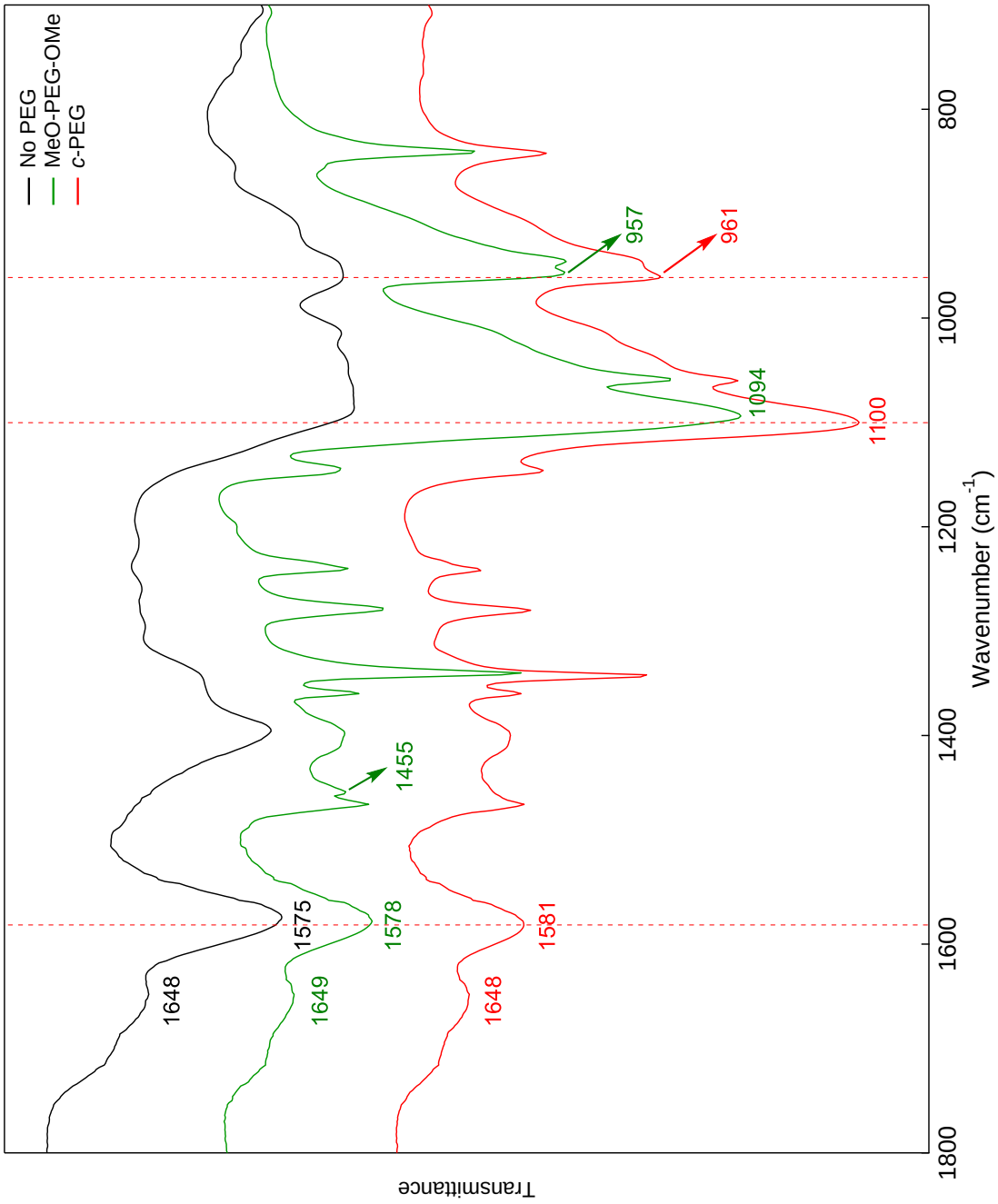

Figure 2.20 FT-IR spectra of AuNPs$_{15}$/No PEG (black), AuNPs$_{15}$/MeO–PEG$_{3k}$–OMe (green), and AuNPs$_{15}$/*c*-PEG$_{3k}$ (red). Red dotted lines indicate the peak top wavenumbers of AuNPs$_{15}$/*c*-PEG$_{3k}$.

Table 2.5 Absorption wavenumbers in the FT-IR spectra of $AuNPs_{15}$/No PEG, $AuNPs_{15}$/MeO–PEG_{3k}–OMe, and $AuNPs_{15}$/*c*-PEG_{3k}.

	AuNPs/No PEG (cm^{-1})	AuNPs/MeO–PEG–OMe (cm^{-1})	AuNPs/*c*-PEG (cm^{-1})
C–O, C–C stretching, CH_2 rocking of PEG[1]	–	841	842
CH_2 rocking, CH_2 twisting of PEG[1]	–	946	946
CH_2 rocking, CH_2 twisting of PEG[1]	**–**	**957**	**961**
C–O, C–C stretching, CH_2 rocking of PEG[1]	–	1059	1060
C–O, C–C stretching of PEG[1]	**–**	**1094**	**1100**
C–O stretching, CH_2 rocking of PEG[1]	–	1145	1146
CH_2 twisting of PEG[1]	–	1240	1242
CH_2 twisting of PEG[1]	–	1279	1280
CH_2 wagging of PEG[1]	–	1340	1343
Symmetric stretching of COO^- of sodium citrate[2]	1396	1398	1399
CH_2 scissoring of PEG[1]	**–**	**1455**	**–**
CH_2 scissoring of PEG[1]	–	1466	1466
Asymmetric stretching of COO^- of sodium citrate[2]	**1575**	**1578**	**1581**
Asymmetric stretching of COO^- of Au–citrate[2]	1648	1649	1648

Noticeable differences are shown in bold.

2.3.12 Animal experiments by AuNPs/PEG

Applications of nano-sized particles have been extensively developed for bio-medical area, and, especially, AuNPs are widely utilized into biosensing, diagnosis, and in vivo drug delivery.[42-46] Thus, further research into the plasma clearance and tumor accumulation by using tumor bearing mouse would clarify the potential usability of AuNPs/*c*-PEG in vivo. As seen in Figure 2.21a. $AuNPs_5$/*c*-PEG_{3k} exhibited slow blood clearance (43.8% dose/plasma at 10 min, and 18.8% dose/plasma at 60 min), while no stable circulations were observed for $AuNPs_5$/No PEG and $AuNPs_5$/MeO–PEG_{3k}–OMe, indicating the topology-dependent utility of surface-modification through *c*-PEG. Tumor accumulation also represented the advantage of $AuNPs_5$/*c*-PEG_{3k} (Figure 2.21b). However, on the basis of the previous reports,[47-49] the absolute amount of $AuNPs_5$/*c*-PEG_{3k} accumulated into tumor was relatively low values. In fact, $AuNPs_5$/*c*-PEG_{3k} in this study is assumed to be accumulated by the enhanced permeability and retention (EPR) effect,[50, 51] and the relationship between particle size and time course are fundamentally important to obtain EPR-driven tumor accumulation, especially vs hypervascular tumors, i.e., murine colon adenocarcinoma (C26).[47, 52] Therefore, the increments in tumor accumulation of nano-sized particle through EPR effect might require additional fine tuning of AuNPs, e.g., particle size, and such additional modification is ongoing. Overall, these results highlight the importance and usability of *c*-PEG as a stabilizer for metal nanoparticle, and the in vivo experiments exhibit the potential effectiveness of AuNPs/*c*-PEG, prepared through simple physisorption of *c*-PEG against AuNPs, for bio-medical applications.

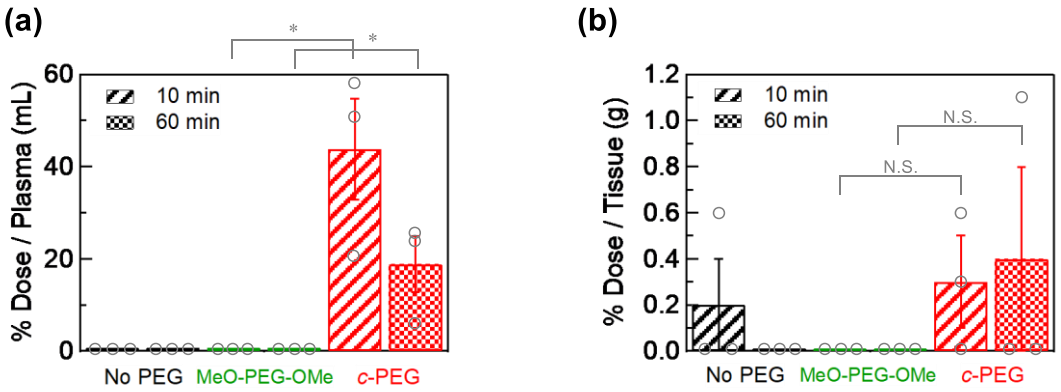

Figure 2.21 Biodistribution of Au in (a) blood and (b) tumor of mice after 10 and 60 min of the injection of $AuNPs_5$/No PEG, $AuNPs_5$/MeO–PEG_{3k}–OMe, and $AuNPs_5$/*c*-PEG_{3k}. Data represent mean ± s.e. from three independent experiments performed in triplicate. *, $p < 0.05$; N.S. = not significant.

2.4. Conclusions

Concerning the cause of the strong affinity of *c*-PEG to the surface of AuNPs, the less entropic penalty upon adsorption is expected to be the major factor. In other words, the number of conformations that unadsorbed *c*-PEG can take is less than that of the unadsorbed linear PEG (HO−PEG−OH and MeO−PEG−OMe) due to their topology. Thus, the entropic penalty upon adsorption onto the surface of AuNPs is smaller for *c*-PEG, where the adsorption is an entropically unfavorable and enthalpically favorable process. Since HO−PEG−OH, MeO−PEG−OMe, and *c*-PEG are consisted of the same PEG repeating units, their enthalpic energy released upon adsorption should be essentially identical, leading to that the adsorption of *c*-PEG is more favorable than HO−PEG−OH and MeO−PEG−OMe in terms of the free energy to form the thicker PEG layer for the enhanced dispersion stabilization.

The stronger affinity of cyclic polymers was also observed against silica nanoparticles.[53] Moreover, the stronger adsorption of cyclic polymers onto a surface have been suggested by theoretical and computational studies.[54-57] Cosgrove and coworkers conducted a detailed study on the difference between the surface adsorption of cyclic and linear polymers from solutions by the extended lattice theory (Scheutjens−Fleer (SF) theory).[58] When the surface adsorption energy parameter (χ_s) is small, a larger amount of the cyclic polymers is adsorbed than the linear analogues. The difference in the adsorption efficiency between linear and cyclic polymers becomes small with increasing χ_s. This result indicates that the difference between the linear and cyclic chains is negligible when the adsorption is strongly controlled by enthalpy, while the cyclic chain is advantageous when the adsorption enthalpy and entropy are comparable.

In summary, the drastic enhancement in the dispersion stability of AuNPs by physisorption of *c*-PEG was shown. This methodology allows for AuNPs dispersions to be frozen, lyophilized,

heated, and exposed to physiological conditions with even better stability than the most commonly used chemisorption of HS–PEG–OMe. Moreover, the AuNPs/*c*-PEG system was applied for an animal experiment, finding the advantages of $AuNPs_5$/*c*-PEG_{3k} in blood circulation in contrast to $AuNPs_5$/No PEG and $AuNPs_5$/MeO–PEG_{3k}–OMe. The combination of the dispersion stability against high temperature and physiological conditions, coupled with the accumulation in tumor, would be most suitable to future applications toward photothermal therapy using gold nanoparticles and nanorods. Furthermore, cyclization and physisorption require no chemical modification on the repeating units of the polymer chain, which is excellent match for the biocompatibility of PEG. Likewise, the physisorption would allow for expedient postfunctionalization through chemisorption.

2.5 References

1. Kelly, K.L., Coronado, E., Zhao, L.L. & Schatz, G.C. *J. Phys. Chem. B* 2003, **107**, 668-677.

2 Kim, Y.J., Johnson, R.C. & Hupp, J.T. *Nano Lett.* 2001,**1**, 165-167.

3. Anker, J.N. et al. *Nat. Mater.* 2008, **7**, 442-453.

4. Hasobe, T. et al. *J. Am. Chem. Soc.* 2005, **127**, 1216-1228.

5. Yan, N., Xiao, C. & Kou, Y. *Coord. Chem. Rev.* 2010, **254**, 1179-1218.

6. Wiley, B., Sun, Y.G. & Xia, Y.N. *Acc. Chem. Res.* 2007, **40**, 1067-1076.

7. Radziuk, D., Skirtach, A., Sukhorukov, G., Shchukin, D. & Möhwald, H. *Macromol. Rapid Commun.* 2007, **28**, 848-855.

8. Dong, H.C. et al. *J. Am. Chem. Soc.* 2008, **130**, 12852-12853.

9. Zhang, X., Servos, M.R. & Liu, J.W. *J. Am. Chem. Soc.* 2012, **134**, 9910-9913.

10. Kralik, M. *Chem. Pap.* 2014, **68**, 1625-1638.

11. Zhang, G. et al. *Biomaterials* 2009, **30**, 1928-1936.

12. Nam, S., Parikh, D.V., Condon, B.D., Zhao, Q. & Yoshioka-Tarver, M. *J. Nanoparticle Res.* 2011, **13**, 3755-3764.

13. Boisselier, E. & Astruc, D. *Chem. Soc. Rev.* 2009, **38**, 1759-1782.

14. Ling, K., Jiang, H. & Zhang, Q. *Nanoscale Res. Lett.* 2013, **8**, 538.

15. Seo, E. et al. *Polym. Chem.* 2017, **8**, 4528-4537.

16. Jia, Z. & Monteiro, M.J. *J. Polym. Sci., Part A: Polym. Chem.* 2012, **50**, 2085-2097.

17. Laurent, B.A. & Grayson, S.M. *Chem. Soc. Rev.* 2009, **38**, 2202-2213.

18. Kricheldorf, H.R. & Schwarz, G. *Macromol. Rapid Commun.* 2003, **24**, 359-381.

19. Yamamoto, T. & Tezuka, Y. *Soft Matter* 2015, **11**, 7458-7468.

20. Honda, S., Yamamoto, T. & Tezuka, Y. *J. Am. Chem. Soc.* 2010, **132**, 10251-10253.

21. Honda, S., Yamamoto, T. & Tezuka, Y. *Nat. Commun.* 2013, **4**, 1574.

22. Baba, E., Yatsunami, T., Tezuka, Y. & Yamamoto, T. *Langmuir* 2016, **32**, 10344-10349.

23. Morgese, G. et al. *Angew. Chem., Int. Ed.* 2016, **55**, 15583-15588.

24. Morgese, G. et al. *Angew. Chem., Int. Ed.* 2017, **56**, 4507-4511.

25. Morgese, G., Cavalli, E., Rosenboom, J.-G., Zenobi-Wong, M. & Benetti, E.M. *Angew. Chem., Int. Ed.* 2018, **57**, 1621-1626.

26. Cooke, J. et al. *Macromolecules* 1998, **31**, 3030-3039.

27. Tang, Q., Wu, Y., Sun, P., Chen, Y. & Zhang, K. *Macromolecules* 2014, **47**, 3775-3781.

28. Liu, R. et al. *Talanta* 2013, **112**, 37-42.

29. Smith, A.M. et al. *Anal. Chem.* 2015, **87**, 2771-2778.

30. Bain, C.D., Biebuyck, H.A. & Whitesides, G.M. *Langmuir* 1989, **5**, 723-727.

31. Kang, T. et al. *ACS Nano* 2016, **10**, 930-937.

32. Du, Y., Jin, J., Liang, H. & Jiang, W. *Langmuir* 2019, **35**, 8316-8324.

33. Pamies, R. et al. *J. Nanopart. Res.* 2014, **16**, 2376.

34. Rahme, K. et al. *RSC Advances* 2013, **3**, 6085-6094.

35. Tao, S.L., Popat, K.C., Norman, J.J. & Desai, T.A. *Langmuir* 2008, **24**, 2631-2636.

36. Damodaran, V.B., Fee, C.J., Ruckh, T. & Popat, K.C. *Langmuir* 2010, **26**, 7299-7306.

37. Uz, M., Bulmus, V. & Altinkaya, S.A. *Langmuir* 2016, **32**, 5997-6009.

38. Wang, Y., Qin, W. & Qiu, D. *Langmuir* 2014, **30**, 5170-5175.

39. Oh, E. et al. *ACS Nano* 2011, **5**, 6434-6448.

40. Vrandečić, N.S., Erceg, M., Jakić, M. & Klarić, I. *Thermochim. Acta* 2010, **498**, 71-80.

41. Wulandari, P. et al. *J. Colloid Interface Sci.* 2015, **438**, 244-248.

42. Elsabahy, M. & Wooley, K.L. *Chem. Soc. Rev.* 2012, **41**, 2545-2561.

43. Sutton, D., Nasongkla, N., Blanco, E. & Gao, J.M. *Pharm. Res.* 2007, **24**, 1029-1046.

44. Agasti, S.S. et al. *Adv. Drug Delivery Rev.* 2010, **62**, 316-328.

45. Knop, K., Hoogenboom, R., Fischer, D. & Schubert, U.S. *Angew. Chem., Int. Ed.* 2010, **49**, 6288-6308.

46. Otsuka, H., Nagasaki, Y. & Kataoka, K. *Adv. Drug Delivery Rev.* 2003, **55**, 403-419.

47. Cabral, H. et al. *Nat. Nanotechnol.* 2011, **6**, 815-823.

48. Bae, Y. et al. *Bioconjugate Chem.* 2005, **16**, 122-130.

49. Cabral, H., Nishiyama, N., Okazaki, S., Koyama, H. & Kataoka, K. *J. Control. Release* 2005, **101**, 223-232.

50. Matsumura, Y. & Maeda, H. *Cancer Res.* 1986, **46**, 6387-6392.

51. Maeda, H., Tsukigawa, K. & Fang, J. *Microcirculation* 2016, **23**, 173-182.

52. Miura, Y. et al. *ACS Biomater. Sci. Eng.* 2015, **1**, 1067-1076.

53. Patel, A., Cosgrove, T. & Semlyen, J.A. *Polymer* 1991, **32**, 1313-1317.

54. Stratouras, G.K. & Kosmas, M.K. *Macromolecules* 1991, **24**, 6754-6758.

55. Stratouras, G. & Kosmas, M. *Macromolecules* 1992, **25**, 3307-3308.

56. Zhang, L., Xia, A. & Xu, Y. *Eur. Polym. J.* 2000, **36**, 847-850.

57. Sikorski, A. *Macromol. Theory Simul.* 2001, **10**, 38-45.

58. van Lent, B., Scheutjens, J. & Cosgrove, T. *Macromolecules* 1987, **20**, 366-370.

Chapter 3

Size Control and Enhanced Stability of Silver Nanoparticles by Cyclic Poly(Ethylene Glycol)

3.1 Introduction

Metal nanoparticles are widely used in catalysis[1], bio-sensors[2], optics[3], electronic components[4], and biomedical treatments[5] in recent years. Due to the surface plasmon resonance (SPR) interaction between light and the surface of metal nanoparticles, various particle intrinsic properties such as size and shape affect the colour and dispersion statuses of the colloidal solution[6]. In order to preserve their properties, the stability of the nanoparticles is a crucial aspect which has to be taken into account. Generally, nanoparticles are kept in solution since their agglomeration is facilitated in the dry state due to the presence of capillary forces. However, the stability of nanoparticles in solution is often disturbed by a range of factors such as light[7], heat[8], salt[9], and pH[10], resulting in aggregation of nanoparticles or changes in the colour of colloidal solution. In order to contain these phenomena, small molecules or polymers are dispersed into the colloidal solution which then adsorb on the particle surface. While molecules such as sodium citrate[11] and cetyltriethylammonium bromide (CTAB)[12] can stabilize particles from ag-glomeration as a result of electrostatic repulsion through the presence of negative and positive charges, respectively, incorporated in their structures, neutral polymers such as poly(ethylene glycol) (PEG) and poly(vinyl pyrrolidone) (PVP) mainly create steric hindrance in order to protect the particle surface which is reported to be more effective than the charge stabilization mechanism[13]. On the other hand, polymers equipped with charges in their backbone structure such as poly(sodium acrylate) can combine both stabilization mechanisms[14].

In the last decade, PEG with long alkoxy chain received more attention from re-searchers due to its water solubility and biocompatibility, which can provide steric hindrance for the preparation of gold nanoparticles (AuNPs) or silver nanoparticles (AgNPs)[15]. In this relation, PEG coverage on the surface of nanostructures was reported to be crucial for the ligand exchange

process[16] and for controlling the shape of nanocrystals[17]. In addition, PEG is also often used to disperse/stabilize AuNPs or AgNPs in immunoassays, thus maintaining the dispersion of the particles and avoiding tracking by the immune system[18]. In particular, the physiological environment is an important factor in vivo and in vitro experiments, and increasing salt concentration or ionic strength can lead to the aggregation or dissolution of nanoparticles[19]. In general, the addition of NaCl to a metal nanoparticle solution together with the presence of oxygen leads to the catalyzed dissolution of the particles attributed to the corrosive nature of the chloride ions[20]. Furthermore, Li et al. reported the bridging of individual particles by secondary precipitates of AgCl when AgNPs were exposed to chloride-containing solutions[19]. AgNPs incubated in an aqueous solution of PEG with M_n = 8,000 Da prevented agglomeration at a NaCl concentration between 10–100 mM upon increasing the concentration of PEG from 1 to 5 mg/mL. At a PEG concentration as low as 10–100 nM, steric protection is already initiated[21]. Nevertheless, an increase in the salt concentration leads to a deterioration in the stabilizing ability of PEG[22].

On the other hand, topological effects of polymers are gaining attention and it becomes another important parameter of polymer in addition to molecular weight[23] and repeating units[24] in recent years. Many researchers synthesized and successfully isolated polymers with various topological shapes such as monocyclic, multicyclic, H-shape, etc.[25]. Among all topologies, cyclic polymers without end-groups exhibit unique physical/chemical properties such as higher glass transition temperature[26], reduced hydro-dynamic volume[27], higher density[28], lower viscosity[29], higher resistance of their micelles towards salt[30] and temperature[31], and higher interfacial activity[32] com-pared to their respective linear counterparts. In particular, superior dispersion stability of AuNPs[33] and AgNPs[34] was drastically enhanced by the physisorption of cyclic PEG were reported. With these previous works in mind, the present research investigates the utilization of PEG in the

preparation process of AgNPs, where the influences of the linear and cyclic polymer topologies as well as the chain-end groups on the AgNPs' size and stability against NaCl were investigated.

3.2 Experimental section

3.2.1 Materials

Silver nitrate ($AgNO_3$) (ACS reagent, < 99 %) and poly(ethylene glycol) (PEG) of M_n = 2,000 Da (HO–PEG_{3k}–OH) were purchased from Sigma Aldrich, while dichloromethane (CH_2Cl_2), tetrahydrofuran (THF), *n*-heptane, potassium hydroxide (KOH), sodium hydroxide (NaOH), chlorobenzene, maltose monohydrate, sodium chloride (NaCl), ammonia (28–30%), iodomethane (> 99.5%), and PEG of Mn = 4,000 Da (HO–PEG_{5k}–OH) and 6,000 Da (HO–PEG_{10k}–OH) were obtained from Kanto Chemicals.

3.2.2 NMR

^1H NMR (400 MHz) and ^{13}C NMR (100 MHz) were measured in $CDCl_3$ using a JEOL JNM-ESC400 instrument at ambient temperature.

3.2.3 SEC

SEC was performed at 40 °C in THF (flow rate, 1.0 mL/min) using a Shodex GPC-101 gel permeation chromatography system (Shodex DU-2130 dual pump, Shodex RI-71 reflective index detector, and Shodex ERC-3125SN degasser) equipped with a Shodex KF-G guard column (4.6 mm × 10 mm; pore size, 8 μm) and two Shodex KF-804L columns (8 mm × 300 mm) in series. Polystyrene standard samples were used for calibration.

3.2.4 TEM

TEM measurements were performed with a Japan Electron Optics Laboratory JEM-2010 operated at 200 kV. The size distribution of AgNPs was determined by the average of 150–200 observed particles.

3.2.5 MALDI–TOF MS

MALDI–TOF mass spectrometry was carried out using a Bruker Daltonics Ultraflex-S at the Open Facility, Hokkaido University.

3.2.6 UV–Vis Spectroscopy

UV–Vis absorption spectra were recorded on a JASCO 4100 spectrophotometer at 25 °C. Relative UV–Vis absorption intensity ($A/A_0 \times 100\%$) of AgNPs without and with NaCl was compared at λ_{max} (409, 405, and 420 nm for HO–PEG_{5k}–OH, *c*-PEG_{5k}, and MeO–PEG_{5k}–OMe, respectively).

3.2.7 Synthesis of AgNPs Through the Tollens Process

AgNPs were prepared according to a reported procedure[35]. Thus, to a mixture of $AgNO_3$ (17 mg, 0.10 mmol), PEG (10–200 mg, 0.22–4.4 mmol), an aqueous solution of ammonia (28–30%, 34 μL) in deionized H_2O (90 mL), an aqueous solution of NaOH (10 mL, 0.10 mM) was added under vigorous stirring. Thereafter, solid maltose monohydrate (360 mg, 1.0 mmol) was added, and the resulting mixture stirred overnight. As prepared AgNPs dispersions were characterized and used without further purification.

3.3 Results and Discussion

3.3.1 Synthesis of AgNPs

AgNPs were prepared by the Tollens method similar to the report by Kvítek et al. with a modification which consisted of using PEG instead of poly(acrylic acid) as a polymeric stabilizer[35]. In this set of experiments, the molar ratio of PEG to $AgNO_3$ (ω) was varied from 2.2 to 44, while other reaction parameters were kept constant (Table 3.1). Hydroxy-terminated linear PEG with M_n of 3,000, 5,000 and 10,000 Da, HO–PEG_{3k}–OH, HO–PEG_{5k}–OH, and HO–PEG_{10k}–OH, respectively, as well as their corresponding cyclic counterparts, *c*-PEG_{3k}, *c*-PEG_{5k}, and *c*-PEG_{10k}, respectively, were used as a polymeric stabilizer.

Table 3.1 Summary of the TEM-Measured Size of AgNPs Prepared in the Presence of HO–PEG–OH, *c*-PEG, and MeO–PEG–OMe with Various Molecular Weight and *ω*.

Polymer	ω[1]	TEM-Measured Size of AgNPs (nm)		
		HO–PEG–OH	*c*-PEG	MeO–PEG–OMe
PEG_{3k}	2.2	55 ± 8	52 ± 8	-
	11	43 ± 8	45 ± 8	-
	44	33 ± 4	30 ± 7	-
PEG_{5k}	2.2	58 ± 13	42 ± 9	48 ± 6
	11	36 ± 5	31 ± 4	44 ± 10
	44	40 ± 7	21 ± 4	48 ± 9
PEG_{10k}	2.2	50 ± 8	30 ± 3	-
	11	48 ± 10	35 ± 4	-
	44	37 ± 7	26 ± 4	-

[1]ω is given by the molar ratio of PEG repeating units to $AgNO_3$ used in the preparation of AgNPs.

In addition, linear PEG (M_n = 5,000) with methoxy termini (MeO–PEG_{5k}–OMe) was also tested to investigate the effects of the end groups. AgNPs that were prepared in this work featured a similar particle size spectrum to the observation made by Kvítek et al. at comparable polymer concentrations[35]. Here, PEG was primarily used as a stabilizing agent, while the reducing environment was provided through the use of maltose monohydrate. The pH of the reaction was adjusted to ~11 by using NaOH which was responsible for the completion of the reaction within minutes. The formed particles were characterized by transmission electron microscopy (TEM) and UV–Vis spectroscopy (Figures 3.1, 3.2, 3.3 and 3.4).

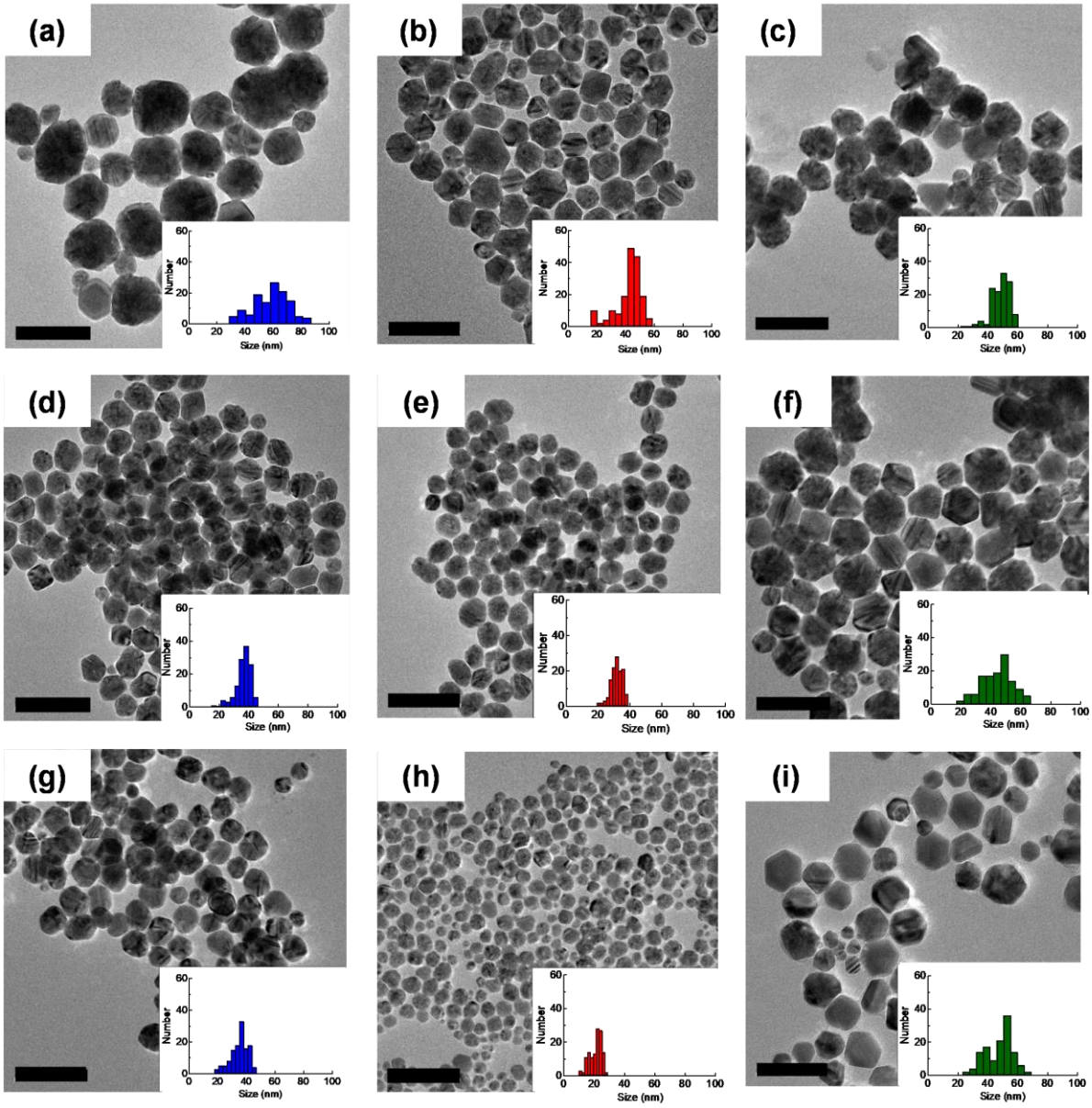

Figure 3.1 TEM micrographs of AgNPs prepared in the presence of (**a**) HO–PEG_{5k}–OH (ω = 2.2), (**b**) *c*-PEG_{5k} (ω = 2.2), (**c**) MeO–PEG_{5k}–OMe (ω = 2.2), (**d**) HO–PEG_{5k}–OH (ω = 11), (**e**) *c*-PEG_{5k} (ω = 11), (**f**) MeO–PEG_{5k}–OMe (ω = 11), (**g**) HO–PEG_{5k}–OH (ω = 44), (**h**) *c*-PEG_{5k} (ω = 44), and (**i**) MeO–PEG_{5k}–OMe (ω = 44) (Scale bar: 100 nm).

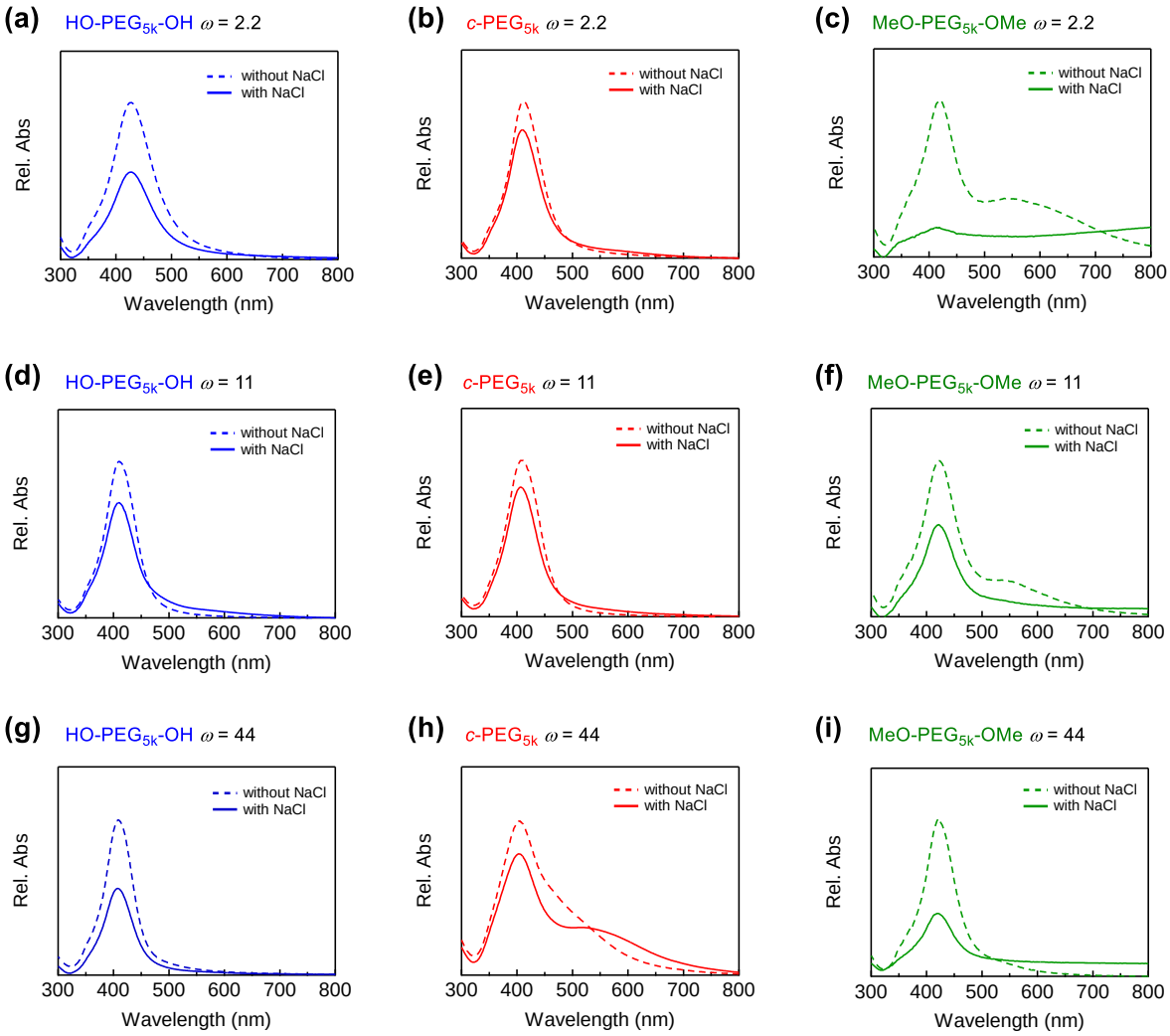

Figure 3.2 Relative UV–Vis absorption spectra of AgNPs without NaCl (dashed line) and with 37.5 mM of NaCl (solid line) in the presence of (**a**) HO–PEG$_{5k}$–OH, (**b**) *c*-PEG$_{5k}$, (**c**) MeO–PEG$_{5k}$–OMe at ω = 2.2, (**d**) HO–PEG$_{5k}$–OH, (**e**) *c*-PEG$_{5k}$, (**f**) MeO–PEG$_{5k}$–OMe at ω = 11, (**g**) HO–PEG$_{5k}$–OH, (**h**) *c*-PEG$_{5k}$, and (**i**) MeO–PEG$_{5k}$–OMe at ω = 44.

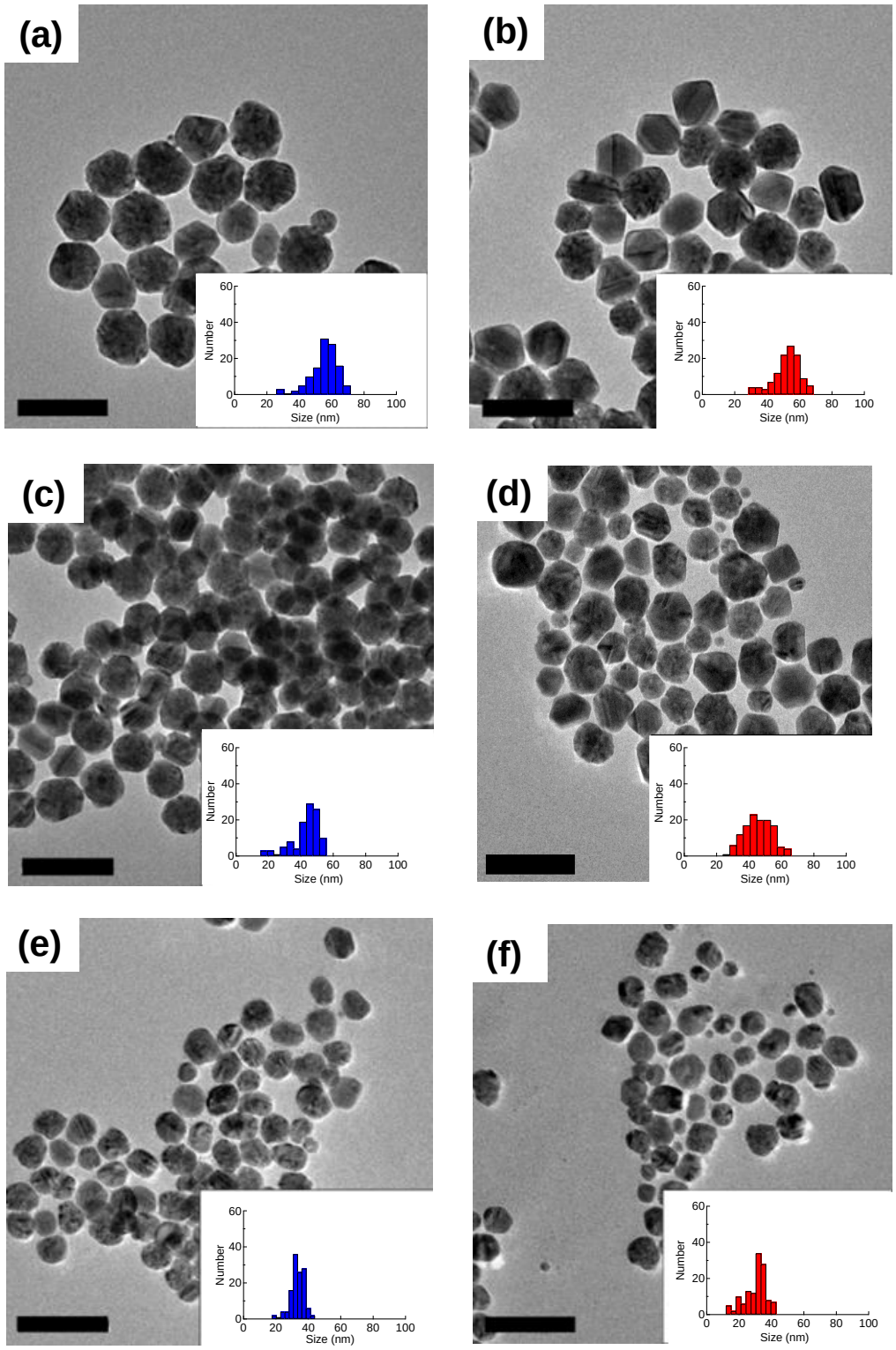

Figure 3.3 TEM micrographs of AgNPs prepared in the presence of (**a**) HO–PEG_{3k}–OH (ω = 2.2), (**b**) *c*-PEG_{3k} (ω = 2.2), (**c**) HO–PEG_{3k}–OH (ω = 11), (**d**) *c*-PEG_{3k} (ω = 11) (**e**) HO–PEG_{3k}–OH (ω = 44), and (**f**) *c*-PEG_{3k} (ω = 44) (Scale bar: 100 nm).

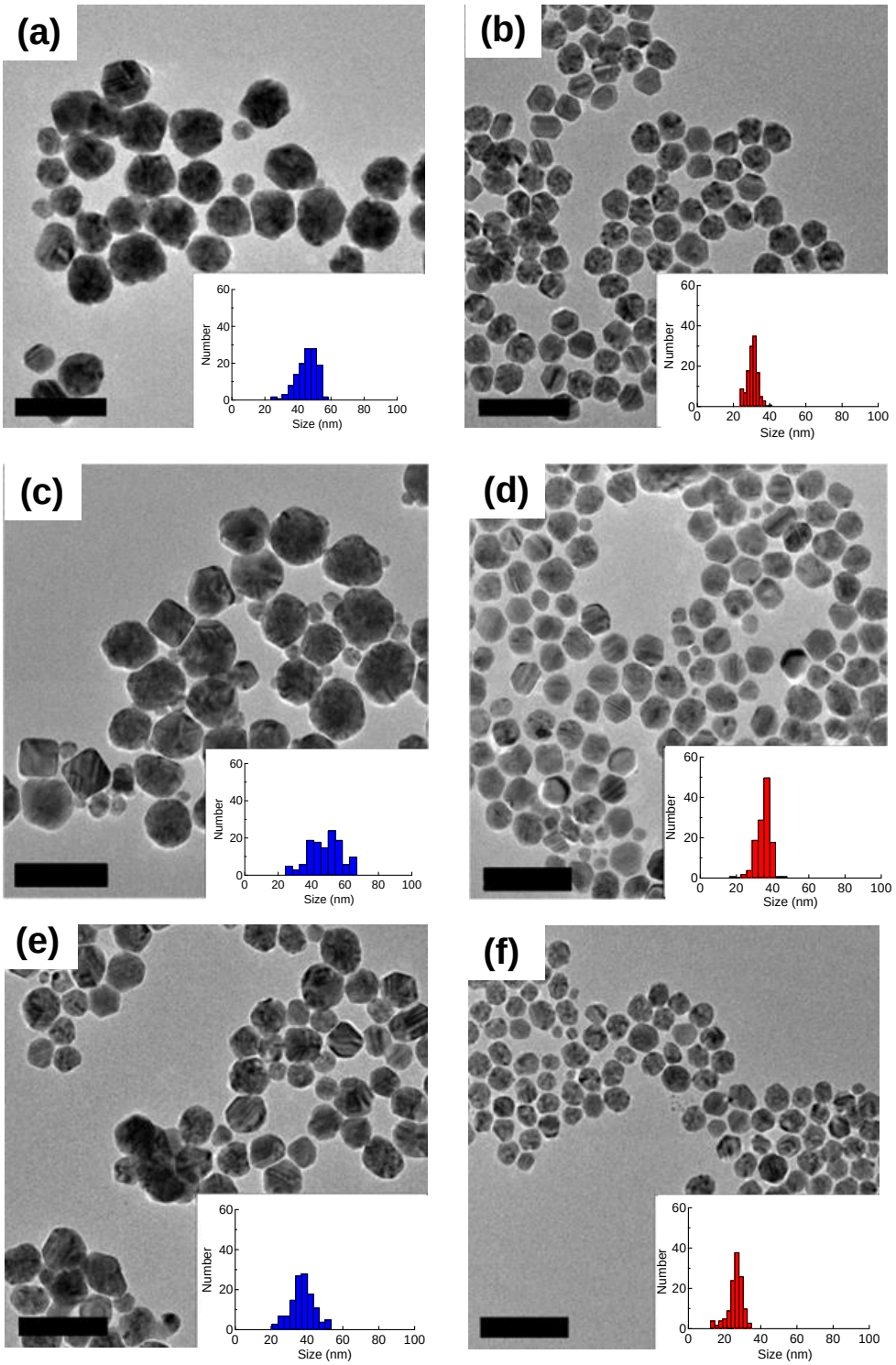

Figure 3.4 TEM micrographs of AgNPs prepared in the presence of (**a**) HO–PEG_{10k}–OH (ω = 2.2), (**b**) *c*-PEG_{10k} (ω = 2.2), (**c**) HO–PEG_{10k}–OH (ω = 11), (**d**) *c*-PEG_{10k} (ω = 11) (**e**) HO–PEG_{10k}–OH (ω = 44), and (**f**) *c*-PEG_{10k} (ω = 44) (Scale bar: 100 nm).

The particle size obtained from the experiments using *c*-PEG_{5k} and *c*-PEG_{10k} was significantly smaller, compared with the cases of corresponding HO–PEG_{5k}–OH and HO–PEG_{10k}–OH, respectively (Table 3.1, Figures 3.1 and 3.4). For example, at ω = 44, 21 ± 4 nm for *c*-PEG_{5k} was substantially smaller than 40 ± 7 nm for HO–PEG_{5k}–OH. Nonetheless, the average particle size remained similar when HO–PEG_{3k}–OH and *c*-PEG_{3k} were used at the respective ω values (Table 3.1 and Figure 3.3). For example, at ω = 44, 30 ± 7 nm for *c*-PEG_{3k} was comparable to 33 ± 4 nm for HO–PEG_{3k}–OH. On the other hand, an increase in the ω value using a same type of polymer generally led to a decrease in the average particle size. Taking *c*-PEG_{5k} as an example, the size decreased from 42 ± 9 nm at ω = 2.2 to 31 ± 4 nm at ω = 11, and eventually to 21 ± 4 nm at ω = 44. These results likely arose from an increase in the potential interaction sites between the silver ions (in the form of $[Ag(NH_3)]_2^+$) and the PEG chain, suppressing the growth of the nanoparticles. The oxyethylene units of PEG complexed with the Ag^+ ions, which were then reduced to form particles[40]. Initially, primary nanoparticles were formed, which underwent coalescence with their neighboring species to form the more stable secondary nanoparticles. In this regard, Shin et al. stated that when the concentration of the polymer is increased, the number of primary AgNPs at close range decreases, thus reducing the possibility of coalescence and eventually yielding small particle sizes[41].

The increase in the ω value meant that it is accompanied by the increase of the number of the hydroxy end groups for HO–PEG–OH, while no hydroxy end groups existed in *c*-PEG. In order to eliminate the effects of the hydroxy end groups, to determine the strict topology effects, PEG with methoxy end groups (MeO–PEG_{5k}–OMe) was synthesized and subjected to the same AgNPs formation experiment. Interestingly, the size of AgNPs formed in the presence of MeO–PEG_{5k}–OMe was basically unchanged (44–48 nm), despite the ω value (Table 3.1, Figure 3.1c,f,i).

This result suggested that the increase in the concentration of the hydroxy end groups leads to the decrease in the particle size, and this effect plays a significant role in the nanoparticle size, using HO–PEG–OH. Therefore, the strict topology effects were actually more prominent by comparing the AgNPs sizes of *c*-PEG$_{5k}$ and MeO–PEG$_{5k}$–OMe; 21 ± 4 nm for *c*-PEG$_{5k}$ and 48 ± 9 nm for MeO–PEG$_{5k}$–OMe at ω = 44 as a representative example. It suggests that the smaller hydrodynamic volume and the corresponding denser structure of *c*-PEG, similar to the case of the micelles from amphiphilic block copolymers[42,43], provided more effective shielding of the metal surface from the coalescence of the primary nanoparticles, which led to the reduction of the average particle size.

The size of the AgNPs was also characterized by UV–Vis spectroscopy (Figures 3.2 and 3.5, dotted lines). For example, at ω = 44, the absorption maximum (λ_{max}) was found at 409, 405, and 420 nm for HO–PEG$_{5k}$–OH, *c*-PEG$_{5k}$, and MeO–PEG$_{5k}$–OMe, respectively. The correlation of the mean particle diameter measured by TEM with λ_{max} in the UV−Vis spectrum was reported previously[44], and the present results reasonably matched the report (Figure 3.6). In the meantime, broadened UV–Vis absorption in the longer wavelengths was observed for some samples such as *c*-PEG$_{5k}$ at ω = 44 (Figure 3.2h), MeO–PEG$_{5k}$–OMe at ω = 2.2 and 11 (Figure 3.2c,f). According to Tadano et al., the polymers can sometimes cause the interactions (i.e., hydrogen bonding and van der Waals interaction) between the polymer chains, which eventually trigger the agglomeration of the nanoparticles[45]. The extent of the agglomeration, however, is also dependent on the particle size and surface properties[46]. At this point, the cause of the broadening trend by ω, the molecular weight, or the topology of the polymer was not determined. Nevertheless, this effect also manifested itself in the corresponding UV–Vis spectra, where absorption at higher wavelengths appeared. Dynamic light scattering was also attempted for size characterization. However, no

valuable data were obtained, likely due to the low concentration of the particles, which gave relatively weak and disturbed signals, where the appropriate concentration of samples for DLS is normally in the range of 1–10 mg/mL.

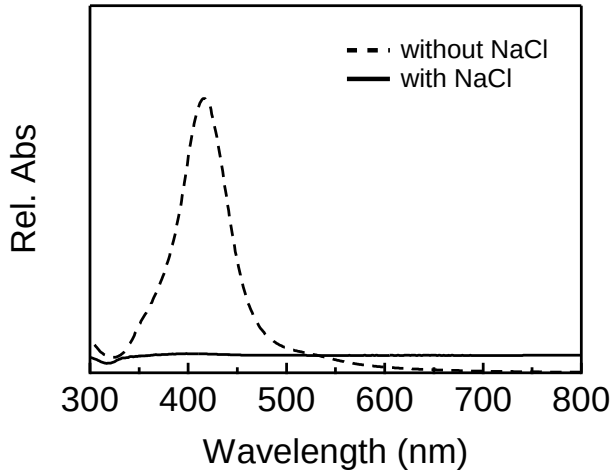

Figure 3.5 Relative UV–Vis absorption spectra of AgNPs without NaCl (dashed line) or with 37.5 mM of NaCl (solid line) in the absence of PEG.

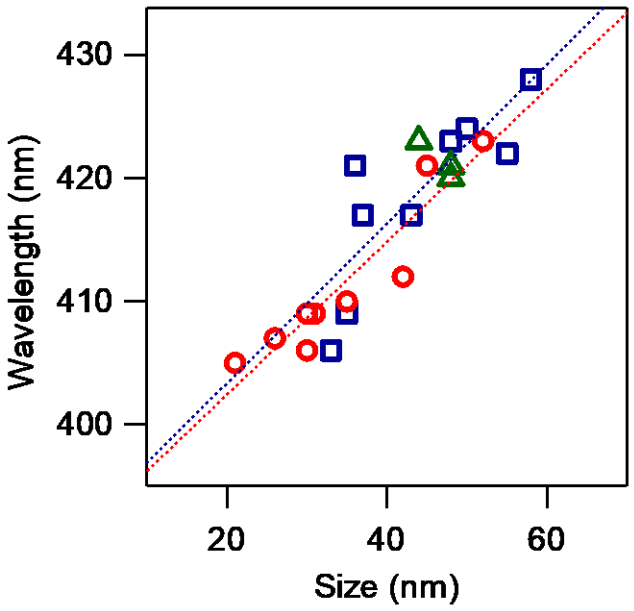

Figure 3.6 Correlation between the particle size of AgNPs extracted from TEM analysis and their λ_{max} measured by UV–Vis spectroscopy for HO–PEG–OH (blue square), *c*-PEG (red circle), and MeO–PEG–OMe (green triangle). The linear regression lines calculated for ones prepared with HO–PEG–OH (blue) and *c*-PEG (red) are included in the plot.

3.3.2 Stability of AgNPs

The prepared AgNPs were subjected to stability tests by exposing them to a solution containing various concentrations of NaCl. The effect of the salt on the intensity of the absorption at λ_{max} was monitored by UV–Vis spectroscopy. The AgNPs prepared in the absence of PEG were susceptible to NaCl, and completely lost the absorption at the salt concentration of 37.5 mM, likely due to aggregation and dissolution (Figure 3.5, solid line). In comparison, AgNPs prepared in the presence of various PEG were more stable. Among them, AgNPs stabilized by *c*-PEG exhibited a higher resistance, compared with those stabilized by corresponding HO–PEG–OH. This phenomenon was illustrated by the *c*-PEG-stabilized AgNPs' ability to preserve the relative UV–Vis absorption intensity ($A/A_0 \times 100\%$) at λ_{max} more efficiently than their linear counterparts, especially at the NaCl concentration range from 37.5 to 50 mM (Figures 3.2, 3.7, 3.8, 3.9, 3.10 and 3.11). For example, at $\omega = 44$ with a NaCl concentration of 37.5 mM, the relative absorption for AgNPs with HO–PEG_{5k}–OH (blue) was 58%, while for *c*-PEG_{5k} (red) it was 80% (Figure 3.7c). Moreover, for MeO–PEG_{5k}–OMe (green), it was only 40% under the same conditions, suggesting the hydroxy end groups also played an important role in the stabilization against NaCl, due to the PEG and AgNPs surface interactions. It is likely that the hydroxy end groups bound to the surface of the AgNPs and protected them from corrosion with chloride anions. Thus, the pure topology effects which were not caused by the hydroxy end groups, on the stabilization of the AgNPs, can be considered as the difference between *c*-PEG_{5k} (80%) and MeO–PEG_{5k}–OMe (40%), despite the fact that AgNPs with *c*-PEG_{5k} were much smaller (21 ± 4 nm) than those with MeO–PEG_{5k}–OMe (48 ± 9 nm). In the meantime, the difference between HO–PEG_{3k}–OH and *c*-PEG_{3k} was not as significant, except for $\omega = 44$ (Figure 3.10), suggesting that the molecular weight and the ω value were also essential factors.

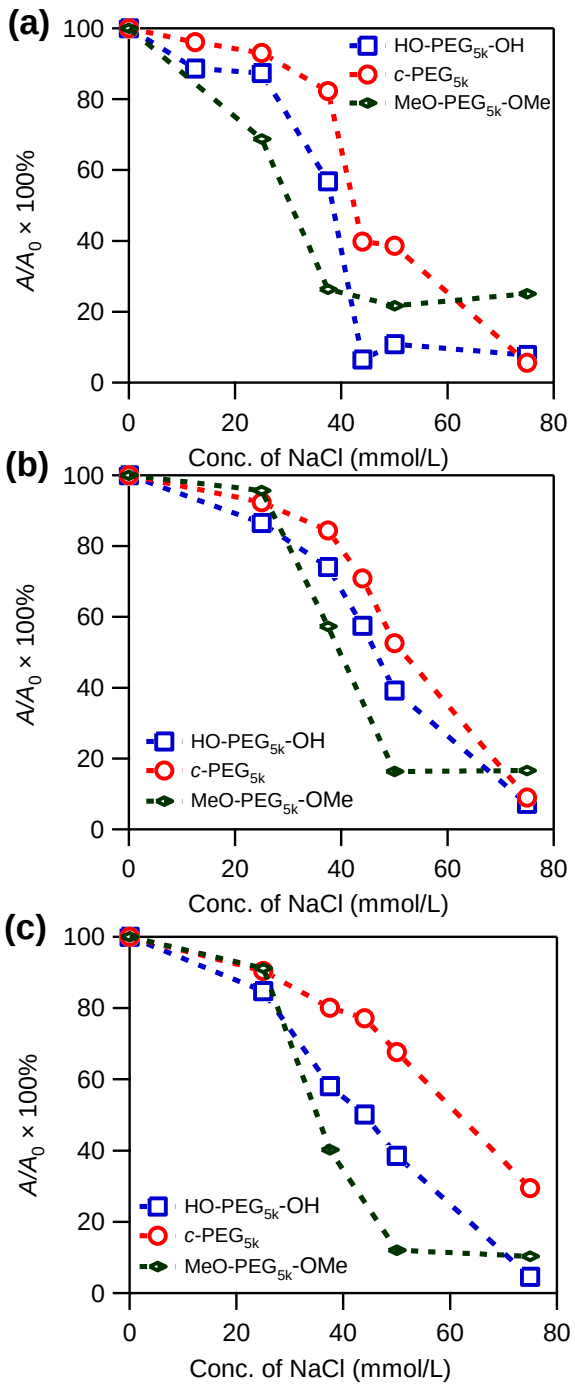

Figure 3.7 Plots of relative UV–Vis absorption intensity (A/A_0 × 100%) at λ_{max} versus the NaCl concentration for AgNPs prepared in the presence of HO–PEG$_{5k}$–OH (blue), *c*-PEG$_{5k}$ (red), and MeO–PEG$_{5k}$–OMe (green) at (**a**) ω = 2.2, (**b**) ω = 11, and (**c**) ω = 44.

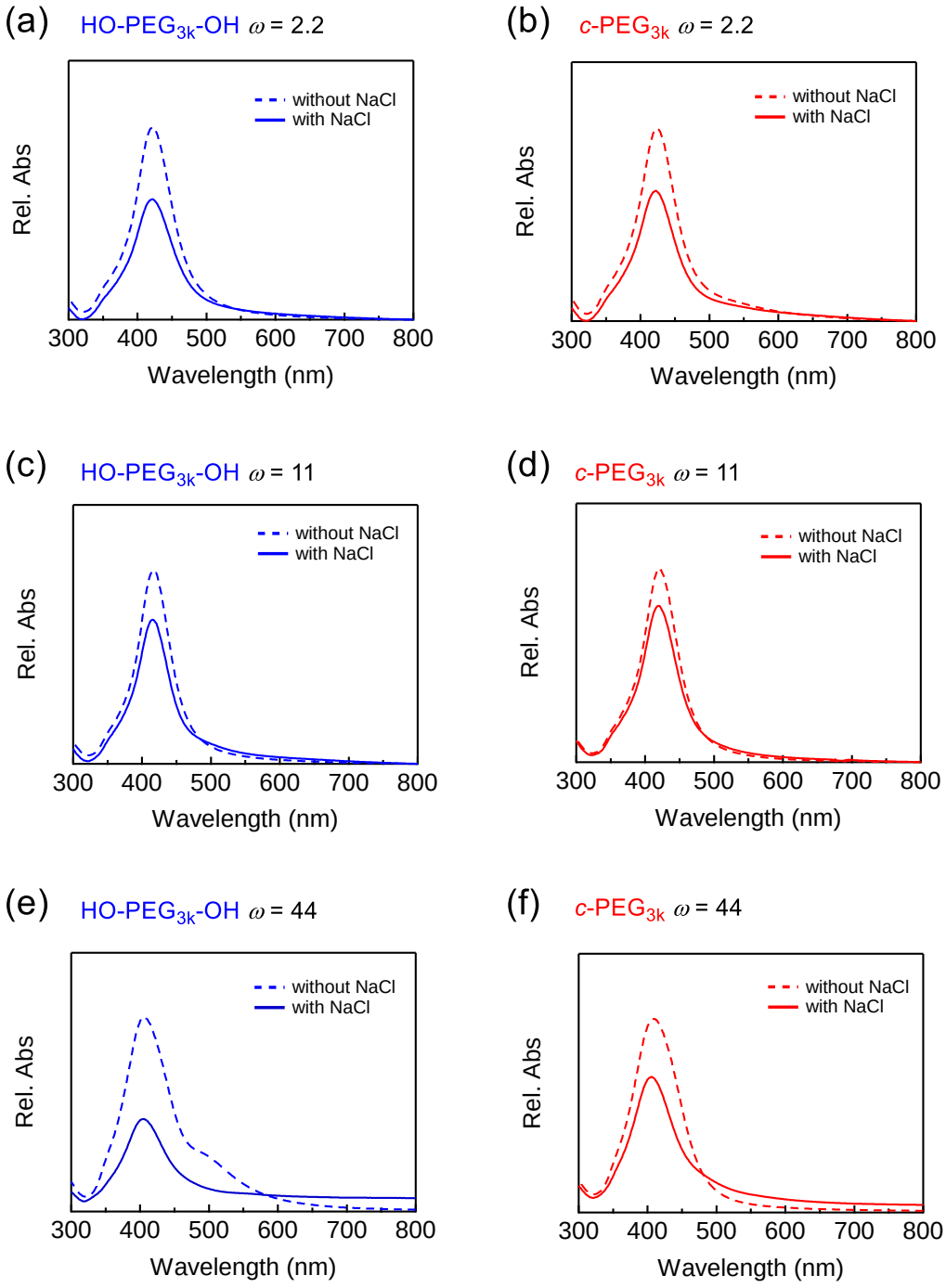

Figure 3.8 Relative UV–Vis absorption spectra of AgNPs without NaCl (dashed line) and with 37.5 mM of NaCl (solid line) in the presence of (a) HO–PEG_{3k}–OH and (b) *c*-PEG_{3k} at ω = 2.2, (c) HO–PEG_{3k}–OH and (d) *c*-PEG_{3k} at ω = 11, (e) HO–PEG_{3k}–OH and (f) *c*-PEG_{3k} at ω = 44.

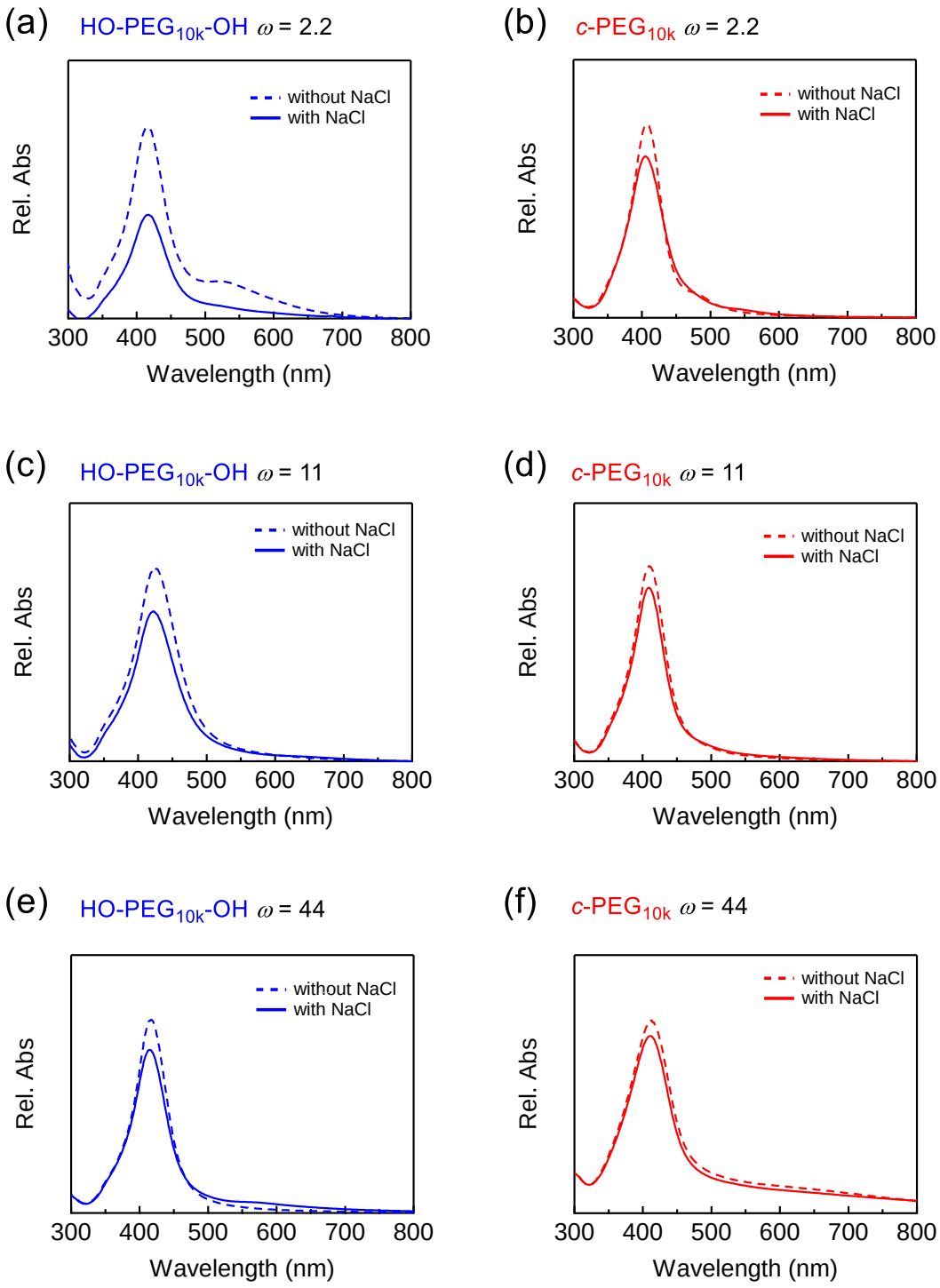

Figure 3.9 Relative UV–Vis absorption spectra of AgNPs without NaCl (dashed line) and with 37.5 mM of NaCl (solid line) in the presence of (a) HO–PEG_{10k}–OH and (b) *c*-PEG_{10k} at ω = 2.2, (c) HO–PEG_{10k}–OH and (d) *c*-PEG_{10k} at ω = 11, (e) HO–PEG_{10k}–OH and (f) *c*-PEG_{10k} at ω = 44.

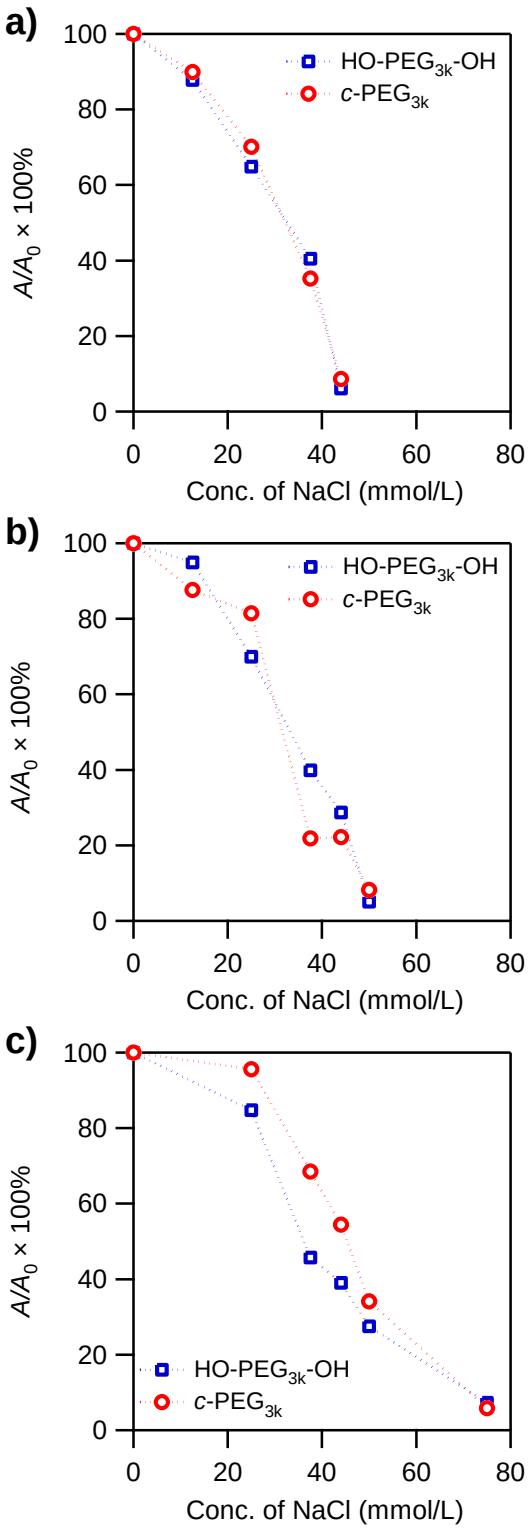

Figure 3.10 Plots of relative UV–Vis absorption intensity ($A/A_0 \times 100\%$) at λ_{max} versus the NaCl concentration for the AgNPs prepared in the presence of HO–PEG_{3k}–OH (blue) and *c*-PEG_{3k} (red) at (a) $\omega = 2.2$, (b) $\omega = 11$, and (c) $\omega = 44$.

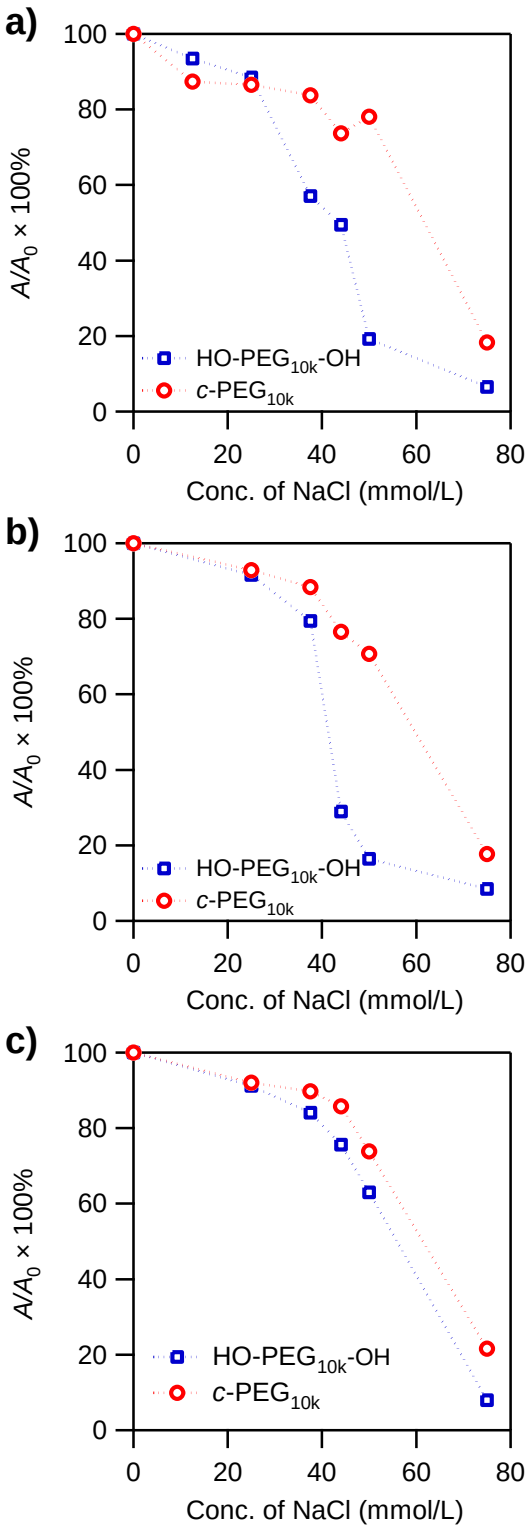

Figure 3.11 Plots of relative UV–Vis absorption intensity ($A/A_0 \times 100\%$) at λ_{max} versus the NaCl concentration for the AgNPs prepared in the presence of HO–PEG_{10k}–OH (blue) and *c*-PEG_{10k} (red) at (a) ω = 2.2, (b) ω = 11, and (c) ω = 44.

3.4 Conclusions

In conclusion, it has been shown that *c*-PEG tends to yield smaller and more narrowly dispersed AgNPs when employed during Tollens' synthesis in comparison with HO–PEG–OH and MeO–PEG–OMe, where smaller and narrowly dispersed metal nanoparticles are desired in various applications. Furthermore, the AgNPs with *c*-PEG exhibited superior stabilizing properties against NaCl, despite the smaller size. Specifically, the pure topological conversion resulted in the drastically improved persistence of the UV–Vis absorption intensity (*c*-PEG_{5k}, 80%; MeO–PEG_{5k}–OMe, 40%). These results clearly indicate that cyclized polymers endow AgNPs with superior stability, compared with their linear counterparts. The enhanced colloidal stability through the use of *c*-PEG would enable applications within biological systems, where the high salt resistance can be exploited. This advantage is coupled with the biocompatibility of PEG itself, where cyclization requires no chemical functionalization on the repeating units of the polymer chain.

3.5 References

1. Kästner, C., Thünemann, A.F. *Langmuir* 2016, **32**, 7383–7391.
2. Beqa, L., Singh, A.K., Khan, S.A., Senapati, D., Arumugam, S.R., Ray, P.C. *ACS Appl. Mater. Interfaces* 2011, **3**, 668–673.
3. Kumbhar, A.S., Kinnan, M.K., Chumanov, G. *J. Am. Chem. Soc*. 2005, **127**, 12444–12445.
4. Hu, M., Chen, J.Y., Li, Z.Y., Au, L., Hartland, G.V., Li, X.D., Marquez, M., Xia, Y.N. *Chem. Soc. Rev*. 2006, **35**, 1084–1094.
5. Anker, J.N., Hall, W.P., Lyandres, O., Shah, N.C., Zhao, J., Van Duyne, R.P. *Nat. Mater*. 2008, **7**, 442–453.
6. Wiley, B.J., Chen, Y.C., McLellan, J.M., Xiong, Y.J., Li, Z.Y., Ginger, D., Xia, Y.N. *Nano Lett*. 2007, **7**, 1032–1036.
7. Mittelman, A.M., Fortner, J.D., Pennell, K.D. *Environ. Sci. Nano.* 2015, **2**, 683–691.
8. Qu, Y.Q., Yang, H.B., Yang, N., Fan, Y.Z., Zhu, H.Y., Zou, G.T. *Mater. Lett*. 2006, **60**, 3548–3552.
9. Hu, S.Q., Huang, P.J.J., Wang, J.X., Liu, J.W. *Anal. Chem*. 2020, **92**, 13354–13360.
10. Zhang, H.Z., Chen, B., Banfield, J.F. *J. Phys. Chem. C* 2010, **114**, 14876–14884.
11. Henglein, A., Giersig, M. *J. Phys. Chem. B* 1999, **103**, 9533–9539.
12. Fenger, R., Fertitta, E., Kirmse, H., Thunemann, A.F., Rademann, K. *Phys. Chem. Chem. Phys*. 2012, **14**, 9343–9349.
13. Tejamaya, M., Romer, I., Merrifield, R.C., Lead, J.R. *Environ. Sci. Technol*. 2012, **46**, 7011–7017.
14. Hussain, I., Brust, M., Papworth, A.J., Cooper, A.I. *Langmuir* 2003, **19**, 4831–4835.
15. Luo, C., Zhang, Y., Zeng, X., Zeng, Y., Wang, Y. *J. Colloid Interface Sci*. 2005, **288**, 444–448.

16. Xia, X., Yang, M., Wang, Y., Zheng, Y., Li, Q., Chen, J., Xia, Y. *ACS Nano* 2012, **6**, 512–522.
17. Li, Y., Lin, H., Zhou, W., Sun, L., Samanta, D., Mirkin, C. *Sci. Adv.* 2021, **7**, eabf1410.
18. Papastefanaki, F., Jakovcevski, I., Poulia, N., Djogo, N., Schulz, F., Martinovic, T., Ciric, D., Loers, G., Vossmeyer, T., Weller, H., Schachner, M., Matsas, R. *Mol. Ther*. 2015, **23**, 993–1002.
19. Li, X., Lenhart, J.J., Walker, H.W. *Langmuir* 2012, **28**, 1095–1104.
20. Li, X.A., Lenhart, J.J., Walker, H.W. *Langmuir* 2010, **26**, 16690–16698.
21. Zhang, X., Servos, M.R., Liu, J. *J. Am. Chem. Soc*. 2012, **134**, 9910–9913.
22. Radziuk, D., Skirtach, A., Sukhorukov, G., Shchukin, D., Möhwald, H. *Macromol. Rapid Commun*. 2007, **28**, 848–855.
23. Kvítek, L., Prucek, R., Panáček, A., Novotny, R., Hrbáč, J., Zbořil, R. *J. Mater. Chem*. 2005, **15**, 1099–1105.
24. Bastakoti, B.P., Guragain, S., Yusa, S., Nakashima, K. *Rsc Adv*. 2012, **2**, 5938–5940.
25. Tezuka, Y., Oike, H. *Prog. Polym. Sci*. 2002, **27**, 1069–1122.
26. Zhang, L.H., Elupula, R., Grayson, S.M., Torkelson, J.M. *Macromolecules* 2016, **49**, 257–268.
27. Kricheldorf, H.R. *J. Polym. Sci. Part A: Polym. Chem*. 2010, **48**, 251–284.
28. Zhang, S.S., Cheng, X.X., Wang, J.Z., Zhang, Z.B., Zhang, W., Zhu, X.L. *Polym. Chem*. 2018, **9**, 5155–5163.
29. Jeong, Y., Jin, Y., Chang, T., Uhlik, F., Roovers, J. *Macromolecules* 2017, **50**, 7770–7776.
30. Honda, S., Yamamoto, T., Tezuka, Y. *J. Am. Chem. Soc*. 2010, **132**, 10251–1025.
31. Honda, S., Yamamoto, T., Tezuka, Y. *Nat. Commun*. 2013, **4**, 1574.
32. Watanabe, T., Chimura, S., Wang, Y.B., Ono, T., Isono, T., Tajima, K., Satoh, T., Sato, S., Ida, D., Yamamoto, T. *Langmuir* 2021, **37**, 6974–6984.

33. Wang, Y., Quinsaat, J.E.Q., Ono, T., Maeki, M., Tokeshi, M., Isono, T., Tajima, K., Satoh, T., Sato, S., Miura, Y., Yamamoto, T. *Nat. Commun*. 2020, **11**, 6089.

34. Oziri, O.J., Wang, Y.B., Watanabe, T., Uno, S., Maeki, M., Tokeshi, M., Isono, T., Tajima, K., Satoh, T., Sato, S.I., Miura, Y., Yamamoto, T. *Nanoscale Adv*. 2022, **4**, 532–545.

35. Panacek, A., Prucek, R., Hrbac, J., Nevecna, T., Steffkova, J., Zboril, R., Kvitek, L. *Chem. Mater*. 2014, **26**, 1332–1339.

36. Sun, T., Yu, G.E., Price, C., Booth, C., Cooke, J., Ryan, A.J. *J. Polymer* 1995, **36**, 3775–3778.

37. Hirose, Y., Taira, T., Sakai, K., Sakai, H., Endo, A., Imura, T. *Langmuir* 2016, **32**, 8374–8382.

38. Lonsdale, D.E., Bell, C.A., Monteiro, M.J. *Macromolecules* 2010, **43**, 3331–3339.

39. Pressly, E.D., Amir, R.J., Hawker, C.J. *J. Polym. Sci. Part A: Polym. Chem*. 2011, **49**, 814–819.

40. Nam, S., Parikh, D.V., Condon, B.D., Zhao, Q., Yoshioka-Tarver, M. *J. Nanoparticle Res*. 2011, **13**, 3755–3764.

41. Shin, H.S., Yang, H.J., Kim, S.B., Lee, M.S. *J. Colloid Interface Sci*. 2004, **274**, 89–94.

42. Heo, K., Kim, Y.Y., Kitazawa, Y., Kim, M., Jin, K.S., Yamamoto, T., Ree, M. *ACS Macro Lett*. 2014, **3**, 233–239.

43. Ree, B.J., Satoh, T., Yamamoto, T. *Polymers* 2019, **11**, 163.

44. Quinsaat, J.E.Q., Testino, A., Pin, S., Huthwelke, T., Nuesch, F.A., Bowen, P., Hofmann, H., Ludwig, C., Opris, D.M. *J. Phys Chem. C* 2014, **118**, 11093–11103.

45. Tadano, T., Zhu, R., Muroga, Y., Hoshi, T., Sasaki, D., Yano, S., Sawaguchi, T. *Polym. J*. 2014, **46**, 342–348.

46. Wang, Y.L., Zhang, Z., Zhang, H., Zhang, Q. *Ind. Eng. Chem. Res*. 2015, **54**, 1646–1655.

Chapter 4

Conclusion

In this thesis, the author announced that *c*-PEG endows a superior dispersion stabilization to metal nanoparticles of gold and silver. Through a novel surface modification of physisorption, not the traditional chemisorption, *c*-PEG is easily adsorbed on the surface of gold nanoparticles due to the less entropic penalty, by compared with the linear counterpart. On the other hand, *c*-PEG exhibits the ability of size control and enhanced stability as a superior dispersant in the synthesis progress of silver nanoparticle. The salt resistant of *c*-PEG towards metal nanoparticles makes it a potential material in a wide range of biomedical and drug delivery system. A summary of the significant findings presented in this research as follows.

Chapter two: The author successfully synthesized, isolated, and characterized various of molecule weight of PEG without end groups and with different end groups of hydroxy, methoxy, and thiol. In the condition of freezing, lyophilization, heating, as well as a physiological condition, AuNPs stabilized by *c*-PEG always remains a red colour due to the SPR of AuNPs. In contrast, AuNPs dispersed by linear counterparts, even by the traditional PEG with thiol end groups, shows aggregation or dissolution of AuNPs. Furthermore, the presence of *c*-PEG layer was confirmed by DLS, ζ-potential, and FT-IR. The thicker PEG layer and the shield effect of ζ-potential from *c*-PEG exhibits a better protective layer on the surface of AuNPs. On the other hand, the AuNPs stabilized by *c*-PEG supplies a prolonged blood circulation and enhanced tumor accumulation in mice. This chapter reveals that the enhanced dispersion stability of AuNPs dispersed by *c*-PEG with no chemical inhomogeneity, supplying sufficient stability toward bio-medical applications, and would be an alternative approach to the gold–sulfur chemisorption. This physisorption would allow for expedient postfunctionalization through chemisorption due to cyclization and physisorption require no chemical modification on the repeating units of the polymer chain.

Chapter three: The author compared the size and salt resistance of synthesized AgNPs by the dispersant of HO–PEG–OH, MeO–PEG–OMe, and *c*-PEG. In the Tollens' synthesis of AgNPs through a *c*-PEG as a stabilizer, smaller size and narrower distribution was found by TEM and UV-Vis, by compared with HO–PEG–OH and MeO–PEG–OMe. Furthermore, the stability of AgNPs was also drastically improved by cyclization. In an aqueous NaCl solution (37.5 mM), the synthesized AgNPs stabilized by *c*-PEG exhibits higher stability (80 %, the relative UV–Vis absorption intensity ($A/A_0 \times 100\%$)) than HO–PEG–OH (58%) and MeO–PEG–OMe (40%). The enhanced colloidal stability through the use of *c*-PEG would enable applications within biological systems, where the high salt resistance can be exploited. This advantage is coupled with the biocompatibility of PEG itself, where cyclization requires no chemical functionalization on the repeating units of the polymer chain.

In conclusion, the author found a novel surface modification of gold and silver nanoparticle by the utilization of *c*-PEG' physisorption. The lack of end chains of *c*-PEG endows superior stabilization to metal nanoparticles, by compared with the linear counterparts. The formulation of cyclic polymer will also be suitable applied on other metal nanoparticles due to the physisorption. In this research, novel surface modification methodology of *c*-PEG will make up the deficiencies of instability, aggregation, and dissolution of metal nanoparticles in bio-medical, photothermal therapy, and drug delivery system field. The utilization of polymer topology effect towards the stability of nanoparticles will open a new vision based on this thesis.